

**DESIGN OF OPTIMAL MEASUREMENT STRATEGIES FOR
GEOMETRIC TOLERANCES CONTROL ON COORDINATE
MEASURING MACHINES**



UNIVERSITÀ DEGLI STUDI DI CAGLIARI

FABIO CONCAS

**Dottorato di Ricerca in Progettazione Meccanica
XIX Ciclo (2003/2006)**

**DESIGN OF OPTIMAL MEASUREMENT STRATEGIES FOR
GEOMETRIC TOLERANCES CONTROL ON COORDINATE
MEASURING MACHINES**



ING. FABIO CONCAS

TUTOR PROF. ING. DANIELE ROMANO

Dottorato di Ricerca in Progettazione Meccanica

XIX Ciclo (2003/2006)

ACKNOWLEDGMENTS

I must express my gratitude towards my advisor, Professor Daniele Romano. His leadership, support, attention to detail, hard work, and scholarship have set an example I hope to match some day.

I wish to thank my family who have always supported me, and most of all Nicoletta for enjoying life together with me.

CONTENTS

ACKNOWLEDGMENTS	iii
CONTENTS	v
INTRODUCTION	xi
1. GEOMETRIC TOLERANCING	1
1.1. Background.....	1
1.2. Geometric tolerancing	3
1.3. Symbols for geometric tolerances.....	4
1.4. Some important concepts from GD&T.....	7
1.4.1. Datum reference frame	7
1.4.2. Maximum Material Condition	10
1.4.3. Least Material Condition	13
1.4.4. Regardless of Feature Size.....	14
1.4.5. Bonus tolerance and datum shift.....	15
1.5. Position tolerances.....	17
1.5.1. Definition of position tolerance zone.....	17
1.5.2. Surface of a Feature Interpretation.....	18
1.5.3. In terms of the Resolved Geometry of a Feature.	21
1.6. Flatness of a surface.....	25
REFERENCES CHAPTER 1.....	28
2. COORDINATE MEASURING MACHINES.....	29
2.1. Background.....	29
2.2. The role of coordinate measuring machines	29
2.3. Types of coordinate measuring machines.....	31

2.3.1.	Cantilever type	31
2.3.2.	Bridge type	32
2.3.3.	Column type	33
2.3.4.	Horizontal arm type	33
2.3.5.	Gantry type	34
2.4.	<i>Modes of operation</i>	35
2.5.	<i>Type of probes</i>	35
2.6.	<i>Probe calibration</i>	39
2.7.	<i>Metrological features</i>	40
	REFERENCES CHAPTER 2	42
3.	UNCERTAINTY IN CMM MEASUREMENTS	43
3.1.	<i>Definition of uncertainty in measurements</i>	43
3.1.1.	The measurement equation	44
3.1.2.	Representation of uncertainty components: standard uncertainty	45
3.1.3.	Evaluating uncertainty components	45
3.1.4.	Combining uncertainty components	46
3.1.5.	Expanded uncertainty and coverage factor	47
3.2.	<i>Uncertainty and traceability in CMM measurements</i>	47
3.3.	<i>Techniques for evaluation of the uncertainty on CMM-based measurements</i>	49
3.3.1.	ISO 15530-1: overview and metrological characteristics	50
3.3.2.	ISO 15530-2: use of multiple strategies in calibration of artefacts	50
3.3.3.	ISO 15530-3: use of calibrated work pieces or standards	51
3.3.4.	ISO 15530-4: estimating task-specific measurement uncertainty using simulation	52
3.3.5.	ISO 15530-5: use of expert judgement, sensitivity analysis and error budgeting	53
3.4.	<i>Critical observations</i>	54

<i>REFERENCES CHAPTER 3</i>	58
4. METHODOLOGY FOR INSPECTION PLAN DESIGN	59
<i>REFERENCES CHAPTER 4</i>	63
5. APPLICATION TO POSITION TOLERANCES	64
5.1. Related work	64
5.2. Measurement process	65
5.2.1. The inspected part	65
5.2.2. DRF evaluation	67
5.2.3. Hole location	70
5.2.4. Position error by surface interpretation at MMC and RFS	70
5.2.5. Position error by resolved geometry interpretation at MMC and RFS ..	73
5.3. Experiment settings on the virtual CMM	75
5.3.1. Input of the part	76
5.3.2. Input of the point sample	76
5.3.3. Input of measurement error	77
5.3.4. DRF computation	78
5.3.5. Point sample on the hole surface	81
5.3.6. Material condition or tolerancing interpretation	83
5.4. Algorithms for estimating the circumference inscribed in n points	89
5.5. Results	90
5.5.1. DRF analysis	91
5.5.2. Position error analysis	92
5.5.3. Final remarks	97
<i>REFERENCES CHAPTER 5</i>	99
6. APPLICATION TO FLATNESS TOLERANCES	101
6.1. Related work	101
6.2. Sample- based estimation of flatness error	102
6.2.1. Orthogonal Least Square method	103

6.2.2.	Boundary Planes method	105
6.2.3.	The Convex Hull method	108
6.2.4.	Reference frame changing method	110
6.3.	<i>Model-based estimation methods</i>	112
6.3.1.	Regression Fit method.....	113
6.3.2.	Improved Regression Fit method.....	113
6.4.	<i>Design of inspection plans for flatness (or straightness) control</i>	115
6.4.1.	The inspected part.....	115
6.4.2.	The planned experiment.....	118
6.5.	<i>Results of the experiment</i>	121
6.5.1.	Analysis of flatness bias.....	121
6.5.2.	Analysis of flatness uncertainty.....	126
6.6.	<i>Application of the Improved Regression Fit method</i>	130
	<i>REFERENCES CHAPTER 6</i>	136
APPENDIX 1: Working Draft ISO/WD 15530-4:		139
	<i>Preliminary remark</i>	139
	<i>A1.1. Scope</i>	139
	<i>A1.2. Terminology: (To be defined; descriptions are given when used first)</i>	140
	<i>A1.3. Overview</i>	140
	<i>A1.4. Elements of the UES</i>	141
	<i>A1.5 Uncertainty Evaluating Software Evaluation (UESE)</i>	145
APPENDIX 2: Architecture of the Software		153
	<i>A2.1. Software configuration in the position tolerance evaluation case.</i>	153
	<i>A2.2. Simulation of nominal measurement points on part surface</i>	155
	<i>A2.3. Assignment of measurement error</i>	159
	<i>A2.4. DRF evaluation</i>	159

<i>A2.5. Definition of measurement error</i>	160
<i>A2.6. Simulation of nominal measurement points on part surface (holes)</i>	160
<i>A2.7. Factorial plan analysis</i>	162
<i>A2.8 Software configuration for the case of flatness (and straightness) tolerance.</i>	172
<i>A2.9. Parameters setting</i>	173
<i>A2.10. Large samples with factorial sampling</i>	175
<i>A2.11. Small samples</i>	177
<i>A2.12. Measurement error and form error attribution</i>	178
<i>A2.13. Flatness error evaluation</i>	178

INTRODUCTION

This study is concerned with a vast industrial problem: the inspection of physical components and subsystems for checking their conformance to dimensional and geometric tolerance specifications. Although a number of non contact optical devices are being currently developed for such a task, Coordinate Measuring Machines (CMM) are still universally adopted thanks to their superiority in terms of accuracy in the measurement of point coordinates. However, their unsurpassed metrological quality for this basic operation is counterbalanced by a fundamental problem that is plaguing practitioners in the sector of industrial metrology. The problem is usually referred to as *methods divergence* and can be stated as follows. On one hand, the machines probe the part surface point-wise and economic constraints force the point sample to be small. On the other end, geometric errors, as defined by tolerance standards, depend heavily on extreme values of the form deviations over the related surface so that a full-field inspection is virtually required. For example, straightness error is the minimum distance between two parallel lines enclosing the actual feature. Thus extreme points are more important than the others in determining the straightness error. This problem, translated in statistical terms, means using a small sample of form deviations to make inference on a quantity dependent on extreme values of the population, thereby unlikely to be in the sample. Thus sample-based evaluation of geometric errors is naturally prone to be substantially biased and uncertain, especially when the surfaces exhibit systematic form deviations. In spite of this, common practice in industry is to probe very few points according to very simple sampling strategy (uniform, random, stratified). The software packages sold with the machines contain algorithms of computational geometry which are selected by purely economic criteria (easy to implement, fast to compute) regardless of their implications on measurement quality. Moreover, user awareness of the importance of evaluating measurement uncertainty in the inspection of geometric tolerances is exceedingly limited. This is no wonder if we consider that the ISO committees have been working for several years on different four methods for uncertainty evaluation in CMM measurement tasks (ISO 15530 family) and still now only one standard has been officially delivered (ISO 15530-3, march 2004). Uncertainty calculation using calibrated objects). Also on the research side there are some deficiencies. The main limit is in that the inherently difficult statistical problems involved in this topic are still not

fully recognized by a research community that is traditionally devoted to engineering design and computational geometry. The research work presented in this dissertation must be referred to this background. It attempts to make the following contributions.

1. A methodology for the design of sound inspection plans for geometric tolerance control is proposed. The methodology is based on experiments to be conducted on a suitable simulation model of the CMM measurement process (the so called *virtual CMM*). Notice that one ISO standard should be soon released on the subject of uncertainty evaluation by the simulation method. Basically the experiments study the effect of the main design variables and options involved in the measurement process on two outputs, i.e. the mean and the random variability of the measurement result. The latter is typically a geometric error, e.g. position error or flatness error, and its first two statistical moments are directly linked to two major metrological properties, namely measurement bias and uncertainty. Design variables can be categorized in two classes: strategies for surface sampling (sampling method and number of probed points), and methods for estimating the geometric error. Also part geometry, both nominal geometry and possible form deviations, take an important role in the design process. Albeit not subject to design, they condition to a large extent the best design choices. As a consequence, the method envisages the extraction of the systematic form error of the involved surfaces for a sound design of the inspection plan.
2. The design methodology is applied to two classes of geometric tolerances, position tolerances and form tolerances (flatness and straightness). The two studies are somehow different. The study of position error is quite compelling as it requires the inspection of more than one surface (up to five). In this case we study the baseline uncertainty of the estimated position error for a nominal geometry part. We discovered an inherent incompatibility between the actual statistical properties of the position error and the nominal properties assumed by the tolerance standards. Then we propose coherent design choices for reducing measurement uncertainty which sometimes contradict explicitly the rule of thumbs adopted in the industrial use of the CMM. Finally a statistical criterion for part acceptance/rejection is proposed. The criterion is based on a genuine vectorial interpretation of the position error which is ignored by the standards.
The second application refers to straightness and flatness tolerances.

As the related geometric errors are easier to estimate, here we consider also the presence of systematic form deviations on the features. A clear distinction is made by sample-based and model-based methods for the estimation of the geometric error, a fundamental difference not always sufficiently acknowledged even in the technical literature. We demonstrate, for a typical form error signature left by milling operations, that sample-based methods, if used *tout-court*, expose the user to the risk of a sizable underestimation of the geometric error, regardless of the sampling method which is used. A natural countermeasure is to design the small point sample by exploiting a-priori information on the actual surface. This may come either from detailed knowledge of the machining processes applied to the part or from a preliminary large-sample inspection of one or a few parts whose form errors can be considered similar to those of the part to be inspected. The latter circumstance occurs in total inspection of lots from batch or mass production: a few parts are densely sampled, then a small-sample plan, designed using that detailed information, is applied to the rest of the lot. Assuming to be in this setting, we propose a new model-based approach to design small-size inspection plans capable of producing accurate estimates of form errors if the similarity conditions hold and warning the user if they do not. The application of the method and its merit are illustrated by a real case-studies referring to straightness tolerances on face-milled surfaces.

The finding of this work indicate that, unless tolerance definitions are changed or CMM are replaced by devices allowing for a full field inspection of parts, acceptable solutions to the “methods divergence” problem can only come from a thorough consideration of the statistical nature of the estimation problem coupled with the full exploitation of any form of reliable knowledge on the parts to be inspected, on the measurement process in use, on the effects of the computational algorithms on the measurement quality.

1. GEOMETRIC TOLERANCING

It is impossible to manufacture workpieces without deviations from the nominal shape. Workpieces always have deviations of size, form, orientation and location. When these deviations are too large the usability of the workpiece will be impaired. Conversely, if during manufacturing attempts are made to keep these deviations as small as possible, in order to avoid the impairment of usability, in general the production is too expensive and the product is hard to sell.

The purpose of this section is to present geometric tolerances with particular reference to position and flatness tolerances. The intent is to briefly illustrate the five types of geometric tolerances showing the advantages of ASME standard interpretation of the geometric dimensioning and tolerancing (GD&T) with respect to the old interpretations (e.g. coordinate tolerances versus position tolerances). Later, position and flatness tolerances are shown using ASME standard definitions.

1.1. Background

Scalable drawings became the medium for defining mechanical parts and entire machines early in the nineteenth century. Dimensions were added to drawings later in the nineteenth century, when affordable steel scales and vernier instruments made precise shop-floor measurement feasible. Tolerances, expressed as plus/minus limits on dimensions, appeared early in the twentieth century. These three constructs, taken together, provided the first reasonably complete system for specifying symbolically the geometry of mechanical products. Note the elements:

- Form was handled by views on orthographic drawings.
- Dimension quantified form
- Variation control, which is essential because human-made artefacts are inherently imprecise, was handled by a mixture of limits on dimensions (e.g. 1.500 ± 0.005) and process callouts (e.g., “hole 1.875 thru”).

An event (World War II, with its vast demands for multisource procurement) stimulated post-war changes in variation-control practice. Process specifications were prohibited to retain maximum manufacturing flexibility, and tolerances became the sole mechanism for variation control. More pervasively, dimensional limit tolerancing (now called

worst-case parametric tolerancing) which suffers from several ambiguities, was replaced with geometric tolerancing. This are based on three central notions:

1. Conformance to a geometric tolerance requires that a surface feature, or an attribute of a feature (e.g. the axis of a hole), lie within a prescribed spatial zone. Note that this is a true geometric criterion, whereas conformance to a parametric tolerance is inherently numeric.
2. A geometric tolerance usually controls explicitly only one specified property of a feature, such as form (flatness) or position. However, subtle interactions between different tolerances on the same feature can complicate matters considerably.
3. Some containment zones (e.g., for form) can be positioned freely in space, whereas others (e.g., for position) are located on parts through reference features called datums. The use of containment zones deals directly with imperfect form and is the hallmark of geometric tolerancing.

These changes were codified in successive editions of the ASME Y14.5 standard (1994a) and required a workforce generation for industry to digest. It is important to realize that geometric dimensioning and tolerancing (GD&T), as defined in Y14.5, is not based on explicit mathematical principles. It is a codification of best practices assembled by practical people with artisan backgrounds, who defined GD&T mainly through examples explained with prose and graphics.

A second event, the “Metrology crisis” of the 1980s, triggered two projects that may mark the start of a new era in tolerancing¹. This divergence was tagged as a “Metrology crisis” requiring attention by the responsible standards committees (Hook 1993)). The first projects sought to “mathematize” Y14.5; it has produced to date a new standard, Y14.5.1M-1994, Mathematical Definition of Dimensioning and Tolerancing Principles (ASME, 1994b). The second project’s goal is a companion standard for Y14.5.1 is somewhat misleading because “principles” are covered only in the narrowest sense. Y14.5.1 is a literal

¹ Industrial use of coordinate measuring machines (CMMs) for part inspection proliferated in the 1980s, but early CMM algorithms produced results different from those obtained with traditional methods (hard gages, open setup).

mathematization: specifically, an enumerative redraft of Y14.5, with Y14.5's prose and graphics replaced by definitions in algebraic geometry of three characteristics for each tolerance class: the containment zone, the conformance criterion, and the actual value. [Actual value means, loosely, the smallest tolerance value (smallest zone) to which a particular physical feature can conform]. Y14.5.1 does not provide a generative reformulation of geometric tolerancing, that is, a sparse set of mathematical principles from which one can construct the various tolerance classes and their three characteristics.

1.2. Geometric tolerancing

Dimensional tolerances prescribe the minimum and the maximum limits within which a dimension is allowed to be. Likewise, geometric tolerances specify the maximum allowable variations, from the perfect geometry implied by the drawing, of form, orientation, position that a geometric entity is allowed to exhibit. The term “geometric” refers to various such entities, such as a plane, a cylinder, a cone, a square, or a axis. These tolerances specify a generally three-dimensional region, called tolerance zone, within which a given geometrical entity must lie if the part is to meet the required accuracy for proper functions and fit. For example, when tolerances of form are not given on a drawing, it is customary to assume that, regardless of form variations, the part will fit and function satisfactorily.

Five types of geometric tolerances can be individuated:

1. **Form tolerance:** this tolerance type is applied to single (individual) features or elements of single features; therefore form tolerances are not related to datums. This tolerance type includes straightness, flatness, circularity (roundness), and cylindricity.
2. **Profile tolerance:** a profile is the outline of an object in a given plane (two dimensional) that is derived from a cross section or projection from a part. The elements of a profile are straight lines, arcs, and other curved lines. With profile tolerancing, the true profile may be defined by basic radii, basic angular dimensions, basic coordinate dimensions, basic size dimensions, undimensioned drawings, or formulas. Profile tolerances include profile of a surface and profile of a line.
3. **Orientation tolerance:** angularity, parallelism, perpendicularity, and in some instances, profile are orientation tolerances

applicable to related features. These tolerances control the orientation of features to one another. All orientation tolerances are defined in relation to datum features.

4. **Location tolerance:** this tolerance type includes position, concentricity, and symmetry used to control the following relationships:
 - a. centre: distance between features such as holes, slots, bosses, and tabs;
 - b. location of a group of features from datum features, such as planer and cylindrical surfaces;
 - c. coaxiality of features;
 - d. concentricity or symmetry of features -centre distanced of correspondingly-located feature elements equally disposed about a datum axis or plane.

5. **Runout tolerance:** runout is a composite tolerance used to control the functional relationship of one or more features of a part to a datum axis. There are two types of runout control, circular runout and total runout. The type used is dependent upon design requirements and manufacturing considerations. Circular runout is normally a less complex requirement than total runout.

1.3. Symbols for geometric tolerances

Methods of indicating geometric tolerances by means of geometric characteristic symbols are recommended rather than by traditional notes. These symbols (ANSI/ASME Y14.5.1) provide an accurate and concise means of specifying geometric characteristics and tolerances in a minimum space. In following table, symbols are reported (Table 1.1).

The ASME Y14.5 specification includes several modifiers that are used to fully describe how a geometric tolerance is to be applied. The selection of a modifier is directly controlled by the functional aspects of the characteristic under consider. The proper selection of a modifier is critical to the ability to manufacture the component and the ease in which the component can be also inspected. Modifiers can be applied to the characteristic being described geometrically and/or to a characteristic serving as a datum.

Table 1.1. Geometric Characteristics Symbols (ASME Y14.5.1)

	TYPE OF TOLERANCE	CHARACTERISTIC	SYMBOL	
FOR INDIVIDUAL FEATURES	FORM	STRAIGHTNESS	—	
		FLATNESS		
		CIRCULARITY (ROUNDNESS)		
		CYLINDRICITY		
FOR INDIVIDUAL OR RELATED FEATURES	PROFILE	PROFILE OF LINE		
		PROFILE OF SURFACE		
FOR RELATED FEATURES	ORIENTATION	PARALLELISM		
		PERPENDICULARITY		
		ANGULARITY		
	LOCATION	POSITION		
		CONCENTRICITY		
		SYMMETRY		
	RUNOUT	RUNOUT	CIRCULAR RUNOUT	
			TOTAL RUNOUT	

Following modifiers are commonly used in GD&T and are shown with their usual abbreviation and symbol used in the drawing feature control frame (see Table 1.2).

Table 1.2. Modifies Symbols (ASME Y14.5.1)

TERM	SYMBOL
AT MAXIMUM MATERIAL CONDITION	
AT LEAST MATERIAL CONDITION	
PROJECTED TOLERANCE ZONE	
FREE STATE	
TANGENT PLANE	
DIAMETER	\varnothing
SPHERICAL DIAMETER	$S\varnothing$
RADIUS	R
SPHERICAL RADIUS	SR
CONTROLLED RADIUS	CR
REFERENCE	()
ARC LENGTH	
STATISTICAL TOLERANCE	
BETWEEN	

- The datum identifying symbol consist of a capital letter in square frame and a leader line extending from the frame to the concerned feature, terminating with a triangle. The triangle may be filled or not filled (see Fig. 1.1). Letters of the alphabet (except I, O, and Q) are used as a datum-identifying letters. A point, line, plane, cylinder or other geometric form assumed to be exact for purposes of computation may serve as datum from which the location or geometric relationship of features of a part may be established.

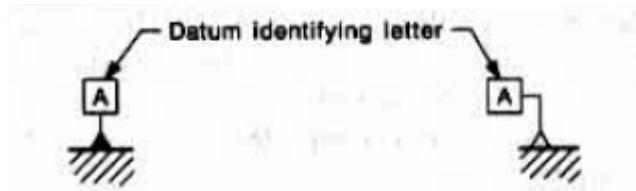


Fig. 1.1. Datum feature triangle may be filled or not filled. Leader may be appropriately directed to a feature

- Supplementary symbols include the symbols for MMC (maximum material condition), (i.e., minimum hole diameter, maximum shaft diameter) and LMC (least material condition), (i.e. maximum hole diameter, minimum shaft diameter). The abbreviation MMC and LMC are also used in notes (Fig. 1.2).

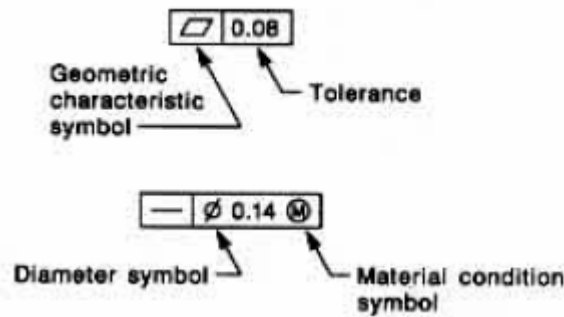


Fig. 1.2. Feature control frame

- Combined symbols are found when individual symbols, datum reference letters, need tolerances, and so on are found in a single frame (Fig. 1.3).

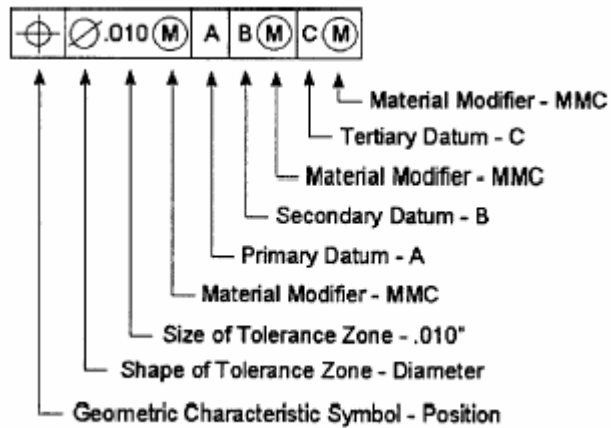


Fig. 1.3. Feature control frame incorporating datums reference

1.4. Some important concepts from GD&T

We have mentioned some important concepts from geometrical tolerances, as datum reference frames (DRF) or material conditions (e.g. Maximum Material Condition). We will now explain briefly their meaning.

1.4.1. Datum reference frame

A datum is a point, line, plane or other geometric surface from which dimensions are measured, or to which geometric tolerances are referenced. A datum has an exact form and represent an exact or fixed locations for purposes of manufacture or measurement. A datum feature is a feature of a part, such as an edge, surface, or hole, which forms the basis for a datum or it is used to establish the location of a datum. Datums are exact geometric points, lines, or surfaces, each based on one more datum features of the part. Surface are usually either flat or cylindrical, but other shapes are used when necessary. Since the datum features are physical surfaces of the part, they are subject to manufacturing errors and variations. For example, a flat surface of a part, if greatly magnified, will show some irregularity. If brought into contact with a perfect plane, this flat surface will touch only at the highest points, (Fig. 1.4). The true datums exist only in theory but are considered to be in the form of locating surfaces of machines, fixtures, and gauging equipment on which the part rests or with which it makes contact during

manufacture and measurement.

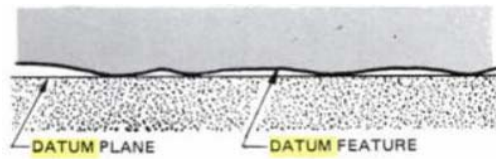


Fig.1.4. Magnified section of a flat surface

Geometric tolerances, such as straightness and flatness, refer to unrelated lines and surfaces and do not require the use of datums. Orientation and locational tolerances refer to related features; that is, they control the relationship of features to one another or to a datum or datum system. Such datum features must be properly identified on the drawing. Usually only one datum is required for orientation purposes, but position relationships may require datum system consisting of two or three datums. These datums are designed as primary, secondary and tertiary. When these datums are plane surfaces that are mutually perpendicular, they are commonly referred as a three-plane datum system or a datum reference frame.

If the primary datum feature is a flat surface, it could be laid on a suitable plane surface, such as the surface of a gage, which would then become a primary datum, Figure 1.5. Theoretically there will be a minimum of three high spots on the flat surface coming in contact with the gages surface.

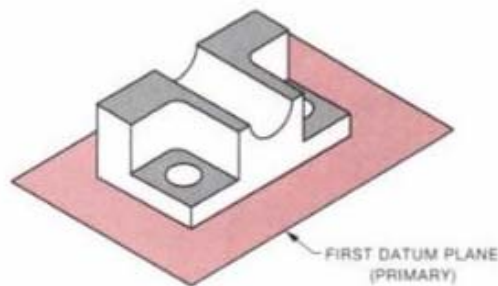


Fig. 1.5. Primary datum

If the part is brought into contact with a secondary plane while lying on the primary plane, it will theoretically touch at a minimum of two points, see Figure 1.6.

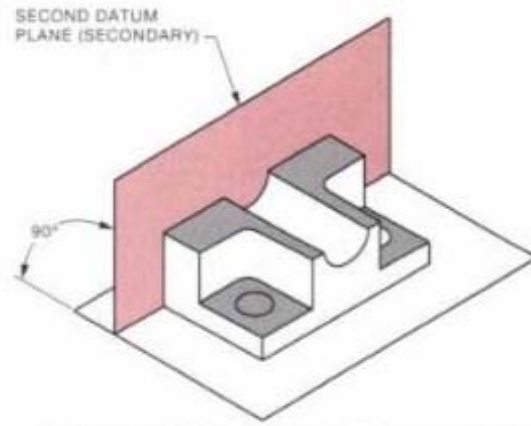


Fig. 1.6. Secondary datum

The part can be slid along while maintaining contact with both the primary and secondary planes until it contacts a third plane, Fig. 1.7. This plane then becomes the tertiary datum and the part will, in theory, touch it at only one point. These three planes constitute a datum system from which measurement can be taken.

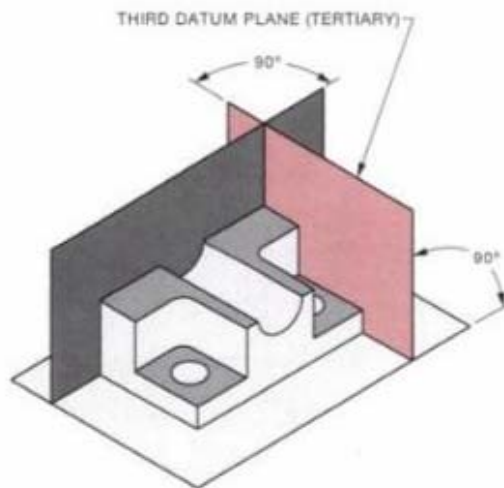


Fig. 1.7. Tertiary datum

Figure 1.8 summarise the sequence of DRF definition

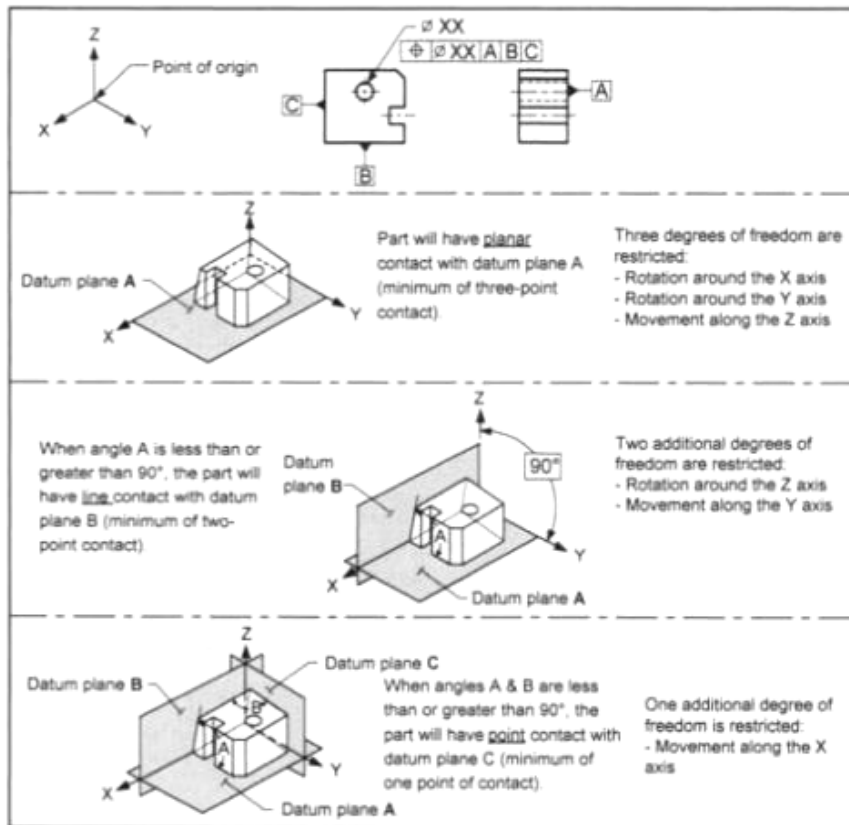


Fig. 1.8. Primary, Secondary and Tertiary Datums

Notice that previous procedure is an example of three virtually orthogonal part surfaces to which the 3-2-1 rule is applied. This rule is inspired by the physical fact that, in order to fix the part, the minimum number of contact points with the primary datum is 3, with the secondary datum is 2, and with the tertiary datum is 1. In this dissertation we will show that this rule is not justified at all when it is used to estimate the DRF as it leads to a highly uncertain estimate (see chapter 5)

1.4.2. Maximum Material Condition

Maximum Material Condition is the condition of a feature wherein the feature contains the most material, it is often thought of as the heaviest feature, it is the smallest hole or the largest shaft. In the ANSI Y14.5 maximum material condition is described as “the condition in which a feature of size contains the maximum amount of material within the

stated limits of size. For example, minimum hole diameter, maximum shaft diameter”. A shaft or other external feature such as a pin, a tab, or a feature made up of opposing external sides of a part are at maximum material condition (MMC) when they are at their largest allowable size. Some like to refer to it as when the feature is the heaviest. For example, a shaft with a size of $\text{Ø } 0.125 \pm 0.010$ would be at MMC when it measures $\text{Ø } 0.135$ or its largest size.

A hole or other internal feature such as a keyway, slot or the feature made up of opposing internal sides of a part are at maximum material condition when they are at their smallest allowable size. If a hole was drilled bigger than its smallest allowable size, more material would have to be removed from the hole, therefore it wouldn't have its maximum amount of material. If a hole with size limits $\text{Ø } 0.480 - 0.500$ was produced at $\text{Ø } 0.480$, it would be at its smallest allowable size, its maximum material condition.

In feature control frames, the MMC concept (circled M) is usually used for mating features. If a shaft is to be inserted into a hole, the shaft's geometry of form, orientation or location need not be as perfect if the shaft is made at a smallest size, just as the hole's geometry can be less perfect if the hole is produced at a larger size. This additional geometric tolerance based on size departure from maximum material condition is often termed 'bonus tolerance'. It allows more parts to pass the inspection procedure based on functional requirements. It lets the inspectors buy off parts that will mate. Many of these parts may not have been allowed to pass the inspection process if they had been controlled on a regardless of feature size basis, even though they may easily have been able to mate with mating features. The MMC concept allows the acceptance of parts that have mating features that may mate with pins more off to one side of the holes rather than directly in the centre of the holes. It allows the acceptance of pins that may lean more inside a mating hole as the pin shrinks in size. If the need is simply that all parts that mate are to be accepted, then the MMC principle may be employed without endangering functionality.

Figures 1.9-1.11 show a hole whose position is specified with respect to two orthogonal surfaces parallel to the hole axis. The centre may lie anywhere within a squared tolerance zone, the sides of which are equal to each tolerances. Thus the total variation along either diagonal of the square allowed by the coordinate method of dimensioning will be 1.4

times greater than the indicated tolerance. Hence, a 0.28-diameter tolerance zone would increase the squared tolerance zone by 54% while guaranteeing the same level of functionality.

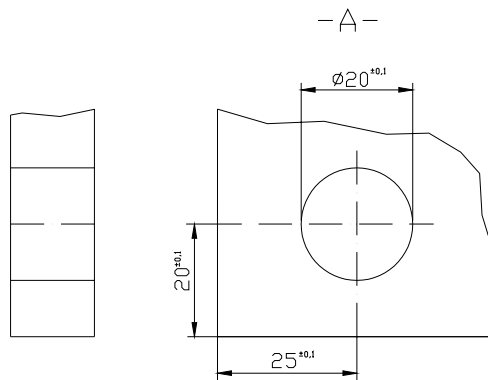


Fig. 1.9. The variation of the hole position is constrained by coordinate tolerancing

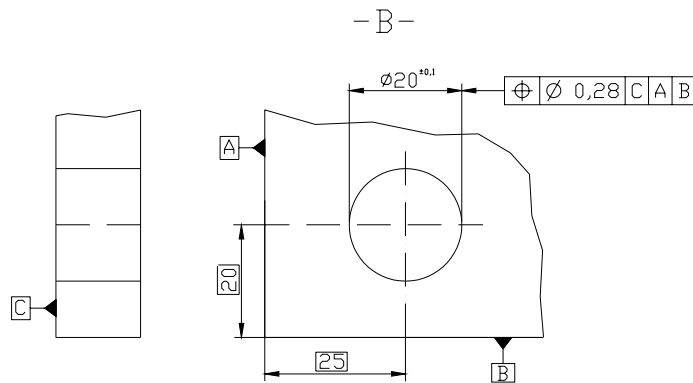


Fig. 1.10. The variation of the hole position is constrained by geometric tolerancing

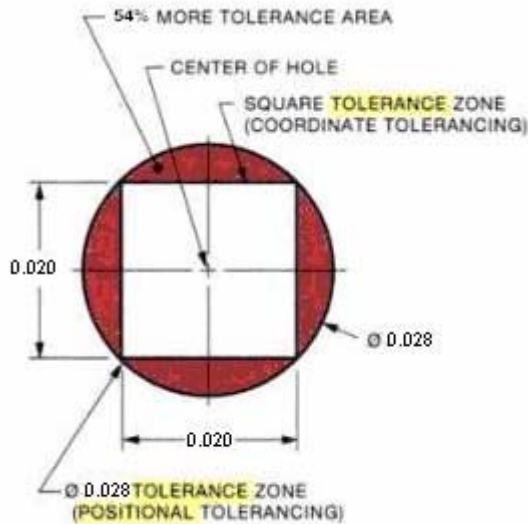


Fig. 1.11. Relationship between the tolerance zone in the two tolerancing systems.

1.4.3. Least Material Condition

Least material condition is the condition of a feature wherein the feature contains the least material. It is often thought of as the lightest feature. It is the largest hole or the smallest shaft. The definition for least material condition is in many ways an opposite of maximum material condition. ANSI Y14.5 lists it as “the condition in which a feature of size contains the least amount of material within the stated limits of size: for example, maximum hole diameter, minimum shaft diameter”.

So, instead of a shaft or tab or other external feature being at its largest size as with maximum material condition, least material condition (LMC) is when that external feature is at its smallest size (having the least material) within its size limits. For example, a shaft with size limits of $\varnothing 0.500 - 0.510$ is at its LMC when it measures $\varnothing 0.500$. An internal feature, however, like a hole or keyway, is at its least material condition when it is at its largest size. For example, a hole with size limits of $\varnothing 0.750 - 0.760$ will be at its least material condition when produced at $\varnothing 0.760$.

In feature control frames, the LMC concept (circled L) is usually used for features when the preservation of material is of great importance and cost is a significant factor. It is used when wall thickness is thought to be

endangered and the holes stand a chance of approaching a breakout condition. It is also used on casting drawings to assure that in subsequent machining operations enough material is available to allow a machine cut to clean up the part surface. It is capable of alleviating the machinist's frustration of starting out machining material and ending up machining nothing but air. Since wall thickness, instead of mating, is of major concern, if a hole is made smaller and a shaft made bigger, a greater position tolerance can be allowed. This additional geometric tolerance, based on size departure from least material condition, is often termed "bonus tolerance" (see §1.4.5.). It allows more parts to pass the inspection procedure based on functional requirements than if the feature had been controlled on a regardless of feature size basis.

1.4.4. Regardless of Feature Size

The regardless of feature size concept (RFS) is used and its symbol implied when the geometric tolerance is to remain the same no matter what size hole or shaft is produced within its limits of size. The geometric tolerance never changes with the size of the feature it controls. The size of the feature must be met and the geometric tolerance must be met as separately verifiable requirements.

The RFS concept is often used where balance is important: for example, on parts that rotate. Spinning parts could be functionally endangered if tolerance of location, such as centring, were allowed to vary with the size of the feature. If function must be preserved in such a way as to have mating features assemble in a specific way, such as a pin more in the centre of a mating hole than the MMC symbol would maintain (since the MMC symbol allows the hole to move out of its perfect position more as the hole grows and the shaft to move out of its perfect position more as the shaft shrinks), then the regardless of feature size concept should be used. Where the MMC symbol (if used after datum features of size) allows a shift of feature patterns making it necessary to shift a part's weight off centre of the datum axis to assemble the mating parts, the RFS concept (if used after datum features of size) allows no pattern shift as the datum feature departs from its MMC. This means that the only parts the inspector can accept are parts that can, at least, be assembled on centre. Although it does not assure that the parts will be assembled on centre in a balanced condition, it does assure that the parts accepted for assembly can be assembled on centre or pushed back to centre. This makes any balancing procedures that are subsequently attempted easier.

It is also worth noting that the use of the RFS concept protects the same worst mating boundary as does the MMC concept and the same worst sweep boundary for wall thicknesses and material preservation as the MMC concept.

The RFS concept would protect the minimum wall thicknesses as well as the LMC concept if two other rules did not interfere. One rule is that with the RFS concept there is no envelope of perfect form required at LMC, but there is one required at MMC. The second rule is that position controls applied at RFS are inspected by verifying the location of the axes or centreplanes of their mating size. For example, a gage pin of the maximum inscribed cylinder generates an axis that must reside within the tolerance zone for a hole that is positioned.

1.4.5. Bonus tolerance and datum shift

Tolerance bonus is an additional tolerance for a geometric control. Whenever a geometric tolerance is applied to a feature of size and a MMC (or LMC) modifier is inserted in the geometric tolerance control frame, a bonus tolerance is allowed. When the MMC modifier is used, the stated tolerance is intended to apply when the features of size is at the maximum material condition. When the actual size of the feature departs from MMC (towards LMC), an increase in the stated tolerance (equal to the amount of the departure) is permitted. This additional tolerance is the tolerance bonus. Figure 1.12. shows how the bonus is calculated when the MMC modifier applies.

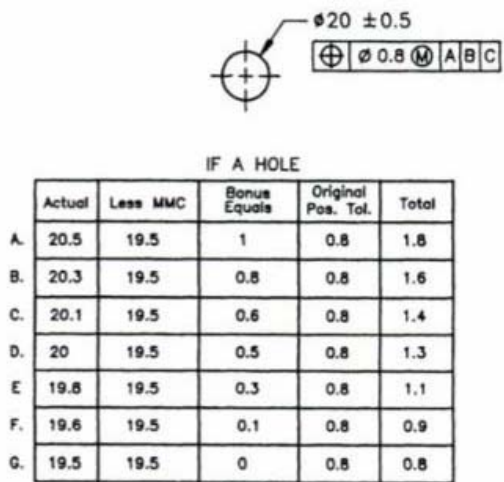


Fig. 1.12. Procedure for tolerance bonus calculation.

Whenever a datum is a feature of size and it is referenced at MMC in the tolerance control frame of a feature, an additional tolerance increase may apply to the feature if the datum departs from MMC. This variable additional tolerance is the datum shift. Its name derives from the consideration of the physical gage which would be used for controlling the tolerance applied to the feature. In fact, in the physical gage, the element that simulates the perfect feature counterpart of the datum is fixed in size but the actual datum feature of size may vary within its size limits. Therefore, there may be some looseness between the part and the gage. Datum shift is the allowable movement or looseness between the part datum feature and the gage.

Figure 1.13 shows an example of datum shift. When a datum feature is at MMC, there is no datum shift allowed. As the actual mating envelope of the datum feature departs from MMC towards LMC, a datum shift becomes available. The amount of datum shift is equal to the amount the datum feature departure from MMC. The maximum amount of datum shift possible is equal to the difference between the gage size and the LMC of the datum feature. The chart in Figure 1.14 shows the amount of datum shift for various datum feature sizes.

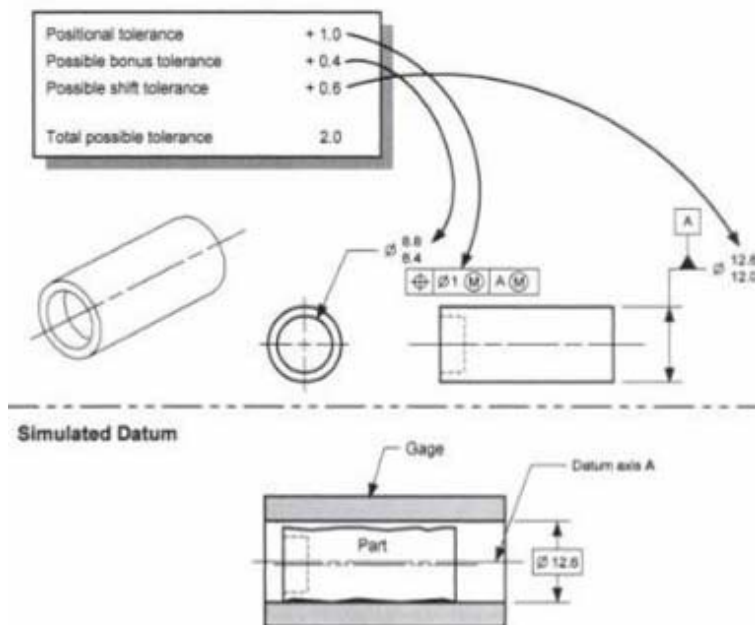


Fig.1.13. Example of datum shift.

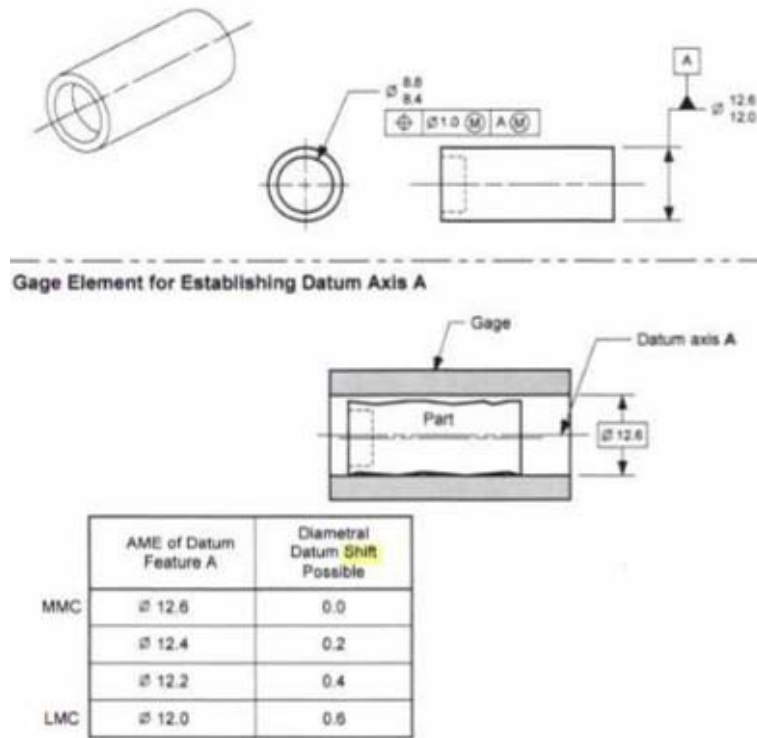


Fig. 1.14. Datum shift.

1.5. Position tolerances

1.5.1. Definition of position tolerance zone

A position tolerance can be explained in terms of a zone within which the resolved geometry (centre point, axis, or centre plane) of a feature of size is permitted to vary from true (theoretically exact) position. Basic dimensions establish the true position from specified datum features and between interrelated features.

A position tolerance applied on an MMC basis may be explained in either of the following ways:

- in terms of the surface of a hole (Surface of a Feature Interpretation). While maintaining the specified size limits of the hole, no element of the hole surface shall be inside a theoretical

boundary having a diameter equal to the minimum limit of size (MMC) minus the position tolerance located at true position.

- in terms of the axis of the hole (Resolved Geometry Interpretation). Where a hole is at MMC (minimum diameter), its axis must fall within a cylindrical tolerance zone whose axis is located at true position. The diameter of this zone is equal to the position tolerance. This tolerance zone also defines the limits of variation in the attitude of the axis of the hole in relation to the datum surface. It is only when the feature is at MMC that the specified position tolerance applies. Where the actual size of the feature is larger than MMC, additional or bonus position tolerance results. This increase of position tolerance is equal to the difference between the specified maximum material limit of size (MMC) and the actual size of the feature.

The problems of tolerancing for the position of holes are simplified when position tolerancing is applied on an MMC basis. Position tolerancing simplifies measuring procedures of functional GO gages.

1.5.2. Surface of a Feature Interpretation

For a pattern of features of size, a position tolerance specifies that the surface of each actual feature must not violate the boundary of a corresponding position tolerance zone. Each boundary is a sphere, cylinder, or pair of parallel planes of size equal to the collective effect of the limits of size, material condition basis, and applicable position tolerance t_0 . Each boundary is located and oriented by the basic dimensions of the pattern. Each position tolerance zone (see Fig. 1.15) is a volume defined by all points P that satisfy the appropriate equation from Table 1.3, where b_0' is a position tolerance zone size parameter (radius or half-width) individuated as indicated in Table 1.4. Notice that "0" subscript, indicate that it is expressed in reference to nominal tolerance t_0

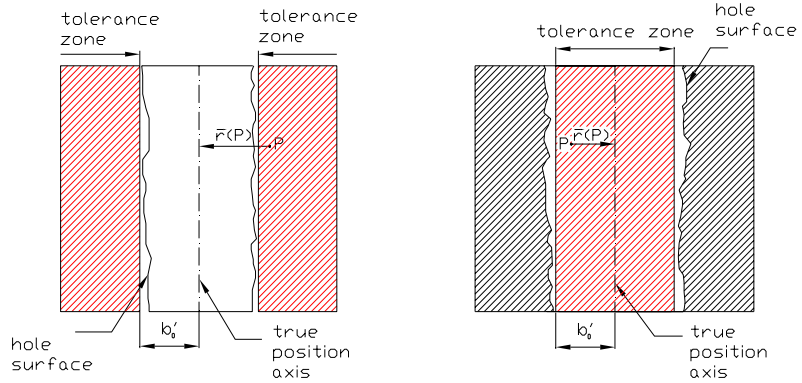


Fig. 1.15. Tolerance zone for a cylindrical hole at MMC or RFS, or a shaft at LMC definition

Table 1.3. Size of position tolerance zone, surface interpretation

Feature type	MMC o RFS	LMC
Internal (hole)	$\bar{r}(P) < b_0'$	$\bar{r}(P) > b_0'$
External (shaft)	$\bar{r}(P) > b_0'$	$\bar{r}(P) < b_0'$

Table 1.4. b_0' parameter definition

Feature type	MMC	RFS	LMC
Internal (hole)	$b_0' = r_{mmc} - \frac{t_0}{2}$	$b_0' = r_{am} - \frac{t_0}{2}$	$b_0' = r_{lmc} + \frac{t_0}{2}$
External (shaft)	$b_0' = r_{mmc} + \frac{t_0}{2}$	$b_0' = r_{am} + \frac{t_0}{2}$	$b_0' = r_{lmc} - \frac{t_0}{2}$

Where

- t_0 position tolerance applied at nominal feature;
- r_{mmc} feature radius at MMC;
- r_{lmc} feature radius at LMC;
- r_{am} actual mating radius.

A feature conforms to a position tolerance t_0 , at a specified material condition basis if all points of the feature lie outside some position zone as defined above with b_0' determined by the appropriate value from

Table 1.4. The surface must conform to the applicable size limits. In the case of an internal feature (spherical hollow, hole, or slot), there is a further condition that the feature must surround the tolerance zone. For MMC or LMC material condition basis, the boundary defined by $r(P)=b_0'$, with b_0 function of r_{mmc} or r_{lmc} and of t_0 , is called the virtual condition.

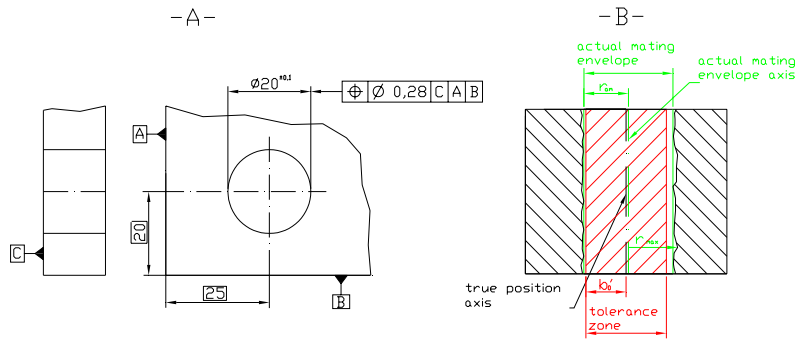


Fig. 1.16. At RFS condition; A) feature, B) feature (hole) conforms to a position tolerance if all points of the feature lie outside position zone defined by cylinder of radius b_0' and if surface conform to the applicable size limits:

$$2r_{am} > (\text{nominal diameter} - \text{size limit}) = 2r_{mmc}$$

$$2r_{max} < (\text{nominal diameter} + \text{size limit}) = 2r_{lmc}$$

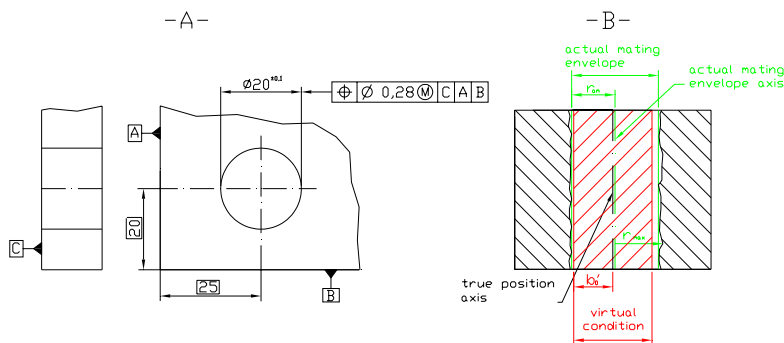


Fig. 1.17. At MMC condition; A) feature, B) feature (hole) conforms to a position tolerance if all points of the feature lie outside position zone (virtual condition envelope) defined by cylinder of radius b_0' and if surface conform to the applicable size limits:

$$2r_{am} > (\text{nominal diameter} - \text{size limit}) = 2r_{mmc}$$

$$2r_{max} < (\text{nominal diameter} + \text{size limit}) = 2r_{lmc}$$

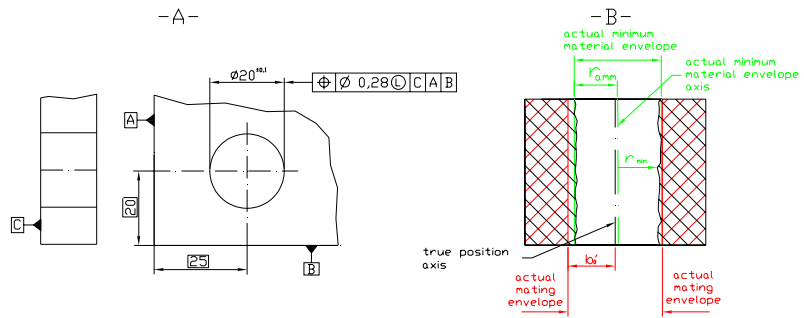


Fig. 1.18. At LMC condition; A) feature, B) feature (hole) conforms to a position tolerance if all points of the feature lie outside position zone (virtual condition envelope) defined by cylinder of radius b_0' and if surface conform to the applicable size limits:

$$2r_{am} > (\text{nominal diameter} - \text{size limit}) = 2r_{mmc}$$

$$2r_{max} < (\text{nominal diameter} + \text{size limit}) = 2r_{lm}$$

The actual value of position deviation t is the smallest value of t to which the feature conforms. For LMC and MMC controls the actual value of deviation can be negative. A negative actual value can be interpreted as the unused portion of the bonus tolerance resulting from the departure of the feature from the applicable limit of size.

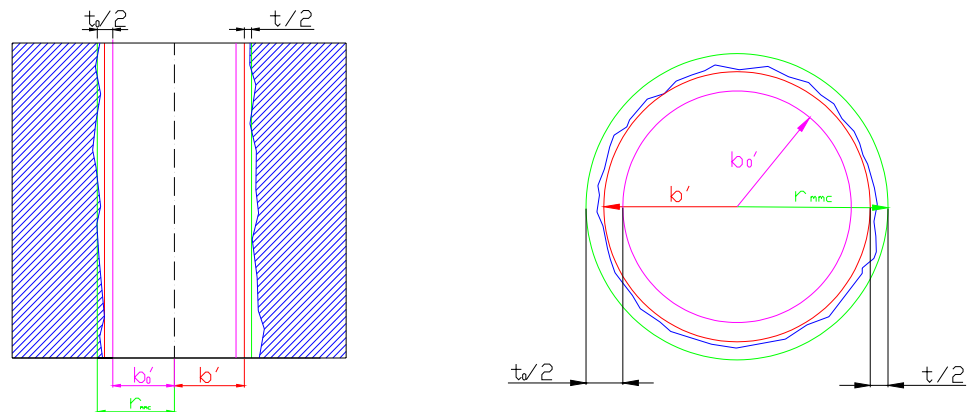


Fig. 1.19. Actual value t for a hole at MMC and surface interpretation

1.5.3. In terms of the Resolved Geometry of a Feature.

For features within a pattern, a position tolerance specifies that the resolved geometry (centre point, axis, or centre plane, as applicable) of each actual mating envelope (for features at MMC or RFS) or actual

minimum material envelope (for features at LMC) must lie within a corresponding position tolerance zone. Each zone is bounded by a sphere, cylinder, or pair of parallel planes of size equal to the total allowable tolerance for the corresponding feature. Each zone is located and oriented by the basic dimensions of the pattern. A position tolerance zone is a spherical, cylindrical, or parallelplane volume defined by all points P that satisfy the equation 1.1.

$$\bar{r}(P) \leq b_0 \quad (1.1)$$

where b_0 is the radius or half-width of the tolerance zone t_0 . The feature axis extends for the full length of the feature. Radius or half-width b_0 is expressed as shown in Table 1.6.

Table 1.5. Size of position tolerance zone, resolved geometry interpretation

Feature type	MMC	RFS	LMC
Internal (hole)	$b_0 = (r_{am} - r_{mmc}) + \frac{t_0}{2}$	$b_0 = \frac{t_0}{2}$	$b_0 = (r_{lmc} - r_{am}) + \frac{t_0}{2}$
External (shaft)	$b_0 = (r_{mmc} - r_{am}) + \frac{t_0}{2}$	$b_0 = \frac{t_0}{2}$	$b_0 = (r_{am} - r_{lmc}) + \frac{t_0}{2}$

Where

- t_0 position tolerance applied at nominal feature;
- r_{mmc} feature radius at MMC;
- r_{lmc} feature radius at LMC;
- r_{am} actual mating at minimum material radius.

Notice that tolerance zone radius b_0 is individuated by the radius of geometrical tolerance applied to the basic dimension of features, to which a bonus is added in case of MMC or LMC conditions.

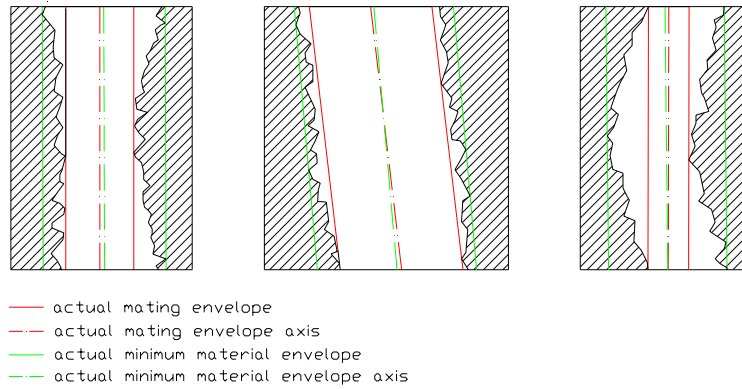


Fig. 1.20. Actual mating envelope (MMC and RFS) and envelope at real minimum material (LMC) with their axis

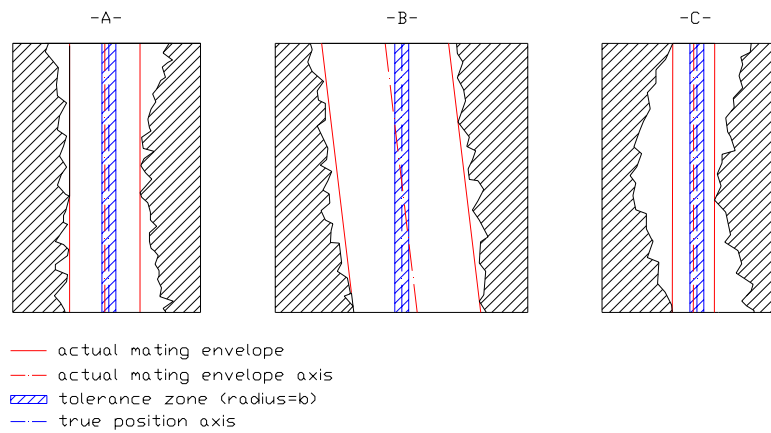


Fig. 1.21. Tolerance zone and conformance for holes with actual mating envelope (MMC or RFS). A and C holes conforms to tolerance, while B does not

A feature conforms to a position tolerance t_0 at a specified material condition basis if all points of the resolved geometry of the applicable envelope (as determined by the material condition basis) lie within some position zone as defined above with b_0 determined by the appropriate formula. Furthermore, the surface must conform to the applicable size limits. All points P must satisfy the equation of the tolerance zone.

$$\bar{r}(P) \leq b_0 \tag{1.2}$$

where b_0 is the radius or half-width of the tolerance zone.

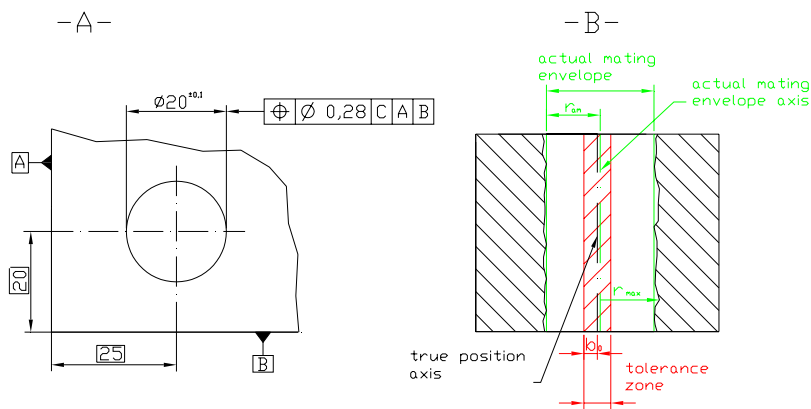


Fig. 1.22. At RFS condition; A) feature, B) feature (hole) conforms to a position tolerance if all points of the feature lie outside position tolerance zone defined by cylinder of radius b_0' and if the surface conform to the applicable size limits:

$$2r_{am} > (\text{nominal diameter} - \text{size limit}) = 2r_{mmc}$$

$$2r_{max} < (\text{nominal diameter} + \text{size limit}) = 2r_{imc}$$

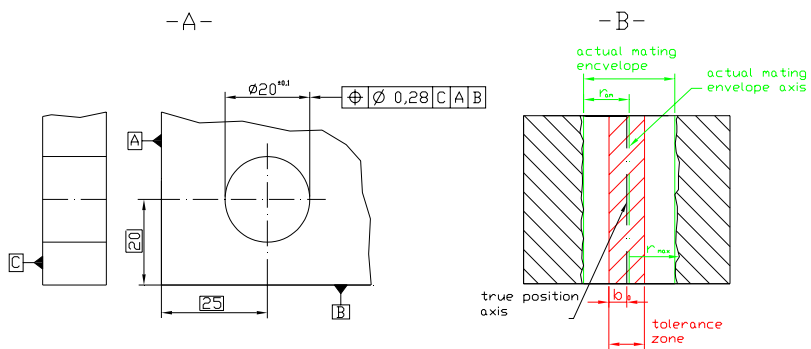


Fig. 1.23. At MMC condition; A) feature, B) feature (hole) conforms to a position tolerance if all points of the feature lie outside position tolerance zone (virtual condition envelope) defined by cylinder of radius b_0' and if the surface conform to the applicable size limits:

$$2r_{am} > (\text{nominal diameter} - \text{size limit}) = 2r_{mmc}$$

$$2r_{max} < (\text{nominal diameter} + \text{size limit}) = 2r_{imc}$$

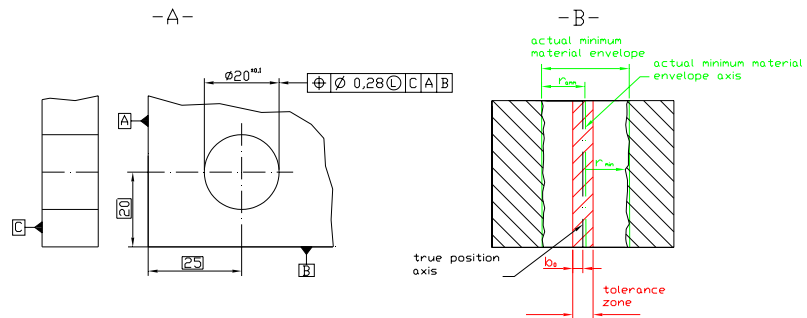


Fig. 1.24. At LMC condition; A) feature, B) feature (hole) conforms to a position tolerance if all points of the feature lie outside position tolerance zone (virtual condition envelope) defined by cylinder of radius b_0 and if the surface conforms to the applicable size limits:

$$2r_{am} > (\text{nominal diameter} - \text{size limit}) = 2r_{mmc}$$

$$2r_{max} < (\text{nominal diameter} + \text{size limit } e) = 2r_{lm}$$

The position deviation t of a feature is the diameter of the smallest tolerance zone (smallest value of b) which contains the centre point or all points on the axis or centre plane (within the extent of the feature) of the applicable actual envelope of the feature.

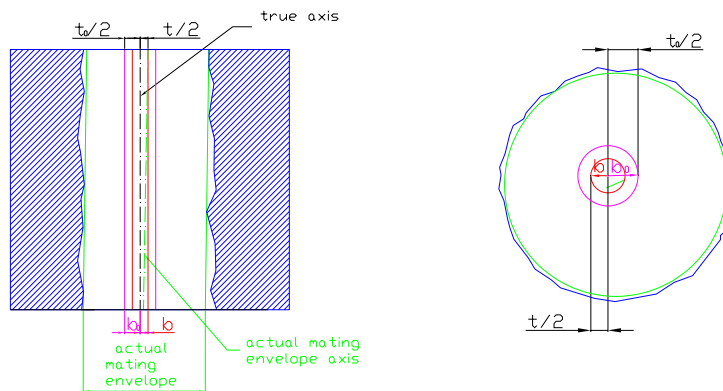


Fig. 1.25. Actual value of tolerance zone t for a hole at RFS at resolved geometry interpretation

1.6. Flatness of a surface

Flatness of a surface is a condition in which all surface elements are in one plane. A flatness tolerance is applied to a line representing the

surface of a part by means of a feature control frame (Fig. 1.26).

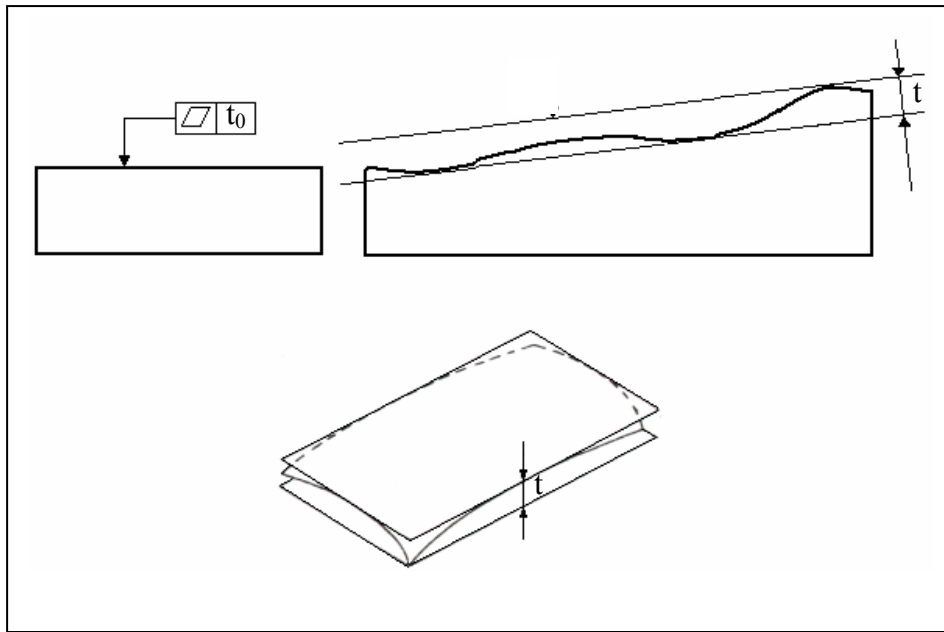


Fig. 1.26. Specifying flatness for a surface

A flatness tolerance means that all points on the surface shall be contained within a tolerance zone consisting of the space between two parallel planes that are separated by the specified tolerance t_0 .

A flatness zone is a volume consisting of all points P satisfying the condition:

$$|\hat{T} \cdot (\vec{P} - \vec{A})| \leq \frac{t}{2} \quad (1.3)$$

where

\hat{T} is the unit direction vector normal to the parallel planes defining the flatness zone

\vec{A} is a position vector locating the mid-plane of the flatness zone

$(\vec{P} - \vec{A})$ is the vector distance from the mid-plane of the flatness zone to any point P

t is the size of the flatness zone (the separation of the parallel planes)

These two parallel planes must lie within the limits of size. These planes may be oriented in any manner to contain the surface; that is, they are not necessarily parallel to the base. The flatness tolerance must be less than the size tolerance and be contained within the limits of size, in other words “a feature conforms to a flatness tolerance to if all points of the feature lie within some flatness zone as defined above, with $t = t_0$. That is, there exist \hat{T} and \bar{A} such that with $t = t_0$, all points of the feature are within the flatness zone. Notice that t is the actual value of flatness for a surface, that is the smallest flatness tolerance to which the surface will conform.

Typical applications of the flatness requirement are for real surfaces, mating surfaces and/or to establish quality datum surfaces. Flatness cannot be verified with functional gages. Flatness must be measured using various setups and instrumentation. The feature can be measured using jackscrews or a wobble plates. Placing a component directly on a surface plate typically results in establishing an unintended datum and will not yield an accurate flatness determination. Flatness can also be verified with optical methods incorporating the use of an optical flat or interferometer. In this work a methodology to verifies flatness by CMM is proposed.

REFERENCES CHAPTER 1

- AMERICAN SOCIETY OF MECHANICAL ENGINEERS, 1995a, "Dimensioning and tolerancing", ASME Y14.5M-1994.
- AMERICAN SOCIETY OF MECHANICAL ENGINEERS, 1995b, "Mathematical definition of dimensioning and tolerancing principles", ASME Y14.5.1M-1994.
- JENSEN, C. H., 2002, "Interpreting Engineering Drawings", (Thomson Delmar Learning).
- MEADOWS, J. D., 1995, "Geometric Dimensioning and Tolerancing: Applications and Techniques for Use in Design", (CRC Press).
- PUNCOCHAR, D. E., 1997, "Interpretation of Geometric Dimensioning and Tolerancing", (Industrial Press).
- ZHANG, H.C., 1997, "Advanced Tolerancing Techniques", (Wiley-Interscience).

2. COORDINATE MEASURING MACHINES

A coordinate measuring machine (CMM) is a computer-controlled device that uses a probe to obtain measurements on a manufactured part's surface, usually one point at a time. Probe movements may be programmed or determined manually by operation of a joystick. CMM's have gained tremendous popularity over hard gauges for dimensional measurement due to their flexibility, accuracy, and ease of automation. Problems arise in their use, however, because tolerancing standards require knowledge of the entire surface but a CMM measures only a few points on the surface.

2.1. Background

It is difficult to say when coordinate measuring machines emerged as a distinct class of instruments, but such metrology pioneers as C. E. Johansson and F. H. Rolt wrote about machines that could measure in three axes.

The Atomic Energy Commission on the 1940s may have been among the first organizations to recognize the potential of CMMs, and their machines kept pace with the explosion in computer technology. The theorists and technicians in the field were quick to recognize the potential and to publicize their accomplishments; unfortunately, the sophistication of CMMs (when compared with commonly used instruments) may have slowed their acceptance.

In the 1960s, CMM began to emerge as a powerful tool; then, as microprocessors became the power in computing, manufactures began to realize the real potential of CMM systems. The combination of the CMM and the computer's ability to process data allows us to apply these measurement systems in the most appropriate and effective ways.

2.2. The role of coordinate measuring machines

Coordinate measuring machines play an important role in a large number of industries, including aerospace, automotive, electronics, food processing, health care, paper, pharmaceuticals, plastics, research and development, and semiconductor.

The ability to quickly and accurately capture and evaluate dimensional data distinguishes the CMM from other types of measurement processes. Sophisticated contact and noncontact sensor, combined with vast computer processing capabilities, make the CMM a practical, cost-

effective solution. CMMs are especially suited for parts with complex geometry and assemblies (Fig. 2.1).



Fig. 2.1. One of most CMM applications

CMMs are particularly suited for the following conditions:

1. Short runs – We may be producing hundreds or even thousands of a part, but the production run is not sufficient to justify the cost of production inspection tooling.
2. Multiple features – When we have a number of features (both dimensional and geometric) to control, CMM is the instrument that makes control easy and economical.
3. Flexibility – Because we can choose the application of the CMM system, we can also do short runs and measure multiple features.
4. High unit cost – Because reworking or scrapping is costly, CMM systems significantly increase the production of acceptable parts.
5. Production interruption – Whenever you have to inspect and pass one part before you can start machining on the next part, a machining center may actually be able to help a manufacturer save more money by reducing down time than would be saved by inspection.

By CMMs, inspection time can be reduced on the order of 80% to 90%; that is reason why manufacture (as well as trade publications and professional journals) are enthusiastic about CMM systems.

2.3. Types of coordinate measuring machines

The basic CMM has three perpendicular axes: x, y and z. Each axis is fitted with precision scale, measuring device, or transducer that continually records the displacement of each carriage a fixed reference. These displacement data are submitted to an indicator or computer for further processing. The carriage on the third axis carries a probe. When the probe comes in contact with a point on a part feature, it reads the displacement for all three axes.

The physical configurations of CMMs vary widely, but they all provide a way to move a probe in three axes with respect to a workpiece. The space that we can contain in the limits of travel in all three axes is known as the *work envelope*. The work envelope does not necessarily limit the size of the workpiece; in many situations, some portions of the workpiece may be outside of the envelope, if the workpiece is adequately supported.

Although 10 configurations are covered by CMM Performance Standard ANSI/ASME B89.1.12M-1990 (Methods for Performance Evaluation of Coordinate Measuring Machines), there are 5 basic configurations that are used most frequently: cantilever, bridge, column, horizontal arm and gantry, see following figures.

2.3.1. Cantilever type

In the cantilever type CMM, a vertical probe moves in the z axis, carried by a cantilevered arm that moves in the y axis. This arm also moves laterally through the x axis. You have easy access to the work area, and the cantilever CMM provides a relatively large envelope without taking up too much floor space.



Fig. 2.2. Cantilever type CMM

2.3.2. Bridge type

The most popular type of CMM, this machine has a moving bridge. It is similar to the cantilever type, because it has a support for the outer ends of the y axis beam on the base.

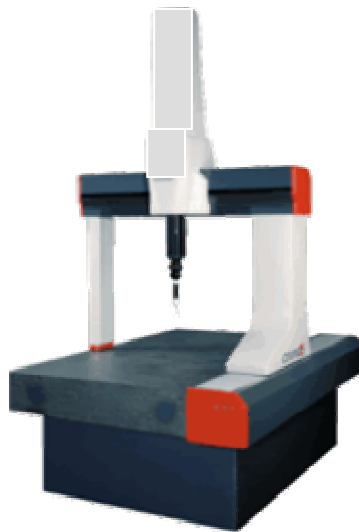


Fig. 2.3. Bridge type CMM

The bridge construction adds rigidity to the machine, but also forces us to make sure that both ends of the y axis track at exactly the same rate. Loading the bridge CMM can be difficult because the bridge has two legs that both touch the base.

In a variation of the bridge CMM, the *fixed bridge* type, the bridge is fixed to the base. This setup eliminates potential tracking problems of the standard bridge CMM, providing superior accuracy and making it useful for gage room applications and production inspection.

2.3.3. Column type

This CMM's construction is similar to the most popular type of jig borer and is often referred to as a *universal measuring machine*, instead of a CMM. The column type CMM's construction provides exceptional rigidity and accuracy, and these machines are usually reserved for gage rooms rather than inspection.



Fig. 2.4. Column type CMM

2.3.4. Horizontal arm type

Unlike the previous machines, the basic horizontal arm type CMM (also referred to as a layout machine) has a moving arm, and the probe is carried along the y axis. This machine's main advantage is that it provides a large, unobstructed work area, which makes it perfect for very

large workpieces like automotive dies. In one variation, called a *fixed arm type*, the probe is fixed to the y axis, and you use a moving work table for the y axis. Manufacturers produce this type of CMM in which both the arm and table move less frequently.



Fig. 2.5. Horizontal arm type CMM

2.3.5. Gantry type

In this type, the support of the workpiece is independent of the x and y axes, both of which are overhead, supported by four vertical columns rising from the floor. This setup allows you to walk along the workpiece with the probe, which is helpful for extremely large pieces.



Fig. 2.6. Gantry type CMM

2.4. Modes of operation

Although there are nearly as many modes of operations as there are CMMs, they can be divided into general categories:

1. Manual
2. Manual computer assisted
3. Motorized computer assisted
4. Direct computer controlled (DCC)

We will use the computer to include computers, microprocessor, and programmable for our discussion.

A manual mode CMM has a free-floating probe that the operator can move along the machine's three axis to establish contact with the part feature it is assessing. The differences among the contact positions are the measurements.

In the manual computer assisted mode, electronic digital displays for these machines are added, making zero setting; changing the sign; converting among inch, decimal-inch, and SI; and printing out data easy and practical. Even without further sophistication, these features save times, minimize calculations, and reduce errors.

A motorized CMM uses a joystick to drive the machine axes, The operator manipulates the joystick to bring the probe sensor into contact with the workpiece.

A direct computer controlled (DCC) coordinate measuring is fully programmable. The CMM uses "taught" locations of CAD data to determine where the probe sensor contacts the workpiece, collecting measurement data. The fully automated CMM allows the operator to place the workpiece in a fixture or on the worktable, run a stored program, collect the data points, and generate an output report. Measurement reports can be saved in the computer to compile a historical record for Statistical Process Control.

2.5. Type of probes

All CMMs consist of a probe and a way to move it along three axes relative to a workpiece. For CMMs, we use the term probe, because early CMMs only provided a solid member to contact the workpiece much as other displacement instruments (vernier calliper or micrometer calliper) did. In a sense, a CMM is three of these instruments placed in an orthogonal array.

The probe is at the heart of the CMM operation, referred to the sensing elements as a “head”. A variety of probe types and designs are available today. CMM users need to understand and distinguish among these various probes in order to select the probe that best meets the application requirements.

Probes fall into two general categories: contact and noncontact. Contact probes are the most common type of probe used on CMMs, contact probes can include touch-trigger probes and analog scanning probes, which maintain contact with the part as they scan along the surface of the part as they measure. Noncontact probes include laser probes and video probes.

Touch probes, as indicated by the name, work by making contact with the workpiece. As the sensor makes contact with the part, the difference in contact resistance indicates that the probe has been deflected. The computer records this contact point coordinate space. An LED light and an audible signal usually indicate contact, see Figure 2.7.



Fig. 2.7. Contact probe

Analog scanning probes are a type of contact probe used to measure contoured surfaces, such as a turbine blade. The analog scanning probe remains in contact with the surface of the part as it moves, and produces analog readings rather than digital signals. Form measurement makes it necessary to collect analyze large amounts of data quickly. Continuous analog scanning system can acquire 10 to 50 times more data than a

traditional touch-trigger probe in a given amount of time.

Analog probes improve the speed and accuracy at which measurement data are collected, particularly for surface mapping complex part shapes. They are often used for measurements of parts where the surface geometry is complex or irregular, such as a crankshaft or prosthetic device. Scanning probes are commonly used to gather data for reverse engineering applications.

One of the limitations of touch-trigger probes is the forces required (a gram or more) to deflect the probe when it makes contact with the part. Measuring flexible or fragile parts can be difficult at best. Soft plastic, rubber, thin wire, or other flexible components can be distorted or damaged by the contact of a touch-trigger probe. Although noncontact probes are the most common solution, low-trigger-force, high-sensitivity-touch probes also are available,



Fig. 2.8. Touch-trigger probes

Advances in technology have made it possible to develop a new type of touch probe that use a high-frequency stylus with a trigger force of less than 10 milligrams to detect touch. The probe body contains a crystal that creates a vibration in the stylus. The probe resonates at 20 to 25 kilohertz. When the stylus makes contact with the part, the motion (vibration) changes. This change is detected by a microprocessor in the electronics box, which records this change as a touch. This touch registers as a data point before part deflection or damage occurs. The vibration in this probe

also eliminates another common problem with low-force touch-trigger probes – “false triggers”. False triggers occur when the machine movement, vibration, or acceleration causes a low trigger force probe to deflect, recording a false measurement point. The vibration in the new touch probe is not affected by changes in machine speed or movement.

Touch probe assemblies consist of three components: probe head, probe, and stylus. This simplest touch probe assemblies are sensitive in the x and y axes, and because these probes record movement in either direction on each axis, we call them *four-way probes*. When we use a probe that has one-way response in the z axis, we call the assembly a five-way probe; and when we use a plus-minus along the z axis, we have a six-way probe, all of which have a built-in provision for overtravel.

The probe head is mounted on the end of one of the CMM’s moving axes. Extensions are commonly added to the probe head for extended reach or positioning. The probe heads can be rotated manually or automatically.



Fig. 2.9. Touch trigger, probes, bodies and styli

The ability to rotate the probe allows the operator to measure features that are on a surface other than the top (xy) plane, eliminating the need to change the part setup. Automatic probe changer racks further enhance the CMM’s capabilities. The operator can select the best stylus for each type of measurement, then program a stylus change to occur automatically during the inspection routine, the correct stylus can increase measurement accuracy. Automating this process saves time.



Fig. 2.10. Automatic probe change rack

2.6. Probe calibration

When we measure in a sequence that progresses in the same direction, result is more inherently reliable than if we make a sequence of measurements that change direction. One of the benefits of a CMM is that we can reverse directions without backlash, hysteresis, and other errors that destroy accuracy. Deflection of the probe is still a problem, but consistent calibration of the probe against a master standard by one of several methods helps keep this problem in check.



Fig. 2.11. Ball Bar with probe

Probe calibration determines the effective working diameter of stylus, which compensates for probe design. Measurement accuracy depends on careful calibration of the probe stylus. The probe stylus is used to measure a very accurate sphere to determine the probe tip's center and radius. When the probe contacts the workpiece, the coordinates of the tip are mathematically offset by the tip's radius. This calculation is performed automatically through the CMM's software.

The accuracy of a measurement with a touch probe also depends on using good probing techniques; an effective probing techniques eliminate many common causes of measurement error.

2.7. Metrological features

CMM manufacturers claim repeatability to or in excess of $+2.54\ \mu\text{m}$ and accuracy of $+10.16\ \mu\text{m}$; however, these values decrease as the size of the CMM increases. These exceptional repeatability and accuracy capabilities might be surprising, considering that the concept of coordinate measuring machine is in no way based in the principles of metrology. Designers and manufacturers take care that their machines, through their function, fulfil the fundamental principles, however, and features like system rigidity and the capability of the probe system make their success possible.

CMMs reduce computational errors, but this reduction must be balanced with any errors that we might find in the programming. Still, it is hard to beat the advantages of a CMM. A manual measurement add systematic error because of the method it is used, even though not even it is easy recognize the errors are there. With the CMM, procedure may be checked without the workpiece, which will reveal errors before the actual measurements are made.

CMMs probably do not diminish thermal errors by being good heat sinks; in fact, they may add thermal errors because their mechanical operations generate heat. CMMs also use a great deal of granite, which is a poor conductor of heat; although it takes a time to warm up, granite also does not release the heat build-up quickly.

CMM structure and part measurement can be affected by thermal expansion (the amount of change in a part due to variations in temperature). Thermal expansion can be used by seasonal temperature changes or by day-to-day factors, such as sunlight, heating and cooling ducts, and the operation of nearby machining operations that produce heat. Because of this, conventional practice has been to limit the use of a

CMM to a temperature- and humidity- controlled environment.

Manufacturing demands for higher quality and faster throughput have resulted in a desire for inspection equipment that works on the shop floor. CMM manufacturers are addressing this need by using construction materials with a low coefficient of expansion and integrating temperature sensors in critical locations.

One material with a low coefficient of expansion that is being incorporated by manufacturers is a nickel alloy material called Invar, a composite of 64% iron and 36% nickel. Invar was developed by Swiss physicist Charles Edouard Guillaume in 1896 to improve the accuracy of precision clocks.

Invar can be combined with the use of thermal expansion sensors to create a CMM that is stable and contracts uniformly for use on the shop floor. This is similar to the process used by civil engineers to compensate for the expansion and contraction of bridges. Transducers measure the growth of the axes due to temperature changes. The sensors measure the growth in microns, and feed back this information to the controller several times a minute. The mathematical algorithms can then compensate for these temperature changes, as they occur.

Similarly, you need to be concerned about vibration. Instead of damping vibrations, some CMMs may be receptive to them.

Coordinate measuring machines do not adhere to Abbe's law because the standard is never in line with the line of measurement; in fact, the standard is often far more removed the line of measurement than it would be with conventional measurement instruments. The essential difference between using conventional instruments and a CMM is that you are responsible for making sure that line of measurement is precisely parallel to the axis of the standard when you are using a conventional instrument. In contrast, this alignment is built into the CMM.

REFERENCES CHAPTER 2

AMERICAN SOCIETY OF MECHANICAL ENGINEERS, 1990, "Methods for Performance Evaluation of Coordinate Measuring Machines", ANSI/ASME B89.1.12M-1990.

HARLOW, R. H., DOTSON, C., 2003, "Fundamentals of Dimensional Metrology", (Delmar Thomson Learning).

3. UNCERTAINTY IN CMM MEASUREMENTS

A correct statement of the uncertainty is becoming increasingly important as more and more companies strive to maintain traceability in accordance with ISO 9000 (and begin to comply with the GPS series of standards. In particular, ISO 14253-1 (1998) states that a proper uncertainty statement is necessary in order to conclude that products are within or outside of specification. The problem is compounded by the expanded outsourcing being used by large corporations and the increasing globalization of the world economy. As the number of production sources used to produce product subsystems increases the necessity for a well functioning and controlled measurement system expands dramatically. Interchangeability in the global marketplace requires traceability and a thorough estimation and understanding of uncertainty.

3.1. Definition of uncertainty in measurements

In general, the result of a measurement is only an approximation or estimate of the value of the specific quantity subject to measurement, that is the measurand, and thus the result is complete only when accompanied by a quantitative statement of its uncertainty. The uncertainty of the result of a measurement generally consists of several components, which may be grouped into two categories according to the method used to estimate their numerical values:

- type A components: those which are evaluated by statistical analysis of series of observations,
- type B components: those which are evaluated by other means.

According to the “Guidelines for Evaluating and Expressing the Uncertainty of NIST Measurement Results” [Barry N. Taylor and Chris E. Kuyatt, NIST Technical Note 1297, 1994], which in turn is based on the comprehensive International Organization for Standardization (ISO) “Guide to the Expression of Uncertainty in Measurement” [ISO, 1995], we can describe and calculate in a correct form the uncertainty of the result of a measurement by a process composed by 5 steps:

1. identify elements that have an influence on the equation expressing the measurand or on the measurement process;

2. examine their uncertainties u_i and classify them according to the type A or B, in other words calculate or obtain them from available sources;
3. add the two different kind of elements and after opportune simplifications, and obtain the composed uncertainty u_c ;
4. define a coverage factor and calculate the expanded uncertainty U ;
5. show the measurement result as the mean of the measurements $\pm U$.

3.1.1. The measurement equation

A case of interest is where the quantity Y being measured, the measurand, is not measured directly, but is determined from N other quantities X_1, X_2, \dots, X_N through a functional relation f , often called the measurement equation:

$$Y = f(X_1, X_2, \dots, X_N) \quad (3.1)$$

Included among the quantities X_i are corrections (or correction factors), as well as quantities that take into account other sources of variability, such as different observers, instruments, samples, laboratories, and times at which observations are made (e.g., different days). Thus, the function f of equation (3.1) should express not simply a physical law but a measurement process and, in particular, it should contain all quantities that can contribute a significant uncertainty to the measurement result.

An estimate of the measurand Y , denoted by y , is obtained from equation (3.1) using input estimates x_1, x_2, \dots, x_N for the values of the N input quantities X_1, X_2, \dots, X_N . Thus, the output estimate y , which is the result of the measurement, is given by

$$y = f(x_1, x_2, \dots, x_N). \quad (3.2)$$

The uncertainty of the measurement result y arises from the uncertainties $u(x_i)$ (or u_i for brevity) of the input estimates x_i that enter equation (3.2).

3.1.2. Representation of uncertainty components: standard uncertainty

Each component of uncertainty u_i , however evaluated, is represented by an estimated standard deviation, termed standard uncertainty and equal to the positive square root of the estimated variance.

An uncertainty component obtained by a type A evaluation is represented by a statistically estimated standard deviation s_i , equal to the positive square root of the statistically estimated variance s_i^2 , and the associated number of degrees of freedom v_i . hence $u_i = s_i$.

In a similar manner, an uncertainty component obtained by a type B evaluation is represented by a quantity u_j , which may be considered an approximation to the corresponding standard deviation; it is equal to the positive square root of u_j^2 , which may be considered an approximation to the corresponding variance and which is obtained from an assumed probability distribution based on all the available information. For such a component the standard uncertainty is simply u_j .

3.1.3. Evaluating uncertainty components

A Type A evaluation of standard uncertainty may be based on any valid statistical method for treating data. Examples are calculating the standard deviation of the mean of a series of independent observations; using the method of least squares to fit a curve to data in order to estimate the parameters of the curve and their standard deviations; and carrying out an analysis of variance (ANOVA) in order to identify and quantify random effects in certain kinds of measurements (method of variance components).

As an example of a Type A evaluation, consider an input quantity X_i whose value is estimated from n independent observations $X_{i,k}$ of X_i obtained under the same conditions of measurement. In this case, the input estimate x_i is usually the sample mean

$$x_i = \bar{X}_i = \frac{1}{n} \sum_{k=1}^n X_{i,k} \quad (3.3)$$

and the standard uncertainty $u(x_i)$ to be associated with x_i is the estimated standard deviation of the mean

$$u(x_i) = s(\bar{X}_i) = \sqrt{\frac{1}{n \cdot (n-1)} \cdot \sum_{k=1}^n (X_{i,k} - \bar{X}_i)^2} \quad (3.4)$$

A type B evaluation of standard uncertainty is usually based on scientific judgment using all of the relevant information available, which may include:

- previous measurement data,
- experience with, or general knowledge of, the behaviour and property of relevant materials and instruments,
- manufacturer's specifications,
- data provided in calibration and other reports, and
- uncertainties assigned to reference data taken from handbooks.

Broadly speaking, the uncertainty is either obtained from an outside source, or obtained from an assumed distribution.

3.1.4. Combining uncertainty components

The combined standard uncertainty of the measurement result y , designated by $u_c(y)$ and taken to represent the estimated standard deviation of the result, is the positive square root of the estimated variance $u_c^2(y)$ obtained from

$$u_c^2(y) = \sum_{i=1}^N \left(\frac{\partial f}{\partial x_i} \right)^2 u^2(x_i) + 2 \sum_{i=1}^{N-1} \sum_{j=i+1}^N \frac{\partial f}{\partial x_i} \frac{\partial f}{\partial x_j} u(x_i, x_j) \quad (3.5)$$

Equation (3.5) is based on a first-order Taylor series approximation of the measurement equation given in equation (3.1) and is conveniently referred to as the law of propagation of uncertainty. The partial derivatives of f with respect to the X_i (often referred to as sensitivity coefficients) are evaluated at $X_i = x_i$; $u(x_i)$ is the standard uncertainty associated with the input estimate x_i ; and $u(x_i, x_j)$ is the estimated covariance associated with x_i and x_j .

Equation (1.5) often reduces to a simple form in cases of practical interest. For example, if the input estimates x_i can be assumed to be uncorrelated, then the second term vanishes. Further, if the input estimates are uncorrelated and the measurement equation is for example in the following form, then equation (3.5) becomes simpler still.

Measurement equation: a product of quantities X_i , raised to powers a , b , ... p , multiplied by a constant A .

$$Y = A \cdot X_1^a \cdot X_2^b \cdot \dots X_N^p \quad (3.6)$$

Measurement result:

$$y = A \cdot x_1^a \cdot x_2^b \cdot \dots x_N^p \quad (3.7)$$

Combined standard uncertainty:

$$u_{c,r}^2(y) = a^2 u_r^2(x_1) + b^2 u_r^2(x_2) + \dots p^2 u_r^2(x_N) \quad (3.8)$$

Here $u_r(x_i)$ is the relative standard uncertainty of x_i and is defined by $u_r(x_i) = u(x_i)/|x_i|$, where $|x_i|$ is the absolute value of x_i and x_i is not equal to zero; and $u_{c,r}(y)$ is the relative combined standard uncertainty of y and is defined by $u_{c,r}(y) = u_c(y)/|y|$, where $|y|$ is the absolute value of y and y is not equal to zero.

3.1.5. Expanded uncertainty and coverage factor

Although the combined standard uncertainty u_c is used to express the uncertainty of many measurement results, for some commercial, industrial, and regulatory applications (e.g., when health and safety are concerned), what is often required is a measure of uncertainty that defines an interval about the measurement result y within which the value of the measurand Y can be confidently asserted to lie with a given probability. The measure of uncertainty intended to meet this requirement is termed expanded uncertainty, suggested symbol U , and is obtained by multiplying $u_c(y)$ by a coverage factor k ($U = k u_c(y)$). In general, the value of the coverage factor k is chosen on the basis of the desired level of confidence to be associated with the interval defined by U . Typically, k is in the range 2 to 3. When the normal distribution applies and u_c is a reliable estimate of the standard deviation of y , $U = 2u_c$ (i.e., $k = 2$) defines an interval having a level of confidence of approximately 95 %, and $U = 3u_c$ (i.e., $k = 3$) defines an interval having a level of confidence of approximately 99.7 %.

3.2. Uncertainty and traceability in CMM measurements

As explained in the previous paragraph, uncertainty is expressed as a range of values within which, at a specified level of confidence, the true value of the quantity measured is believed to lie. In CMM-based measurements, a task-specific uncertainty for each Geometric Dimensioning and Tolerancing (GD&T) parameter is necessary. Required are statements like, "The uncertainty of the diameter of this particular 75.00-mm diameter hole (produced under specific manufacturing conditions) is ± 0.05 mm at 95 percent confidence (when determined with this particular measurement system, using this particular measuring protocol, under this particular set of environmental conditions). As suggested by the parenthetic phrases in the last sentence, many factors will contribute to task-specific measurement uncertainties. The same power and versatility that make the CMM attractive as a measuring device also make assessing these measurement uncertainties a formidable task. First, consider two important roles that measurement uncertainty plays in CMM applications. The first is in measurement traceability; the second is in conformance decisions.

The ISO defines traceability as "the property of the result of a measurement or the value of a standard whereby it can be related to stated references, usually national or international standards, through an unbroken chain of comparisons all having stated uncertainties." The prominent role of uncertainty in completing the traceability chain is evident. Simply having a CMM calibrated does not make its measurement results traceable. If CMM-derived GD&T measurements are traceable, defensible task-specific uncertainty evaluations should be included in a report (see Fig. 3.1).

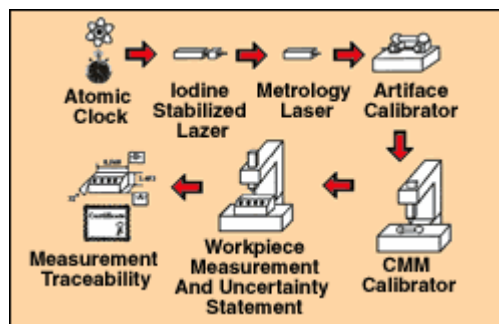


Fig.3.1. An example of the CMM traceability chain.

The importance of uncertainty evaluation has been further emphasized in recent standards, e.g. ISO 14253-1 (1998) and ASME B89.7.3.1 (2001),

which create guidance for the decision rule formulation to govern the acceptance or rejection of commercial products. Figure 3.2 shows that if a decision rule requires that the specification zone be reduced by the measurement uncertainty to determine the zone of acceptable values, there is a clear economic penalty for greater uncertainty.

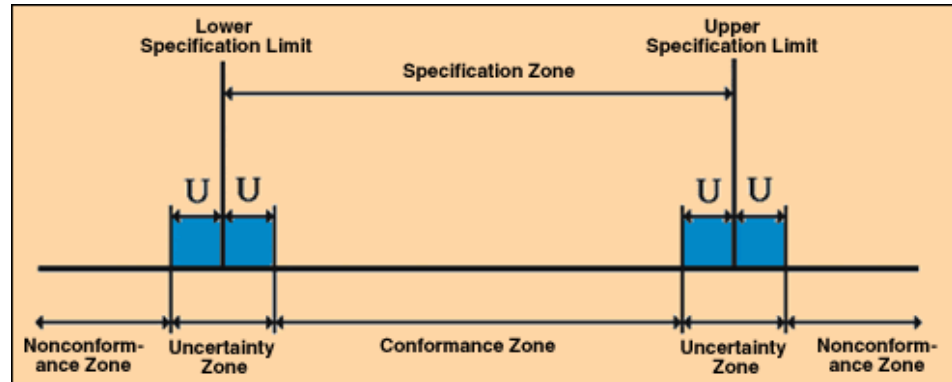


Fig. 3.2. This chart illustrates the role of measurement uncertainty in product conformance/non-conformance.

Many factors can contribute to the uncertainty in a CMM-based measurement of a GD&T parameter. The number of these influences and the complexity of their interactions make the application of traditional "error budget" approaches to measurement uncertainty largely impractical for CMMs. The ISO 15530 (Geometrical Product Specifications (GPS) -- Coordinate measuring machines (CMM): Technique for determining the uncertainty of measurement) series offers several alternative approaches.

3.3. Techniques for evaluation of the uncertainty on CMM-based measurements

The ISO 15530 series of International Standards is intended to provide terminology, techniques, and guidelines for estimating the uncertainty of CMM measurements. Although the technical committee ISO TC 213 has been working on it since more than a decade it is still largely incomplete. CMMs are considered to be complex GPS measuring equipment, and the estimation of the uncertainty of CMM measurements often involves more advanced techniques than those described in ISO 14253-2 (1999). The techniques presented in the ISO 15530 series are compliant with both and the GUM.

The following paragraphs show a synthesis of ISO 15530 standards. (Geometric Product Specification (GPS) – Coordinate Measuring Machines (CMM): techniques for determining the uncertainty of measurement)

- Part 1: Overview and metrological characteristics.
- Part 2: Use of multiple strategies in calibration of artefacts.
- Part 3: Use of calibrated work pieces or standards.
- Part 4: Use of computer simulation.
- Part 5: Use of expert judgement, sensitivity analysis and error budgeting

3.3.1. ISO 15530-1: overview and metrological characteristics

ISO 15530-1 aims to introduce the techniques for determining the uncertainty of measurement for a CMM, providing the proper terminology and a reference list of metrological characteristics, i.e. a list of factors that can potentially affect the measurements produced by a CMM. The document is still in a draft version.

ISO 15530-1 is based on the following key concepts: task specific measurement uncertainty and metrological characteristic of a measuring device.

Task specific measurement uncertainty is the expanded uncertainty U including the uncertainty contributors related to the overall process concerning a work piece measured by a CMM. The metrological characteristic of a measuring device is defined as the characteristic of a measuring device which may influence the results of measurements and which can determine an immediate uncertainty contribution.

3.3.2. ISO 15530-2: use of multiple strategies in calibration of artefacts

ISO 15530-2 (the document is still in a draft version) aims to introduce the technique of multiple measurement strategies, for determining the uncertainty of measurement related to a work piece measured by a CMM. The multiple measurement strategy aims to combine several orientations of the work piece and point distributions on its surface in order to get a better estimation for the conventional true value of the measurand. More specifically, the work piece must be measured in at least three (default four) different orientations corresponding to positions capable of guaranteeing good measurement conditions. In each orientation, the work

piece must be measured with at least five different point distributions. In case distance/size measurements are required on the work piece, subsidiary measurements on a material standard of size similar in its length to the above distance/size, must be performed along the three CMM coordinate axes and repeated three times each. The calibration value, and related calibration uncertainty are determined by proper calculation based on the database generated by all of the measuring results obtained.

3.3.3. ISO 15530-3: use of calibrated work pieces or standards

ISO 15530-3 aims to provide a technique for a simple uncertainty evaluation of measurements performed by a CMM. This technique applies to specific measuring tasks and to CMM results obtained from both uncorrected and corrected measurements. The standard was published in March 2004.

It is based on three key concepts: non substitution measurement, substitution measurement, similarity condition. Non substitution measurements are results in which the CMM indication is not corrected by systematic errors. On the opposite, in substitution measurement, the CMM indication is corrected by systematic errors, where both the work piece and a proper material standard of size are measured. Similarity conditions define the constraints binding the work piece and the material standard of size in the uncertainty assessment (i.e. dimensions and materials, the procedure used for measuring them, the environmental conditions, the CMM stylus configuration).

In case of a non-substitution strategy, calibrated artefacts are measured on a CMM in at least ten measurement cycles, each composed of the handling of each artefact and its consequent measurement. A total of at least 20 measurement repetitions must be achieved in different conditions simulating the real measuring process, including position and orientation of the work piece. This means that, in case only one artefact is involved in the assessment, the above cycle must be repeated 20 times.

The uncertainty contributors include the following:

- the calibration uncertainty stated in the artefact certificate;
- the standard uncertainty assessed by the above procedure;
- the standard uncertainty resulting from the variations of form errors, roughness, CTE, and other relevant parameters in different corresponding workpieces.

In case of a substitution strategy, the same procedure as stated above applies, i.e. the measuring cycle comprises the handling of the calibrated artefact, its consequent measurement, the handling of the work piece, and its consequent measurement.

3.3.4. ISO 15530-4: estimating task-specific measurement uncertainty using simulation

ISO 15530-4 aims to define criteria for simulation techniques applied to task-specific uncertainty evaluations. The target of these techniques is to provide measurement results combined with the related measuring uncertainty. Their application will enable the user to take immediate decisions about the consistency of the measuring process and the conformance or non-conformance of the work piece to the specification as required by ISO 14253-1.

ISO 15530-4 is the result of several years of research activities focused on simulation techniques applied to coordinate metrology (Virtual CMM). In Virtual CMM (VCMM), the VCMM model is assessed on the basis of a set of input parameters by means of proper CMM measurements of sphere/hole plates and of environmental parameters: using VCMM, it is possible to generate calibrated artefacts, i.e. to associate to the measurement result with the related uncertainty.

ISO 15530 is still in the DTR (Draft Technical Report) phase, namely it is an unpublished document in the first phase of the TR status which does not have the full status of an International standard.

Key concepts ISO 15530-4 is based on the following key concepts:

1. Concept of UES (Uncertainty Evaluating Software).
2. Concept of UES model.
3. Concept of UES validation.

The UES is a software used to provide uncertainty evaluation by simulating the overall CMM measuring process on a work piece: it can be resident inside the software equipping the CMM, or in another system working in conjunction with it. UES model can be based on mathematical and/or numerical procedures able to handle input quantities (like the temperature of the air) and to determine the related uncertainty contribution. UES can consider only a part of the metrological characteristics and related uncertainty contributions in its evaluating

process: in this case, the uncertainty evaluation must be based on a combination of uncertainty evaluation techniques, some of which are derived from pure simulation, and others of which are based on an experimental approach (as described in ISO 15530-3).

The UES manufacturer must provide:

- a list of CMM metrological characteristics managed by the UES;
- proper documentation of the techniques used for the uncertainty evaluation.

UES can be validated by the following two different approaches:

- experimental approach consisting of proper testing with a CMM on a calibrated artefact and/or on a proper calibrated material standard of size. Iterative testing, combined with proper analytical tests focused on some specific factors like scale and probing errors, can consolidate the basis of the uncertainty analysis.
- computer-aided techniques (CVE, Computer aided Verification and Evaluation). The process can be based on error vector field analysis, comprising the vector applied to the expected (“true”) measured point and its direction versus the determined position of the measured one. By proper perturbation of a reference “true” condition, based on the input of different input quantities it is possible to achieve an uncertainty evaluation related to the metrological characteristic under examination. Uncertainties caused by perturbation of contact points derived from a set of reference input in the UES under examination can thus be compared with ones related to contact points given by a testing body by means of coherently simulated instances. Historical data referred to proper predefined tasks can be considered too.

3.3.5. ISO 15530-5: use of expert judgement, sensitivity analysis and error budgeting

ISO 15530-5 aims to define the criteria of the technique for uncertainty evaluation based on expert judgement. The use of expert judgement can be particularly important when type B standard uncertainty is considered in the uncertainty budget. Personnel aiming to provide expert judgements must be properly qualified. ISO 15530-5 is still in draft status.

Key concept: concept of qualified personnel.

Qualified personnel, is here defined as personnel possessing the academic qualifications, experience and educational background in the field of accreditation and is required to provide an expert judgement. It is expected that any signatory representing a calibration laboratory accredited according to ISO/IEC 17025 (General requirements for the competence of testing and calibration laboratories, 2005) by a national accreditation body is able to provide proper judgements.

3.4. Critical observations

ISO 15530-2 e ISO 15530-3 are two different methods of evaluation measurement uncertainty.

In the first standard, the uncertainty of measurement is obtained by a non-calibrated objects method. The uncertainty is the result of three contributions: repeatability of measurements (evaluated by changing position of probe points); geometric errors of the piece (by measurement of the same piece in different orientations); error of scale. In the second instead, uncertainty is obtained by a calibrated object method. It's the result of systematic error (difference between measurand and reference object), repeatability of measurements (evaluated by changing position of probe points) and uncertainty of calibration and reference object.

These methods define uncertainty measurement by an aggregate way, while ISO 15530-4 analytically characterise each uncertainty contribution in the measurement volume of the machine. This is the way promoted by PTB (German metrological Institute), which firstly introduced the concept of "virtual machine".

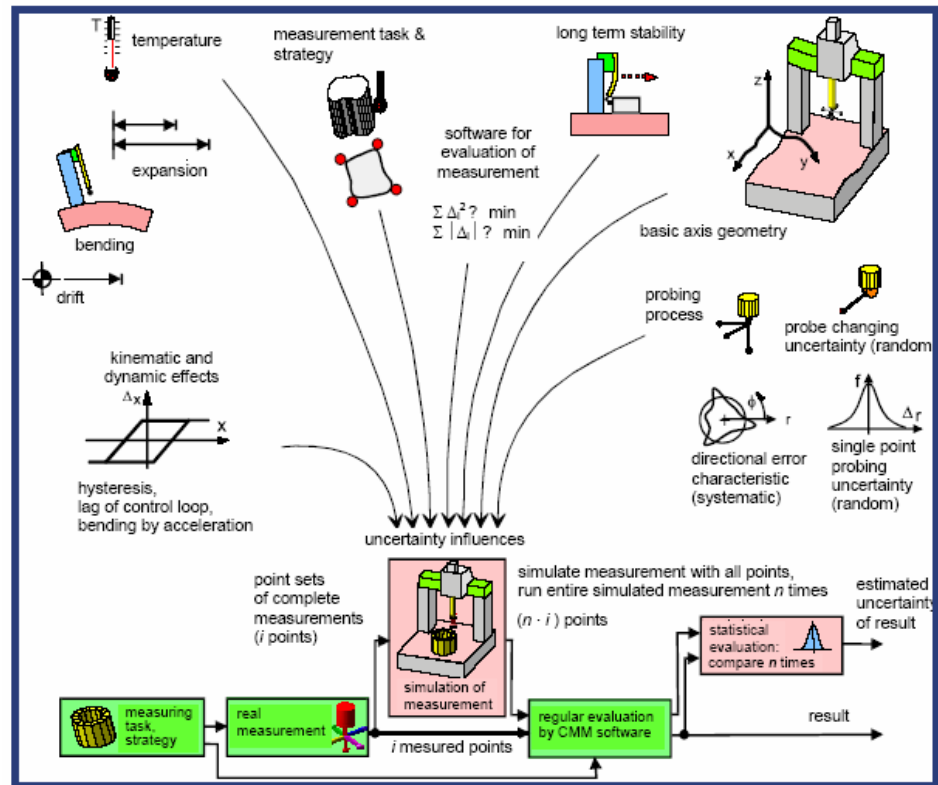


Fig. 3.3. The virtual machine concept

The virtual coordinate measuring machine (VCMM) approach estimates an uncertainty statement for a particular measurement task on a particular CMM according to Monte Carlo simulation results. "Basically the virtual CMM performs a point by point simulation of measurements, emulating the measurement strategy and the physical behaviour of the CMM with the dominating uncertainty contributions disturbing the measurement" (Trapet, E., Waldele, F., 1996; van Dorp et al., 2001). The simulated measurement should have all the facets of the real measurement that can significantly contribute to the measurement uncertainty. Practical systems include probe qualification and workpiece orientation but in practice may not always cover all contributions. The original developers of the technique considered that there were three basic contributions to uncertainty, known systematic influences, unknown systematic influences and random influences. They also distinguish between on-line and off-line simulations. This approach is illustrated in Figure 3.4 as an extension of a normal CMM measurement.

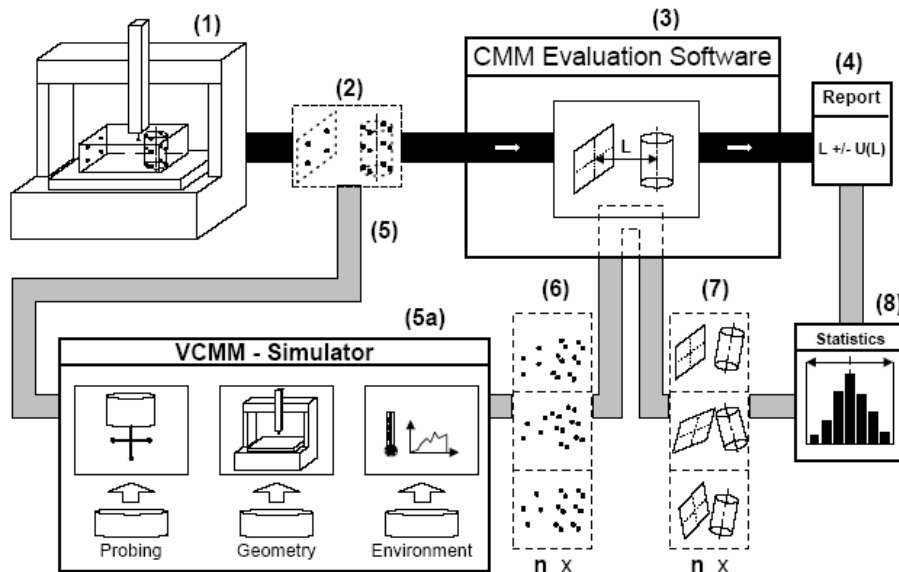


Fig. 3.4. The virtual CMM concept.

The thick black lines show data flow for a normal CMM measurement while the thick grey lines show the additional data flow that is employed to achieve a VCMM estimate. In a normal CMM measurement, a machine with a probe (1) is used to develop a set of points for each feature of interest in the measurement (2). These points are then used with CMM evaluation software to compute substitute geometric elements (3) and derive geometric parameters. These parameters are listed in a measurement report to arrive at an estimate of conformance (4) for each measured feature. When operating the VCMM, initial input is the set of points (5) to be sampled on a particular feature. These points are specified with respect to the ideal geometry of the design specification. For each sample point on a particular feature, the VCMM simulator (5a) generates a perturbed point that represents an estimate of what a particular CMM would have reported when measuring that commanded point. The perturbed point is generated by modelling variations that may result from part geometry, probing errors, machine motion errors, environmental influences, and other measurement uncertainty contributors. Each error is simulated using a probability density function (PDF) and each point estimate in the simulation is generated by considering all of the PDFs that contribute uncertainty to the measurement result. For any particular feature, a set of simulated results

is generated (6) and then input to typical CMM evaluation software to produce a set of computed substitute geometric elements (7). By evaluating each substitute geometry element, a PDF of the reported parameter can be computed to characterize its uncertainty. This PDF represents the difference between simulated measurements with uncertainty influences present and the same simulated measurement made with no uncertainty influences present. Statistics (8) associated with this PDF can then be used to report the uncertainty of the measurement following the notation of the GUM. To operate a VCMM, uncertainty contributors must be assessed or estimated for each particular CMM under specific environmental conditions. For each CMM, data files characterizing these uncertainties are used as input for VCMM simulations. These contributors include standard deviations of probing processes, residual errors of CMM motion (scale, straightness, and rotation), permissible temperature gradients, and expansion coefficients. In the next chapter we will illustrate a methodology for inspection plan design application, where the virtual CMM concepts will be largely employed although in a wider meaning.

REFERENCES CHAPTER 3

- AMERICAN SOCIETY OF MECHANICAL ENGINEERS, 2001, "Guidelines for decision rules: considering measurement uncertainty in determining conformance to specifications", ASME B89.7.3.1.
- INTERNATIONAL STANDARDS ORGANIZATION, 1995, "Guide to the expression of uncertainty in measurement".
- INTERNATIONAL STANDARDS ORGANIZATION, 1998, "Geometrical Product Specifications (GPS) – Inspection by measurement of workpieces and measuring instruments – Part 1: Decision rules for proving conformance or non conformance with specification", ISO 14253-1:1998.
- INTERNATIONAL STANDARDS ORGANIZATION, 1999, "Geometrical Product Specifications (GPS) -- Inspection by measurement of workpieces and measuring equipment -- Part 2: Guide to the estimation of uncertainty in GPS measurement, in calibration of measuring equipment and in product verification", ISO 14253-2:1999.
- INTERNATIONAL STANDARDS ORGANIZATION, 2000, "Quality Management Systems and supporting documents", ISO 9000:2000.
- TAYLOR, B. N. AND KUYATT, C. E., 1994, "Guidelines for Evaluating and Expressing the Uncertainty of NIST Measurement Results", NIST Technical Note 1297.
- TAKAMASU, K., FURUTANI, R., KUROSAWA, T., TAKATSUJI, T., WÄLDELE, F., SCHWENKE, H., BROWN, N., JAATINEN, E., 2001, "International Standard Development of Virtual CMM", final research report for New Energy and Industrial Technology Development Organization (Japan).
- TRAPET, E., WALDELE, F., 1996, "The virtual CMM concept, in advanced mathematical tools in metrology II", (World Scientific), 238-247.
- VAN DORP, B., HAITJEMA, H., DELBRESSINE, F., BERGMANS, R., SCHELLEKENS, P., 2001, "Virtual CMM using Monte Carlo methods based on frequency content of the error signal.", Proc. SPIE 4401 Recent Developments in Traceable Dimensional Measurements', J.E. Decker and N. Brown, Eds., SPIE.
- VAN DORP, B., DELBRESSINE, F., HAITJEMA, H., AND SCHELLEKENS, P., 2001, "Calculation of measurement uncertainty for multi-dimensional machines, using the method of surrogate data", Advanced Mathematical and Computational Tools in Metrology V.

4. METHODOLOGY FOR INSPECTION PLAN DESIGN

The main objective is to focus on obtaining reduced sample size (cost) for the accurate evaluation (minimum uncertainty and zero bias) of geometric errors in parts obtained from batch or mass production.

The measurement process combines a physical and a numerical part, see Figure 4.1. For a required measurement task, the CMM inspects the part by probing the relevant surfaces at a sample of points. Then, suitable numerical algorithms elaborate the Cartesian coordinates of the sample in order to calculate the measurement result which has to be assessed against the tolerance specification.

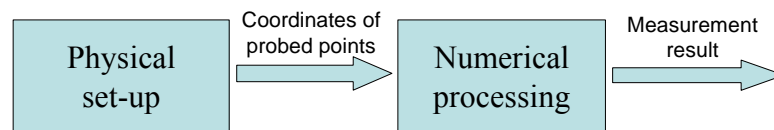


Fig. 4.1. Schematic representation of the CMM measurement process.

Both parts of the process involve design options. For the physical part, design refers to machine set-up (selection of the probing system, ball calibration procedure, part orientation and fixturing) and probing operations (number and location of the points to be probed, path and speed of the probe); for the numerical part to the methods of estimation of the geometrical entities and the tolerance interpretation criterion.

It is essential to point out that CMM inspection poses a peculiar metrological problem. On one hand, being a discrete point sampling device, sampling error is a distinctive major source of uncertainty, and even more so given that the economic constraint requires samples to be small. On the other hand, according to the principles of geometric dimensioning and tolerancing (GD&T), as mathematically codified in A. (Sun, Y. T., et al., 2002) the geometric error strongly depends on the extreme values of the population of form deviations so that a full-field inspection is ideally required. This incompatibility, known as “methods divergence”, originates an ill-posed statistical problem, namely the use of small-sample statistics for estimating extreme-value properties. Estimates will be largely biased unless prior information on the population is assumed. One should bear this in mind for the subsequent argumentations.

Providing a good solution of the design problem requires knowing how measurement performance, bias and uncertainty, is affected by all

possible design choices. As in the measurement process there are several sources of uncontrolled variation, the measurement result is a random variable with bias and uncertainty being directly related to its mean and variance.

In this dissertation a numerical model of the actual surface including its systematic error coming from the manufacture process is used. Identification of the characteristics of a surface resulting from a manufacturing process require an attentive analysis by a detailed inspection of a representative number of pieces taken from a production lot. In the case when the rest of lot differs from the virtual part designed, the inspection plan might be not appropriate, thereby some tests for tightly identify the discrepancy would be useful, for example a lack of fit test if the model is a statistical one.

The methodology proposed involve the following stages:

- (a) detailed inspection of some parts representative of the lot;
- (b) identification of the best model simulating the part geometry from the measurement data;
- (c) design of the reduced inspection on succeeding specimens using Design of Experiment and virtual CMM;
- (d) application of the designed inspection plan to the rest of the lot;
- (e) use of tests to identify differences between virtual part designed and parts of the lot inspected;
- (f) computation of the geometric error and attribution of uncertainty.

Given an homogenous lot of N parts, first step require a physical CMM, that scans the surface of n_0 parts sampled from the lot, by k_0 measurement points. Because we not have any CMM, we centre the research around the virtual measurement process design, whose implementation scheme is reported in Figure 4.2.

For a given measurement task, the design procedure requires to run repeated measuring cycles on the computer for all the design settings of interest. An effective way to do this combines Design of Experiments (DoE) and Monte Carlo simulation, where the first allows for an intelligent exploration of the design space and the second produces samples of the measurement result large enough to ensure reliable estimates of its mean and variance.

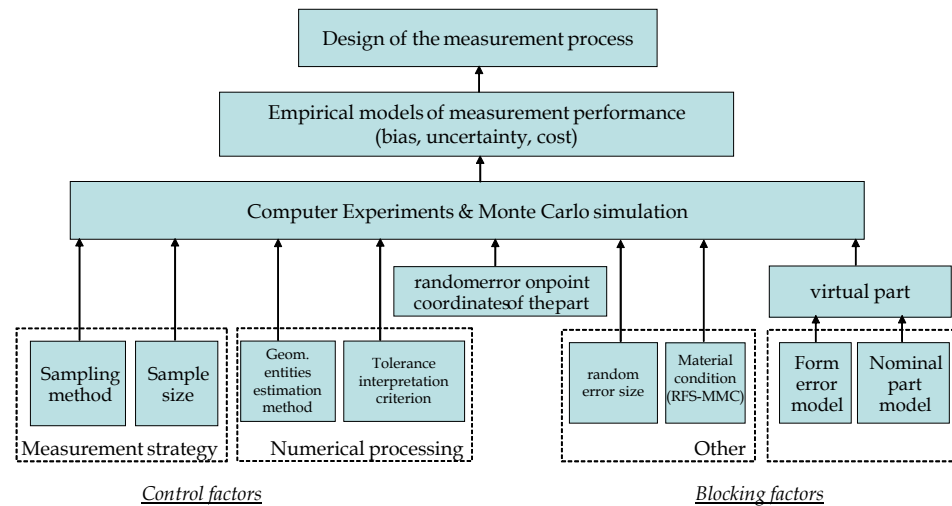


Fig. 4.2. An implementation scheme of the design procedure in virtual CMM

Technically, for every trial of the planned experiment a Monte Carlo simulation is run with 10^4 repetitions. During repetitions the simulation model is not changed apart from the random measurement error. The experimental factors are of two kinds, control factors and blocking factors. The former belong to the measurement process, the latter to the part geometry.

According to which geometrical tolerance will be considered, control factors will be chosen and their influence in finding optimal measurement process may be analysed. For example, when form tolerances are involved, interpretation criterion and material condition are not relevant.

Control factors are subdivided into measurement strategy factors, includes number and location of the parts and in factors of numerical processing, include always possible alternative method for geometrical entities estimation. The blocking factors are made up of the virtual part and of the other factors. The virtual part, results by the sum of error model and the nominal part model. This better is the nominal geometry of the parts and possible factor are the dimensions of the part. Other factors may be introduced to design optimal measurement plan, i.e. material condition (MMC/RFS).

In the following pages and in chapters 5 and 6, we will illustrate factorial plans used to analyze some geometrical tolerances by virtual CMM: position tolerances and flatness tolerances. The intent is explain that these two case studies will provide a more detailed exploration of the methodology. Position tolerance, that is the most complex geometrical

tolerance, is used to design inspection plane in the case of one or two holes calculation, but also to individuate its uncertainty (see chapter 5). In this case form error is not considered, but is simulated as a random error that modify nominal probe points. The second tolerance is less difficult to evaluate, thereby form error model has been considered (see chapter 6).

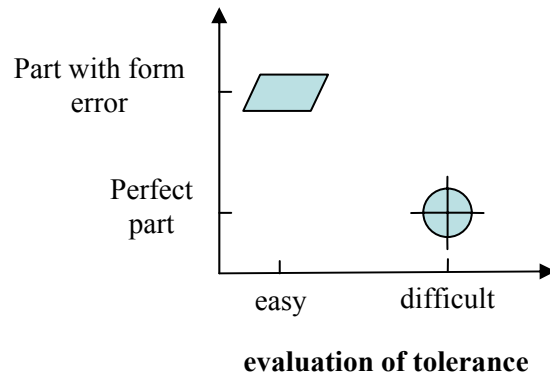


Fig. 4.3. Two case studies illustration

After definition of optimal set of inspection parameters, we will make physical measurement of the $N-n_0$ specimens and we can calculate their uncertainty. In this phase it is also necessary to check by some rigorous tests similarity of the $N-n_0$ pieces with the virtual part. If estimate coefficients of surfaces are significant, geometric error t will be calculated, if not, will be prudent to increase sample size k_0 . This operation may be conducted using a sequential procedure, to choose following points according to a sensible criterion and stops when an exit criterion is verified.

REFERENCES CHAPTER 4

- SUN Y. T., ANAND S., TANG J. S. Y., 2002, "Comprehensive design of experiments-base framework for optimal CMM inspection and uncertainty analysis of form tolerances", *International Journal of Production Research*, vol. 40, no. 9, 2097-2123.
- ROMANO, D., AND VICARIO, G., 2003, "Assessing Part Conformance by Coordinate Measuring Machines", *Proc. of ESREL 2003 - European Safety and Reliability Conf.*, Maastricht (NL), June, T. Bedford and P.H. van Geldereds., Balkema Publishers, Lisse (NL), 1329-1336.
- VICARIO, G., AND ROMANO, D., 2002, "Inspecting Geometric Tolerances: Uncertainty In Position Tolerances Control On Coordinate Measuring Machines", *SMA (Statistical Methods & Applications)*, vol. 11 no. 1, Springer Verlag, Berlin Heidelberg (DE), 83-94.

5. APPLICATION TO POSITION TOLERANCES

This chapter presents the application of the framework introduced in chapter 4. to the design of the measurement process by which position tolerance of mechanical parts are checked on Coordinate Measuring Machines (CMM) .

The process combines a physical and a numerical part. The CMM inspects the part by exploring the relevant surfaces at a sample of points. Then suitable numerical algorithms elaborate the Cartesian coordinates of the sample in order to calculate the geometric error, which has to be assessed against the tolerance specification.

The design of the measurement process consists in selecting the number and the location of points explored on each surface as well as the numerical algorithms. Uncertainty is generated by two sources - the random measurement error on Cartesian coordinates and the sampling error inherent to the way CMMs operate – and then it is inflated by the numerical processing. The first source of uncertainty accounts for several physical effects. These effects can be attributed to the environment (especially temperature), the machine (e.g. errors in the geometry of the slides, errors in the probing system), the fixturing system, and the part (e.g. form errors, cleanness, surface roughness).

Effective design requires an investigation on how uncertainty is affected by the measurement strategies (size and type of the inspection sample), the numerical algorithms for the computation of the geometric error, the part geometry, both nominal and actual, and any other option which the user may have when deciding upon the measurement process.

As we have already seen in previous chapter, the method used is based on the substitution of the physical process with a suitable numerical model that simulates the measurement error. Then an extensive experimentation performed on the simulated process allows to estimating the link between the design options and measurement uncertainty. The adopted experimental procedure combines Design of Experiments and Montecarlo simulation.

5.1. Related work

Several scientific works have addressed the design problem of the CMM measurement process. On the main they study the effect of the sampling

strategy (sampling method and sample size) and the form-fitting criterion on measurement uncertainty in the case of form tolerances. Among those accounting also for machining errors, we mention Lin, Z.C., et al., 1997, Capello, E., and Semeraro, Q., 2001, Dowling, M. M., et al., 1997, Sun, A. Y. T., et al., 2002, Summerhays, K. D., et al., 2002. The first two consider sampling strategy whereas the remainders also different form-fitting criteria. As far as our knowledge may reach, no study has dealt with position tolerances in a systematic way and the tolerance interpretation criterion (“resolved geometry” vs. “surface”), where it applies, has never been considered among the design options. In this dissertation we explicitly consider also this option. Moreover, the position tolerance on fully cylindrical holes is examined for different material conditions (RFS and MMC) and different part geometries, thus spanning a large set of practical situations.

Although a number of studies have been reported in evaluating measurement uncertainty, only a few have applied the design of experiments to systematically examine factors which may affect uncertainty. Feng et al. (2006) apply a fractional factorial experimentation to investigate the effect of the factors and their interactions on the measurement uncertainty, as defined by the GUM. While they mainly use typical factors regarding the set-up of the machine (stylus speed, stylus length, probe ratio, %offset), we mainly analyse effects of factors pertaining to the measurement strategy and the numerical data processing. In fact, we pool the physical effects in the random measurement error of the point coordinates.

5.2. Measurement process

In this section we describe the steps of the measurement process involved in the control of position tolerance on a CMM. Each step gives a specific contribution to the overall uncertainty of the estimated position error. The description of the measurement process is preceded by the presentation of the part used in the case-study. Once a point sample is probed on each of the part surfaces involved in the position tolerance control, main process steps are: estimation of the Datum Reference Frame (DRF), estimation of the feature location, and estimation of the position error. At each step main user options and design parameters are highlighted.

5.2.1. The inspected part

Inspection is applied to a part with perfect shape. There is a specific

reason for it. In fact, the objective of the study is to analyse the baseline contribution to measurement uncertainty arising from (1) the CMM measurement error, (2) the CMM sampling error and (3) the quite complex method of geometric calculus needed for estimating the position error. Hence, the contribution due to possible form error on the inspected surfaces (and its interaction with the sampling strategy) is purposely left aside. The selected is a plate (dimensions $l_u \times l_a \times h$) with a circular hole (diameter d) in the middle. The hole axis is perpendicular to a reference horizontal plane A at a nominal location indicated by X_c and Y_c , as represented in Figure 5.1.

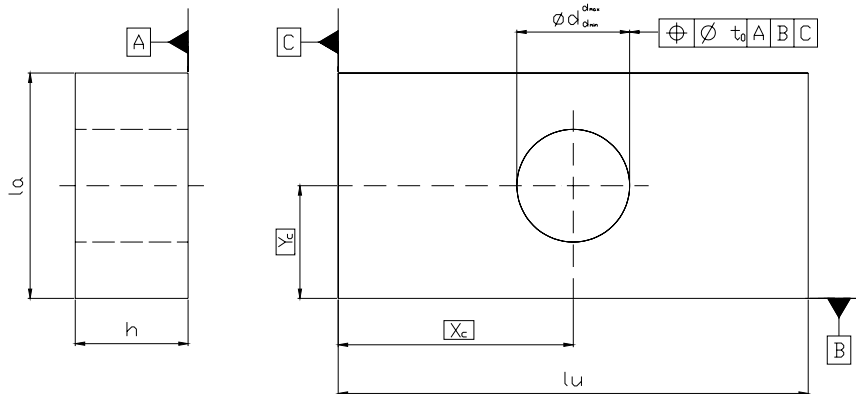


Fig. 5.1. The inspected part: a plate with a central hole.

Both a dimensional and a geometric tolerance apply to the hole: for part conformance the hole diameter must range from d_{\min} to d_{\max} and its axis must lie within a cylindrical zone of diameter t_0 around the nominal location.

Figure 5.2 shows the true DRF system (needed for position tolerance evaluation) for such a part. Point O is the DRF origin. It results from the intersection of three mutually orthogonal planes corresponding to the planes A, B, C referenced in the drawing. As already pointed out they are called datums and they are not the surfaces on the actual part, but perfectly flat mating counterparts of the actual surfaces. As the geometry of the part is the nominal one, the true DRF system coincides with the coordinate planes, its origin is the part corner O $[0,0,0]$, its unit vectors are $\vec{i}, \vec{j}, \vec{k}$ and the hole axis joins the points $C_1[X_c, Y_c, 0]$ and $C_2[X_c, Y_c, h]$. As a consequence the true position error for such a part is zero.

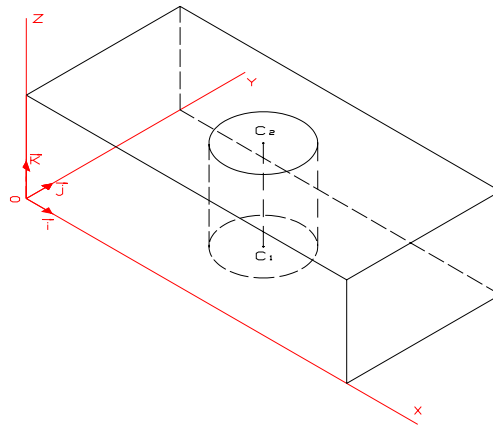


Fig. 5.2. The true DRF for the part of perfect geometry.

5.2.2. DRF evaluation

Actual identification of the DRF follows a procedure which has already been described in § 1.4.1. However it is summarized in the following steps.

1. The part is placed in the CMM work volume.
2. A set of points is probed on the horizontal face of part and datum A is estimated using a selected method (e.g. the Orthogonal Least Squares (OLS) or a minimum zone method). Then datum B is estimated analogously with the additional constraint of being perpendicular to datum A; datum C is finally estimated with a double orthogonality constraint (to both A and B). Thus DRF coordinate planes are identified. Notice that the order of datums is not irrelevant.
3. The intersection of A, B and C defines the origin of the DRF.

Because of the measurement error, the estimated DRF is in general different from the true DRF. We use the OLS method for estimating the three datums. It aims at minimizing the sum of squared distances (δ) of the measured points from the estimated plane, as illustrated in Figure 5.3 for a two-dimensional case. Notice the difference from the ordinary Least Square method, which would consider deviations of each point from the line only in the vertical direction. In fact, OLS requires a non linear estimation of the plane coefficients. Details of the OLS method will be provided in chapter 6.

$$\min \sum (\delta^2) \quad (5.1)$$

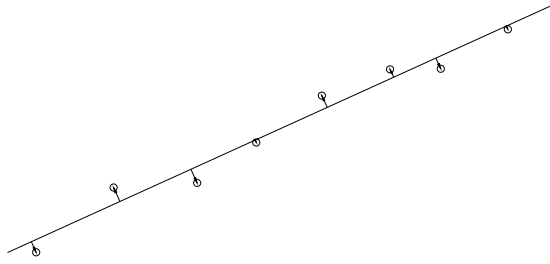


Fig 5.3. OLS method for datum estimation.

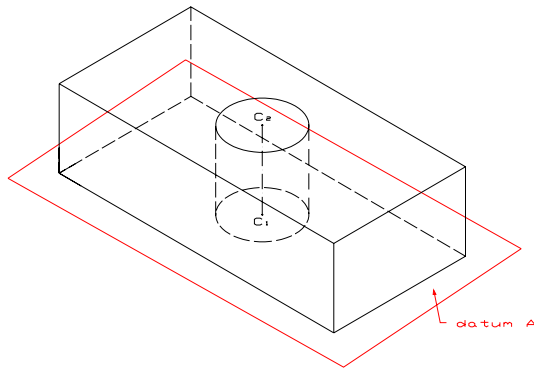


Fig. 5.4. Estimation of datum A.

After datum A is estimated by OLS method, another set of points is probed on the surface corresponding to the secondary datum B, from which the datum is estimated. In this case a constrained OLS estimation is applied to fulfil the condition that datum B is orthogonal to datum A.

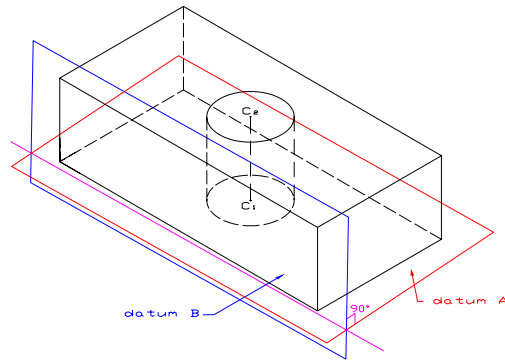


Fig. 5.5. Estimation of datum B.

The same logic applies to the estimation of tertiary datum C. As it must be orthogonal to datums A and B, its orientation is fully determined and OLS only serves to locate the plane.

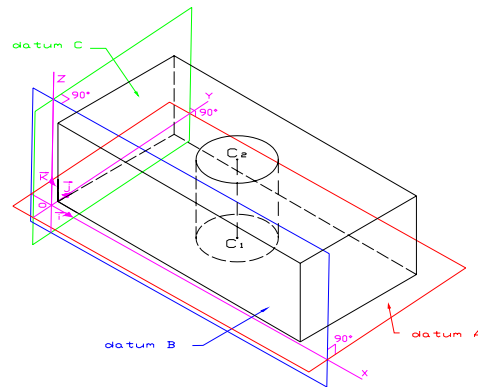


Fig. 5.6. Estimation of datum C.

By intersection of surfaces A, B and C, DRF origin is obtained. Mathematically coordinates of origin are the result of a linear system of three equations:

$$\begin{cases} \alpha_A x + \beta_A y + \gamma_A z + \delta_A = 0 \\ \alpha_B x + \beta_B y + \gamma_B z + \delta_B = 0 \\ \alpha_C x + \beta_C y + \gamma_C z + \delta_C = 0 \end{cases} \quad (5.2)$$

Notice that here we did not apply the envelope principle, that would have

required to move the datum until the furthest exterior point. As we work on a nominal geometry the application of the principle would only catch the measurement error of the CMM producing an up-ward bias. When real surfaces are inspected just the opposing happens. There even the use of the envelope principle might not prevent the estimate from a downward bias since we are relying on a usually small sample of points.

The estimated DRF is the coordinate system respect to which the hole axis is located and the successive geometric computations are done. Therefore the error in DRF calculation is a first important error contribution in the evaluation of the position error.

5.2.3. Hole location

Next step is probing a set of points on the hole surface. Using coordinates of probed points, the hole location in the DRF is determined. Standards offer two options at this regard. The hole can be located either by locating its axis (which is an abstract entity!) or by locating a functional counterpart of the hole surface. This latter is called the actual mating envelope, namely the largest diameter cylinder still able to enter the hole. The two options correspond to two different criteria for interpreting position tolerance: the resolved geometry interpretation (when the axis is located) and the surface interpretation (when the actual mating envelope is located). One objective of the study is to compare the extent to which the two interpretations for hole location affect the uncertainty of the position error. The two criteria are described in detail in the next sections considering both the MMC and the RFS material conditions for the hole.

5.2.4. Position error by surface interpretation at MMC and RFS

The actual value of position error t is the smallest value of position tolerance to which the feature conforms. According to the surface interpretation a feature conforms to a position tolerance at a specified material condition basis if all points of the feature lie outside a specified three-dimensional tolerance zone. Notice that, for the surface interpretation, the tolerance zone is a zone forbidden to any point of the feature. In the case of the hole, the tolerance zone is defined by a cylinder of radius b' with axis positioned in theoretical hole location. The latter is defined in the DRF by the boxed dimensions X_C and Y_C specified in the drawing, see Figure 5.1. b' is referred to as the size parameter of the

tolerance zone (Fig. 5.7).

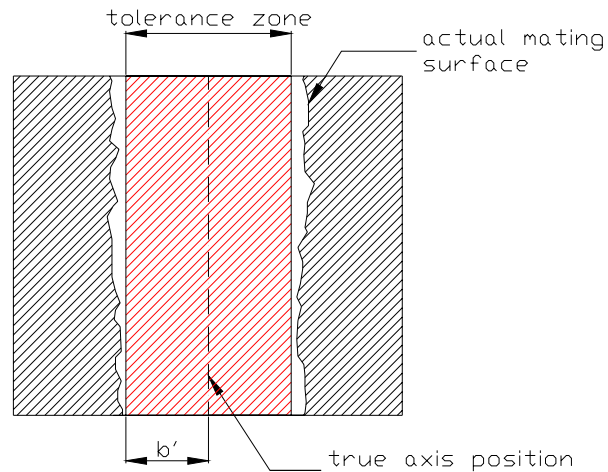


Fig. 5.7: Tolerance zone in the case of an internal feature according to the surface interpretation

The size parameter b' is calculated in different ways according to the material condition which is set in the specification. In the next two subsections the RFS and MMC conditions are examined.

5.2.4.1. RFS case

At RFS, radius b_0' of the cylindrical tolerance zone is defined by:

$$b_0' = r_{am} - \frac{t_0}{2} \quad (5.3)$$

Where t_0 is the position tolerance and r_{am} is the radius of actual mating envelope of the hole.

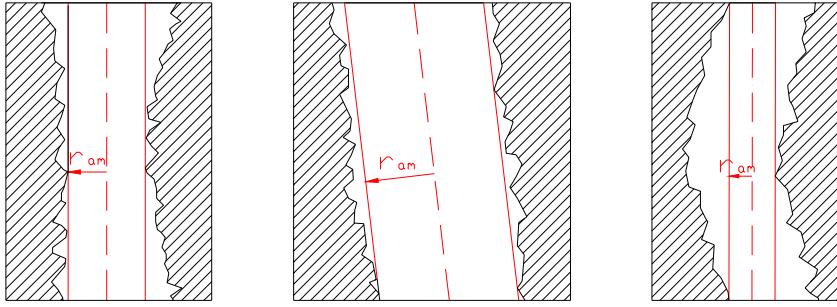


Fig. 5.8. Actual mating envelope (in red) and its size r_{am} for three holes.

Use of surface interpretation of position tolerance is completely adequate when conformance is checked by a physical gauge, but it is not sufficient when conformance is checked by a CMM. In fact, the sampling operated by the machine gives an uncertain evaluation of the actual mating envelope. As we will see in the sub-section 5.3.6.1., an algorithm is developed to calculate r_{am} from the coordinates of the points probed on the hole surface. The algorithm explores the spatial orientations which the actual mating envelope can have. As the actual value of position error t is the smallest value of position tolerance to which the feature conform, the defining equation for t can be simply obtained from (5.3):

$$t = 2(r_{am} - b') \quad (5.4)$$

where b' is the radius of the largest cylinder defining the tolerance zone with which the actual hole would be accepted. Therefore, recalling the definition of the tolerance zone for the surface interpretation, b' is the radius of the internal envelope of the actual hole with the constraint that the envelope axis is orthogonal to the Z axis of the DRF and passes through its theoretical position. Relying on the point sample it can be computed as the smallest distance between each point $P_i(X_{P_i}, Y_{P_i}, Z_{P_i})$ probed on the hole surface and the axis of the tolerance cylinder:

$$b' = \min_i \left(\sqrt{(X_{P_i} - X_C)^2 + (Y_{P_i} - Y_C)^2} \right) \quad (5.5)$$

5.2.4.2. MMC case

At MMC, radius b_0' of the cylindrical tolerance zone is defined by:

$$b_0' = r_{\text{mmc}} - \frac{t_0}{2} \quad (5.6)$$

where t_0 is the position tolerance and r_{mmc} is the MMC radius of the hole, i.e. $r_{\text{mmc}} = d_{\text{min}}/2$.

Analogously to (5.4), position error t can be expressed as:

$$t = 2 (r_{\text{mmc}} - b') \quad (5.7)$$

where b' is defined as before. Notice that, as in this case t does not depend on r_{am} , there is no need to estimate the actual mating envelope of the hole. As we will see later in the chapter, this is highly beneficial to the uncertainty of the estimated position error. In fact uncertainty of the estimated t only depends on uncertainty of the estimated b'

The hole conforms to a position tolerance t_0 if $t \leq t_0$. Sometimes, especially when using the surface interpretation at MMC, estimate of t can be negative. This means that the position error is overcompensated by the tolerance bonus which applies when the radius of the actual hole is larger than its limit of size r_{mmc} . (see Fig. 5.9).

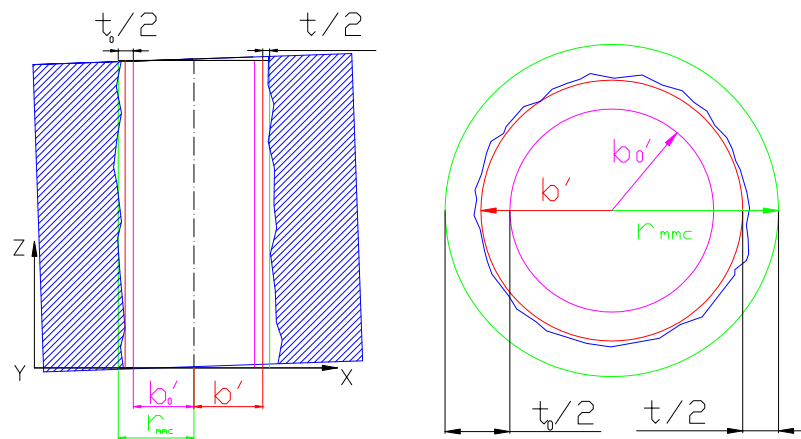


Fig. 5.9. Graphical interpretation of the main parameters defining position tolerance at MMC.

5.2.5. Position error by resolved geometry interpretation at MMC and RFS

According to the resolved geometry interpretation, the actual value of

position error t is the diameter of the smallest tolerance cylinder which contains all points of the axis, within the width of the part, of the actual mating envelope of the hole (see Fig. 5.10). Notice that, contrarily to the surface interpretation where the tolerance zone is a forbidden zone for the actual hole surface, in resolved geometry interpretation the cylindrical tolerance zone is an allowable zone for the actual hole axis.

Likewise surface interpretation, also for resolved geometry interpretation the size of the tolerance zone is calculated in different ways depending on the material condition applied.

5.2.5.1. RFS case

At RFS, radius b_0 of the cylindrical tolerance zone is defined by:

$$b_0 = \frac{t_0}{2} \quad (5.8)$$

where t_0 is the specified position tolerance. As before, inverting (5.8) we obtain position error t as:

$$t = 2b \quad (5.9)$$

where b is the radius of the smallest size tolerance cylinder enveloping the actual axis. Recall that the axis of a tolerance cylinder is parallel to the Z -axis and passes through the theoretical position $(X_C, Y_C, 0)$ in the DRF (see Fig. 5.10). If $t \leq t_0$ the tolerance specification is met.

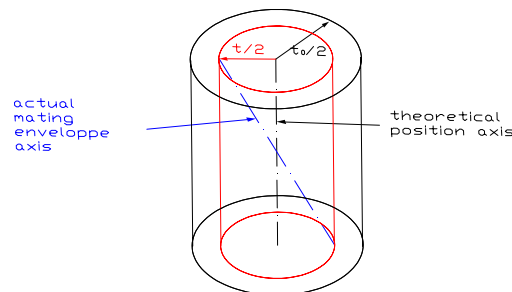


Fig. 5.10. Interpretation of position error t as limit of conformance for the actual hole axis.

5.2.5.2. MMC case

At MMC, radius b_0 of the cylindrical tolerance zone is defined by:

$$b_0 = \frac{t_0}{2} + (r_{am} - r_{mmc}) \quad (5.10)$$

where t_0 is the specified position tolerance. The difference between the radius of the actual mating cylinder (r_{am}) and the radius at MMC (r_{mmc}) is the tolerance bonus. Analogously to (5.9) position error t is the value is given by:

$$t = 2(b - (r_{am} - r_{mmc})) \quad (5.11)$$

5.3. Experiment settings on the virtual CMM

In this section we present how the virtual CMM has been developed and the general structure of the software implementing the experiment on the virtual CMM² (Fig. 5.11).

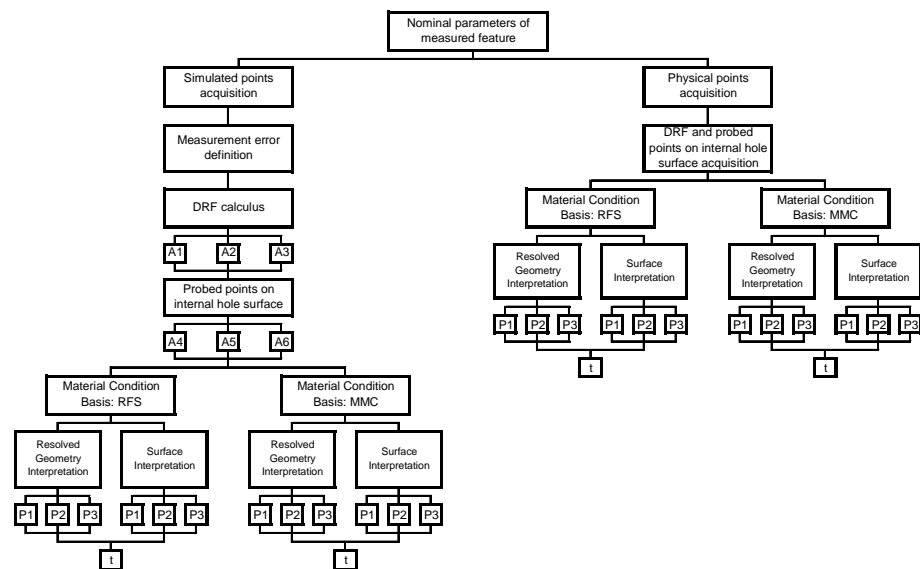


Fig. 5.11. General structure of the developed software showing data flow and main functionalities.

² In appendix II the software is reported and explained.

The software, developed in the Matlab environment, is organized in the form of main program which manages the whole experiment and a collection of ancillary functions implementing ad hoc algorithms which may be called by the main program. In the following pages the measurement process will be explained step by step. In doing this we will introduce all factors included in the experiment and their levels. Notice that the package, in principle, may run either with physically probed points or with simulated points.

5.3.1. Input of the part

The main program acquires the nominal part geometry from an external file. This file contains the basic dimensions as well as the specified dimensional and geometric tolerances. Table 5.1 reports the list of the geometric entities of the part (Fig. 5.1) involved in the case study.

5.3.2. Input of the point sample

Here there is the option to acquire simulated points or physical points (Fig. 5.12). In the case study the first option was used. When simulating a part with systematic form error, the form error model must be available.

Table 5.1. Nomenclature of the geometric parameters of the part selected for the case study.

Plate length	l_u
Plate width	l_a
Plate height	h
Hole diameter	d
Hole centre abscissa	X_c
Hole centre ordinate	Y_c
Hole dimensional tolerance	$\pm\Delta d$
Hole position tolerance	t_0
Primary datum	A
Secondary datum	B
Terziary datum	C

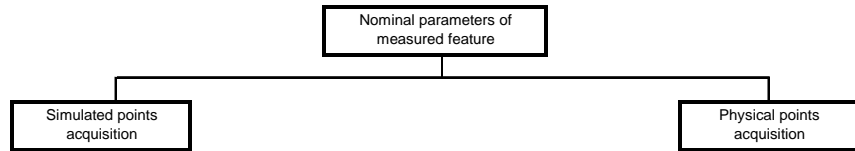


Fig. 5.12. Input data choice.

According to factorial design or just for calculate position tolerance for a set of data input, software can simulate a realistic measured cycle, from probed points to t value, and if the choice is to do some measurements repetitions it would calculate uncertainty of position tolerance. At this stage number of probed points and sampling strategy are required.

5.3.3. Input of measurement error

When point samples are simulated a measurement error must be assigned to the coordinates of each probed point (Fig. 5.13). This error is considered additive and is described by i.i.d. normal random variables with zero mean and common standard deviation, σ . Measurement error cumulatively accounts for a number of errors pertaining to the machine (form errors in the slides, error linked to the approach angle, etc.), the environment, the part and the fixturing system. For sake of simplicity the error size, σ , is taken to be uniform over the whole working volume of the CMM. Levels attributed to σ in the experiment are reported in Table 5.2, spanning a broad set of CMM with different quality.

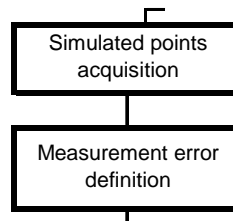


Fig. 5.13. Measurement error input.

Table 5.2. Levels of standard deviation of the measurement error.

	Low level	Central level	High level
σ [mm]	0,001	0,005	0,01

5.3.4. DRF computation

The first step of data processing is DRF computation. It works on the coordinates of the points sampled on the surfaces corresponding to the datums referenced in the drawing. With reference to the part in Figure 5.1 datum surfaces are three mutually orthogonal faces of the plate. n_A , n_B , n_C points are probed respectively on the surfaces corresponding to datums A, B, and C (Fig. 5.14). Table 5.3 contains the relevant levels for sample sizes n_A , n_B , n_C . Levels grow as powers of two (2^k , $k=2,3,4$).

Table 5.3. Levels of the number of probed points on part faces related to datums A, B, and C.

	Low level	Central level	High level
n_A	4	9	16
n_B	4	9	16
n_C	4	9	16

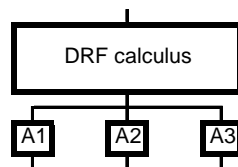


Fig. 5.14. DRF computation.

The sampling strategies applied on the nominally planar surfaces are: stratified non random sampling, stratified-random sampling, and pure random sampling.

- Stratified non-random (factorial), A1: points form a regular grid and maximize coverage (Fig. 5.15). External points are moved towards the face edges in order to maximise coverage; however a clearance distance from the edges is respected in order to avoid that possible edge irregularities are picked. We name this scheme also “factorial” for the similarity with point locations in a full factorial design.

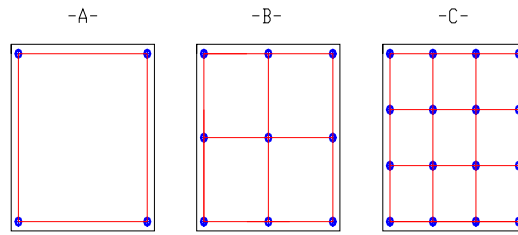


Fig. 5.15. Stratified non-random sampling, A1 .A) $n_p=4$, B) $n_p=9$, C) $n_p=16$.

- Stratified-random sampling, A2: points are drawn randomly inside the cells defined by a regular grid (one point per cell). Here again a clearance distance from the edges is respected (Fig. 5.16).
- Pure random sampling, A3: points are drawn randomly all over the face respecting a clearance distance from the edges (Fig. 5.17).

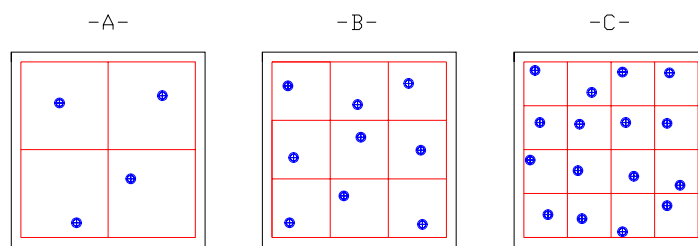


Fig. 5.16. Stratified random sampling, A2. A) $n_p=4$, B) $n_p=9$, C) $n_p=16$.

An unfortunate circumstance is when all points are nearly located along a straight line. In such a case the numerical algorithm which computes the plane may fail. nearly

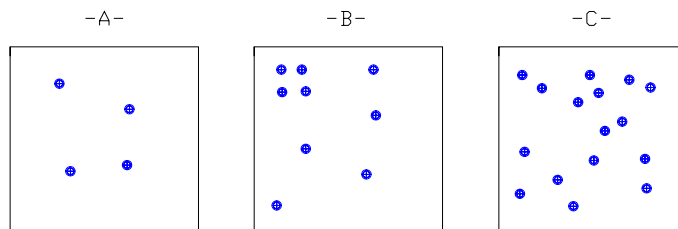


Fig. 5.17. Pure random sampling, A3. A) $n_p=4$, B) $n_p=9$, C) $n_p=16$.

Once the point samples are generated the DRF is computed by OLS method as described in section 5.2.2. Recall that this is only an estimate of the true DRF. In fact, in the repeated runs the computer DRF are different from each other and different from the true DRF, see Figure

5.18.

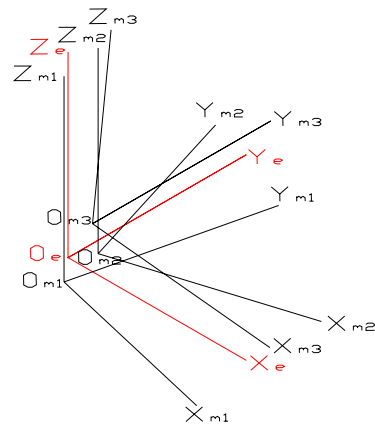


Fig. 5.18: True DRF (in red) and three possible DRF obtained from three different point samples on the three planar surfaces related to datums A, B, and C.

Because of the perfect geometry the Cartesian planes of the DRF coincide with three orthogonal faces of the plate. The coordinate of the point sample, originally expressed in the absolute Cartesian system of the machine, have now to be converted in the estimated DRF. Mathematically, the change of the reference system needs a rotation and a translation.

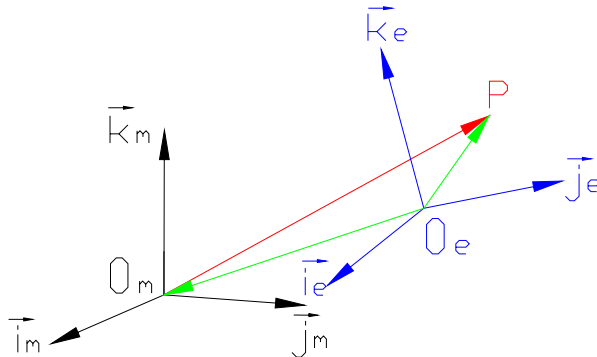


Fig. 5.19. Relative position of true DRF (blue) and estimated DRF (black).

Referring to Figure 5.19, the relation defining reference system transformation is:

$$\overrightarrow{O_m P} = (\overrightarrow{O_e P} - \overrightarrow{O_m O_e}) \circ R_{\omega\varphi\rho} \quad (5.12)$$

where $R_{\omega\varphi\rho}$ is the rotation matrix, function of ω , φ e ρ , the rotation angles around axis X_e , Y_e e Z_e , and $\overrightarrow{O_m O_e}$ is the translation vector from O_e to O_m . Matrix $R_{\omega\varphi\rho}$ is

$$R_{\omega\varphi\rho} = R_\omega \circ R_\varphi \circ R_\rho = \begin{bmatrix} \cos\varphi\cos\rho & -\cos\varphi\sin\rho & \sin\varphi \\ \sin\omega\sin\varphi\cos\rho + \cos\omega\sin\rho & -\sin\omega\sin\varphi\sin\rho + \cos\omega\cos\rho & -\sin\omega\cos\varphi \\ -\cos\omega\sin\varphi\cos\rho + \sin\omega\sin\rho & \cos\omega\sin\varphi\sin\rho + \sin\omega\cos\rho & \cos\omega\cos\varphi \end{bmatrix} \quad (5.13)$$

where

$$R_\omega = \begin{bmatrix} 1 & 0 & 0 \\ 0 & \cos\omega & -\sin\omega \\ 0 & \sin\omega & \cos\omega \end{bmatrix} : \text{rotation matrix around } X_e \text{ axis}$$

$$R_\varphi = \begin{bmatrix} \cos\varphi & 0 & \sin\varphi \\ 0 & 1 & 0 \\ -\sin\varphi & 0 & \cos\varphi \end{bmatrix} : \text{rotation matrix around } Y_e \text{ axis}$$

$$R_\rho = \begin{bmatrix} \cos\rho & -\sin\rho & 0 \\ \sin\rho & \cos\rho & 0 \\ 0 & 0 & 1 \end{bmatrix} : \text{rotation matrix around } Z_e \text{ axis}$$

5.3.5. Point sample on the hole surface

Similarly to the planar faces, a point sample of given size (n_H) is collected with a given sampling method. As before, levels of n_H are 4, 16, and 25 (Table 5.4). As for the sampling method, three methods are selected.

Table 5.4. Levels for the number of points probed on the hole surface

	Low level	Central level	High level
n_H	4	9	16

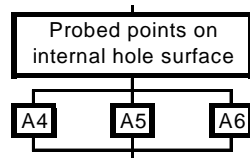


Fig. 5.20. Actual mating envelope cylinder calculus

- Stratified non-random sampling, A4: points are located to maximize coverage. The hole axis is cut by $\sqrt{n_H}$ horizontal planes. Each plane intersects the hole surface along a circumference. On each circumference $\sqrt{n_H}$ points are probed as illustrated in Figure 5.21. Points on different circumferences are vertically aligned.
- Stratified non-random sampling with staggered points, (A5): hole surface is probed by $\sqrt{n_H}$ points located on $\sqrt{n_H}$ vertical planes and staggered in order that each point has one different phase among n_H equispaced phases (Fig. 5.22).
- Stratified random sampling, (A6): hole surface is probed by $\sqrt{n_H}$ randomly drawn points in $\sqrt{n_H}$ equispaced vertical planes (Fig. 5.23).

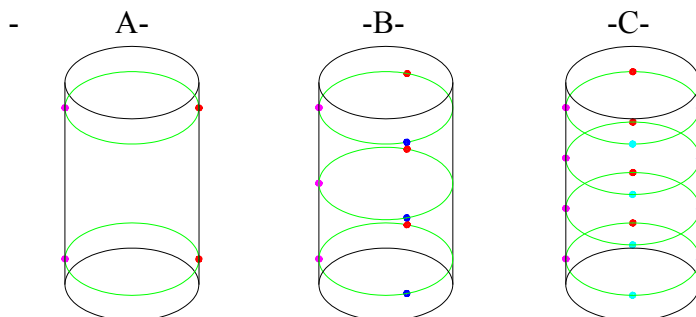


Fig. 5.21. Stratified non-random sampling with aligned points, A4. A) $n_p=4$, B) $n_p=9$, C) $n_p=16$.

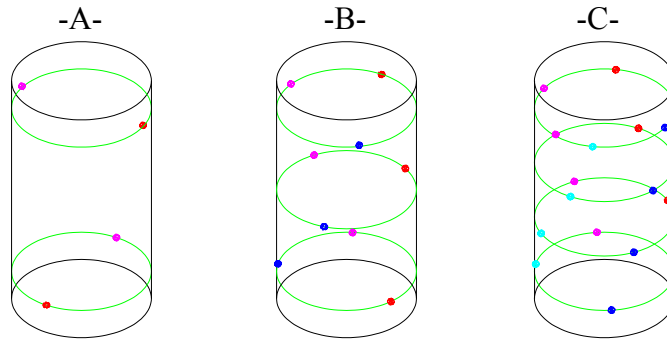


Fig. 5.22. Stratified non-random sampling with staggered points, A5. A) $n_p=4$, B) $n_p=9$, C) $n_p=16$.

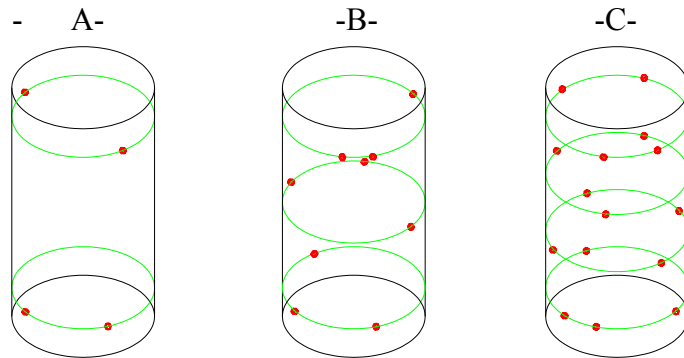


Fig. 5.23. Stratified random sampling, A6. A) $n_p=4$, B) $n_p=9$, C) $n_p=16$.

Analogously to points probed on the planar surfaces, also points probed on the hole surface must be expressed in the DRF system. The coordinate transformation is done by applying both a rotation and a translation to the point coordinates in the original system (Equation 5.13).

5.3.6. Material condition or tolerancing interpretation

Now the virtual CMM has all the information necessary to estimate position error t . However, depending on the material condition and the tolerance interpretation, t must be estimated in four different ways which will be described in the next sub-sections (Fig. 5.24).

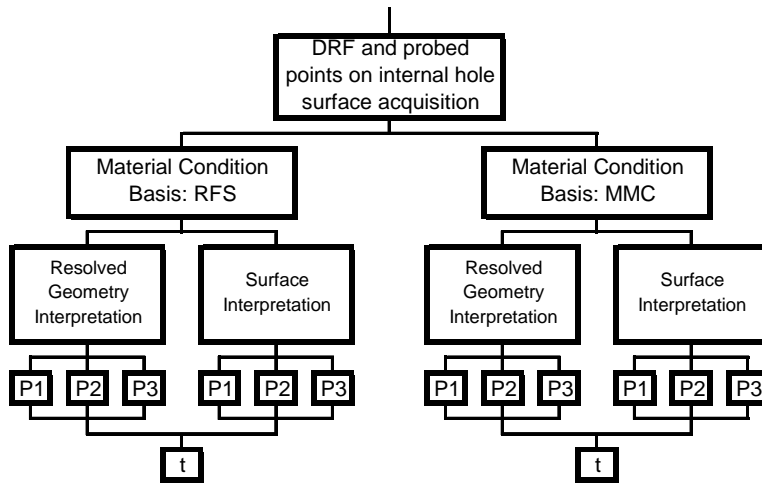


Fig. 5.24. Four ways for position error estimation. They are related to the four combinations of material condition and tolerance interpretation criterion.

5.3.6.1. At RFS and resolved geometry interpretation

From (5.9) position error is $t = 2b$, where b is the radius of the tolerance cylinder, that is smallest radius of a cylinder that, centred in the theoretical position, contains the axis of actual mating envelope cylinder of the hole within the width of the plate (Fig. 5.25).

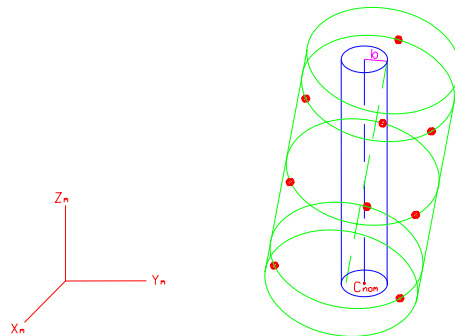


Fig. 5.25. Representation of parameter b .

The actual mating envelope is the surface of the largest virtual pin which still fits the hole. It can be identified by searching for the direction of the axis of a cylinder such that the projection of the probed points onto a plane orthogonal to this direction is internally enveloped by a circle of largest diameter. This logic is implemented in the algorithm described

below.

- Points probed on hole surface are projected on XY plane of the estimated DRF and on planes $(XY)_{\alpha\beta}$ obtained by a rotation of the XY plane around X_m e Y_m by the angles α and β respectively. $(XY)_{\alpha\beta}$ planes are calculated for all the combinations of α and β values within the square $-0.075^\circ \leq \alpha, \beta \leq 0.075^\circ$ with a $0,005^\circ$ discretization step in both angles. Coordinates of the points in a system obtained by rotating the DRF by α and β are given by:

$$P_{\alpha\beta} = P_m \circ R_\alpha \circ R_\beta = [x_m \quad y_m \quad z_m] \circ \begin{bmatrix} \cos \beta & 0 & \sin \beta \\ \sin \alpha \sin \beta & \cos \alpha & -\sin \alpha \cos \beta \\ -\cos \alpha \sin \beta & \sin \alpha & \cos \alpha \cos \beta \end{bmatrix} \quad (5.14)$$

where

$$R_\alpha = \begin{bmatrix} 1 & 0 & 0 \\ 0 & \cos \alpha & -\sin \alpha \\ 0 & \sin \alpha & \cos \alpha \end{bmatrix} \quad \text{rotation matrix around } X_m \text{ axis}$$

$$R_\beta = \begin{bmatrix} \cos \beta & 0 & \sin \beta \\ 0 & 1 & 0 \\ -\sin \beta & 0 & \cos \beta \end{bmatrix} \quad \text{rotation matrix around } Y_m \text{ axis}$$

- For each set of projected points on planes $(XY)_{\alpha\beta}$ the maximum inscribed circumference is computed, according to one of three methods that we will describe at the end of this chapter.
- Among all circumferences found at the previous step, the one with the largest diameter is selected. Let α^* and β^* be the corresponding angle pair. They define the direction of the axis of the actual mating envelope. The axis is identified by imposing that it passes through the centre $C_{\alpha^*\beta^*}$ of the circumference, whose coordinates are $(x_{\alpha^*\beta^*}, y_{\alpha^*\beta^*}, 0)$ in the rotated system. The circumference radius identifies parameter r_{am} . The actual axis is confined within the width (h) of the plate. Therefore it goes from $C_{\alpha^*\beta^*}$ to point $(x_{\alpha^*\beta^*}, y_{\alpha^*\beta^*}, h)$.
- Coordinates of axis endpoints are expressed back in the estimated DRF by applying the transformation:

$$C = C_{\alpha\beta} \circ R_{\beta'} \circ R_{\alpha'} = [x_{\alpha\beta} \quad y_{\alpha\beta} \quad z_{\alpha\beta}] \circ \begin{bmatrix} \cos \beta & \sin \beta \sin \alpha & -\sin \beta \cos \alpha \\ 0 & \cos \alpha & \sin \alpha \\ \sin \beta & -\cos \beta \sin \alpha & \cos \beta \cos \alpha \end{bmatrix} \quad (5.15)$$

where:

$$R_{\beta'} = \begin{bmatrix} \cos \beta & 0 & -\sin \beta \\ 0 & 1 & 0 \\ \sin \beta & 0 & \cos \beta \end{bmatrix} \quad \text{rotation matrix around } Y_{\alpha\beta} \text{ axis}$$

$$R_{\alpha'} = \begin{bmatrix} 1 & 0 & 0 \\ 0 & \cos \alpha & \sin \alpha \\ 0 & -\sin \alpha & \cos \alpha \end{bmatrix} \quad \text{rotation matrix around } X_{\alpha\beta} \text{ axis}$$

- Endpoints of the axis of the actual mating envelope are projected onto the XY plane of the estimated DRF. Let $C_1(x_1, y_1, 0)$ and $C_2(x_2, y_2, 0)$ be their projections.
- Distances of C_1 and C_2 from the theoretical location of the axis in the DRF XY plane $C_{th}: (X_C, Y_C, 0)$ are computed. The longest of the two distances estimates b , the radius of the tolerance cylinder (Fig. 5.26).

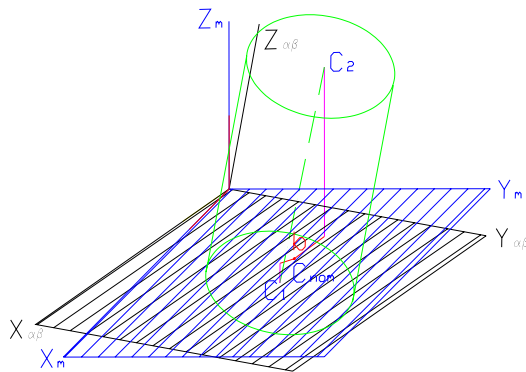


Fig. 5.26. Estimation of the radius of the tolerance cylinder, b .

5.3.6.2. At RFS and surface interpretation

From (5.3) position error is $t = 2(r_{am} - b')$, where r_{am} is the actual mating radius and b' is the radius of the maximum size cylinder, that, being in

the theoretical hole axis location, is still inscribed into the hole (Fig. 5.27).

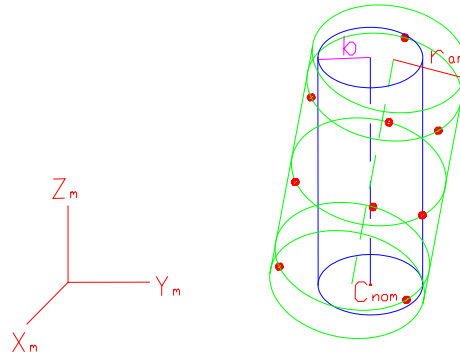


Fig. 5.27. Actual mating envelope (radius r_{am}) and tolerance cylinder (radius b').

Computation of r_{am} has been described in the previous section. Radius b' can be estimated as follows.

- Probed points are projected onto DRF XY plane. Then maximum size circumference inscribed in the projected points is computed, according to one of three methods that we will describe at the end of this chapter. This circumference, with centre $C_t:(x_t, y_t, 0)$ and radius r_t , is displayed in red in Figure 5.28.
- A circumference with centre in the hole axis theoretical location $(X_C, Y_C, 0)$ and tangent to the maximum enveloping circumference is found (green circle in Fig. 5.28). Its radius, b' , is computed as:

$$b' = r_t - \text{dist}(C_C - C_t) = r_t - \sqrt{(X_C - x_t)^2 + (Y_C - y_t)^2} \quad (5.16)$$

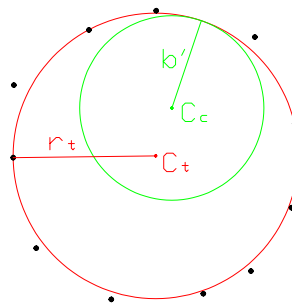


Fig. 5.28. Computation of b' .

5.3.6.3. At MMC and resolved geometry interpretation

From (5.11) position error is $t = 2(b - (r_{am} - r_{mmc}))$, where b is the radius of the tolerance cylinder, r_{am} is the radius of the actual mating envelope and r_{mmc} the minimum size of the hole radius allowed by the dimensional tolerance (Fig. 5.29). The procedure described in section 5.6.3.1 provides the computation of both b and r_{am} .

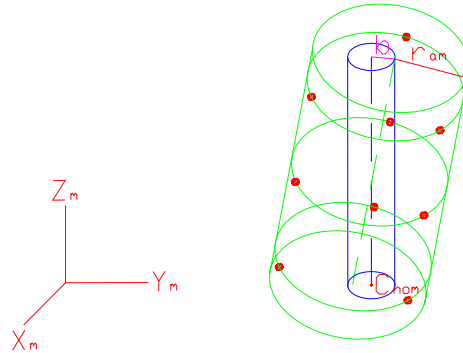


Fig. 5.29. Tolerance cylinder (radius b) and actual mating envelope (radius r_{am}).

5.3.6.4. At MMC and surface interpretation

From (5.7) position error is $t = 2(r_{mmc} - b')$, where r_{mmc} is the minimum size of the hole radius allowed by the dimensional specifications and b' is the radius of the maximum size cylinder, that, being in the theoretical hole axis location, is still inscribed into the hole (Fig. 5.30). The procedure described in section 5.6.3.2 provides the computation of b' .

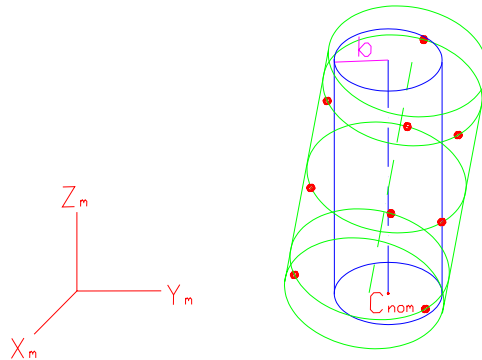


Fig. 5.30. Tolerance cylinder (radius b').

5.4. Algorithms for estimating the circumference inscribed in n points

To estimate the largest size circumference inscribed in n points lying on the same plane, three algorithms have been implemented.

1. Method based on the geometrical property of circles (P1).

Since only one circumference passes through three points, the method finds the circles passing through all subsets of three points from the set of n points. Thus $\frac{n!}{3!(n-3)!}$ circles are obtained, which are sorted by radius

size in descending order. Hence, the first circle in the ordered list satisfying the condition that all n points are distant from its centre not less than its radius is the desired circle. In order to prevent from possible wrong estimates it is necessary to impose that the centre of the circles be close to the barycentre of point set, see Figure 5.31.

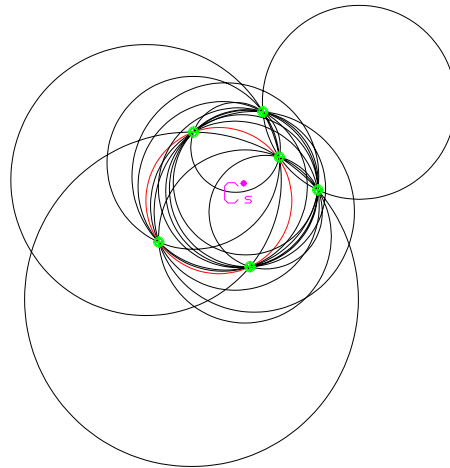


Fig. 5.31: Maximum inscribed circle: method based on the geometrical property (P1).

2. Method based on Non-Linear Optimization (P2).

First the barycentre, C_s in Figure 5.32, of the n -point set is calculated. Then an optimization routine, starting with a circumference centred in the barycentre, search for the largest inscribed circumference by iteratively modifying centre and radius of the current circumference.

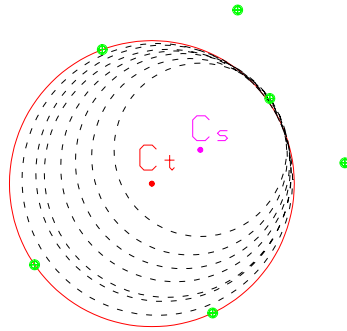


Fig. 5.32. Maximum inscribed circle: method based on the Non-Linear Optimization (P2).

3. Method based on Orthogonal Least Square (P3).

OLS method is applied to n point set to find an OLS circumference centred in the point set barycentre. Then the circle is uniformly shrunk around its centre until all n points are left out.. Notice that at least one point will be on the circumference (Fig. 5.33).

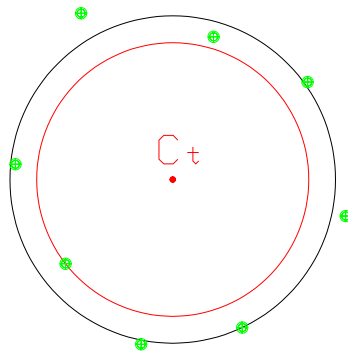


Fig. 5.33. Maximum inscribed circle: method based on the Orthogonal Least Squares (P3).

5.5. Results

A baseline application of the methodology to an ideal part with no form error is described in the following. Nominal geometry is as in Figure 5.1 with $l_u=l_a=200\text{mm}$; other dimensions may vary. Errors in the measurement of the coordinates of the part are assumed i.i.d. Normal random variables with uniform size all over the part, i.e. $\mu_\varepsilon=0$ and $\Sigma_\varepsilon=\sigma^2 I_3 \forall P_{vp}$, where I_3 is the identity matrix of dimension 3. Although the

hypothesis is often unrealistic, the study is expected to reveal the more distinctive features of process design. The design factors considered are sampling strategy (number and location of points) on planar datums and the cylindrical holes, the estimation method and the tolerance interpretation criterion. Factors that are not subject to design but affect the design solution (blocking factors) are the material condition, the error standard deviation σ and the part geometry parameters. Point location on planes is dictated by a sampling mechanism: pure random, stratified random, stratified non random. In the latter scheme external points are moved towards the face edges in order to maximise coverage; we name this scheme “factorial” for the similarity with point locations in a full factorial design. Points on cylindrical surfaces follow a stratified non-random sampling and a uniform distribution on uniformly separated cross sections. Estimation method of the substitute geometry is Orthogonal Least Squares (OLS) for planes and both OLS and Minimum Zone (via non linear optimisation) for cylinders. Technical details on OLS can be found in Vicario, G. and Romano, D.,2002.

5.5.1. DRF analysis

The first analysis refers to the uncertainty in the position of the DRF origin, namely the intersection of datums A, B and C. As only the estimation of three planar datums is required, factors are the sampling method and the sample size (4-9-16 points per plane). A 34 full factorial experiment, with 104 Monte Carlo replications ($\sigma=0.005$ mm), is run and the square root of the trace of the covariance matrix of the DRF coordinates, $(\sigma_x^2 + \sigma_y^2 + \sigma_z^2)^{\frac{1}{2}}$, is the relevant measure of uncertainty. For comparison purpose this measure is normalised with respect to the value corresponding to the basic 3-2-1 strategy (3 points for datum A, 2 for B, 1 for C) usually applied in the practice. How much each sampling method reduces the 3-2-1 uncertainty can be appreciated in Figure 5.34. As figures are averaged over all the combinations of 4,9,16 points on the planes, they correspond to an average of nearly 10 points per plane (the 3-2-1 scheme has only 2). The factorial sampling is by far preferable as it cuts the 3-2-1 uncertainty by a factor 12. Thus maximum surface coverage appears a rewarding criterion. An interesting result is that the patterns of sample size effects are discrepant in the three schemes. Although it always occurs that a larger sample size reduces uncertainty and that n_A affects uncertainty more than n_B and n_B more than n_C these effects are approximately in the ratio 10:4:1 for pure random sampling,

14:3.7:1 for stratified random sampling, 4:2.5:1 for factorial sampling. The best scheme tends to mitigate the difference in the information content attributable to points measured on the three planes. Another important result is that there is substantial correlation among the DRF coordinates as generated by the degrees of freedom lost in the estimation of datums B and C because of the orthogonality constraints. A geometric interpretation of this is provided in Romano, D., and Vicario, G., 2003. This will have implications on the position error uncertainty. Finally, we point out that, since the application of the envelope principle entails an outward rigid translation of the OLS plane, the DRF origin is biased.

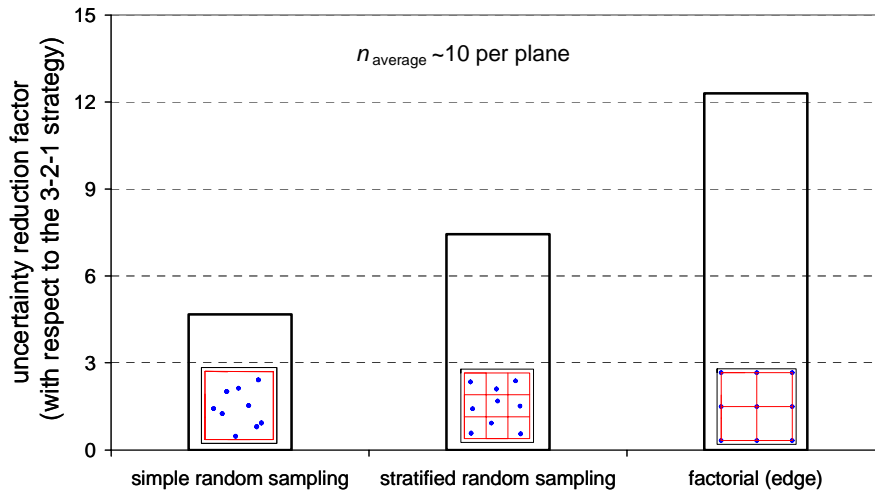


Fig. 5.34. Uncertainty on the DRF origin. The measure of uncertainty

is $\left(\sigma_x^2 + \sigma_y^2 + \sigma_z^2\right)^{\frac{1}{2}}$, where the variance terms refer to the DRF Cartesian coordinates. Numbers are the ratio between the uncertainty for the deterministic 3-2-1 scheme and the one for the sampling method considered.

5.5.2. Position error analysis

It is useful, although the standards does not do it, to define the position error \bar{e}_p as a planar vector on datum A (see Fig. 5.35). Basing on the vectorial interpretation of the position error an even more appropriate measure of uncertainty can be defined.

By making the polar transformation $\bar{e}_p = \rho e^{i\theta}$ a suitable measure of uncertainty is the area of the conjoint confidence region of the two-dimensional random variable (ρ, θ) at the $(1-\alpha)\%$ confidence level, say $I_{1-\alpha}$.

It is possible to find a boundary $\rho(\theta)$, with $0 \leq \theta \leq 2\pi$ of $I_{1-\alpha}$ by using conditional distribution $f_{\rho|\theta}$ and marginal f_θ :

$$\int_I f_{\rho,\theta}(r,t) dr dt = \int_0^{2\pi} \int_0^{\rho(\theta)} f_{\rho|\theta}(r,t) f_\theta(t) dr dt = 1 - \alpha \quad (5.17)$$

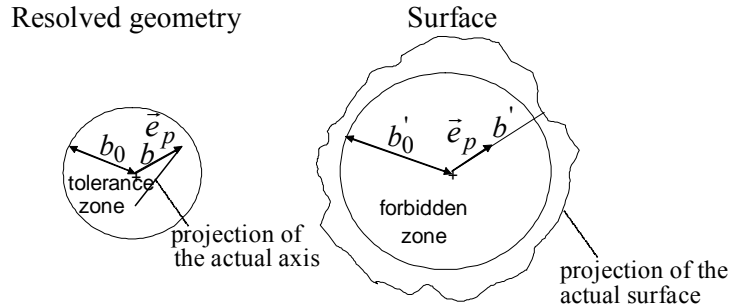


Fig. 5.35. Interpretation criteria of the position tolerance of a cylindrical hole in the plane of datum A. In both cases a position error \bar{e}_p can be defined as a planar vector.

The previously defined position error is analysed here. Firstly, two qualitative design factors, the tolerance interpretation criterion and the estimation method, and one blocking factor, the material condition, are scrutinised. This makes the whole exposition clearer and simplifies the successive analysis of the sampling strategy factors that is done for the best setting of the design factors found at this first stage. Another full factorial (23 with 104 replications) is run and the uncertainty measure is the standard deviation of $2 \cdot |\bar{e}_p|$. Sampling strategy is fixed for the planes (factorial sampling, $n_A = n_B = n_C = 9$) and the hole (stratified non-random sampling, $n_H = 9$). The Pareto chart of the effects is reported in Figure 5.36, together with the explanation of factors and levels. The important result is that the surface interpretation produces an uncertainty that is, on average, nearly 3σ smaller than that for the resolved geometry interpretation. The reason is that it does not require the estimation of the actual hole axis, which is numerically awkward, but only the radius of enveloping circles. The other main effects are much smaller: OLS yields more uncertainty than the minimum zone (but it is computationally ten times faster) and MMC more than RFS. The first fact is explained by a larger uncertainty on b' and r_{am} determined by the enveloping operation that follows the estimation of the OLS circle; the second fact derives from the additional uncertainty due to the estimation of r_{am} needed in the

RFS condition.

Now the sampling strategy factors are analysed in conjunction with the geometrical parameters of the part and the error size whereas the interpretation criterion is “surface”, the estimation method is OLS and the material condition is MMC. Table 5.5 reports factors and their range. The design is a Central Composite Design in the 3-level factors (273 runs) crossed with a full factorial in the 2-level factors (8 runs); the resulting 2184 runs are again replicated 104 times. The uncertainty measure used here is the area of $I_{0.95}$, say $A_{0.95}$. In Figure 5.37 (above) the normal probability plot of the effects of the corresponding 2-level factorial is shown.

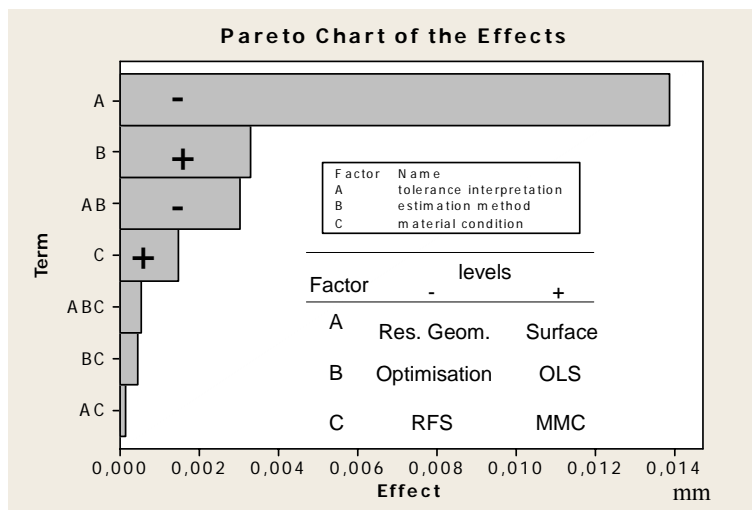


Fig. 5.36. Factorial effects on uncertainty of the position error. The measure of uncertainty is the standard deviation of $2 \cdot \left| \bar{e}_p \right|$.

We see the high leverage of the error standard deviation σ and also its significant interactions with sample sizes n_H , n_A , n_B ; this fact proves that the use of a linear estimation method like ordinary least squares, that would lead to a separation between the effects of sampling error and measurement error on uncertainty, is grossly approximated. Convenience of the factorial sampling for planes is confirmed while the two sampling methods for the hole are practically equivalent. Other large main effects are n_H , n_A , n_B in the order. Note also the large interaction $S_{\pi} \cdot n_A$. To better appreciate it let us restrict to the sub-case where the sampling method on the planes is “factorial” and $\sigma=0.005$. Surprisingly the effect of n_A is much smaller than before; both n_B , and n_C prevail. This is partly due to

the factorial sampling that tends to equalise the effects of sample size on the three planes, as already noted for the DRF uncertainty. But it is also the consequence of the fact that, since position error is evaluated by orthogonally projecting the actual hole axis or the surface on datum A, an erroneous estimate of datum A is partly compensate. On the other hand, errors in the estimate of datum B and C are directly transformed in errors of the nominal location of the hole axis as this is obtained by translating, on datum A, the DRF origin orthogonally to B by X_C and orthogonally to C by Y_C . Also the plate thickness h is significant, alone and in interaction with n_A .

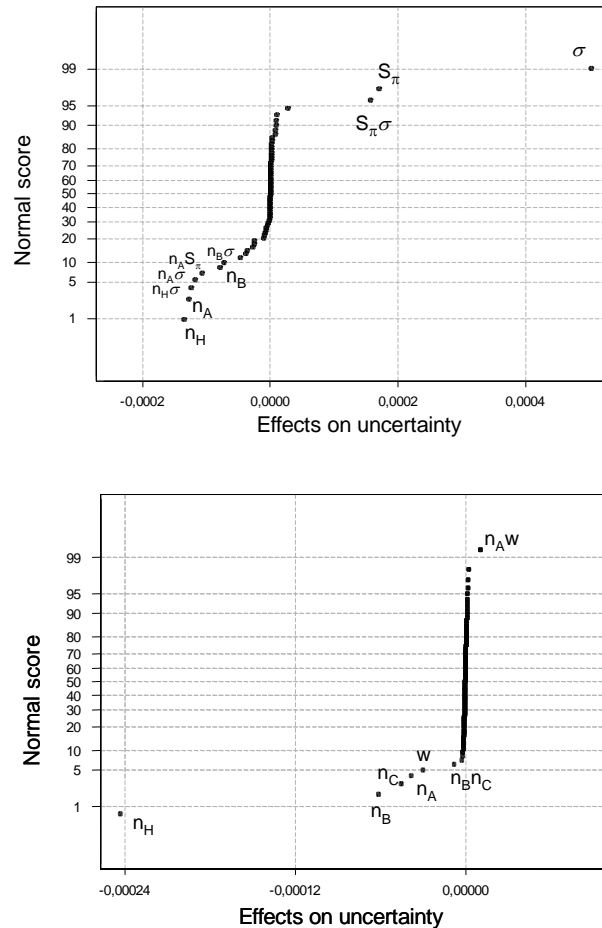


Fig. 5.37. Factorial effects on uncertainty of the position error. The measure of uncertainty is the area of the 95% confidence region of \vec{e}_p . Above: all factors in Table 5.5 are active; below: S_π , S_H and σ are fixed at “factorial”, “stratified non-random sampling” and 0,005 mm respectively.

Table 5.5. Factors and levels in the last experiment.

<i>Symbol</i>	<i>Control factors</i>	<i>Levels</i>		
n_A, n_B, n_C, n_H	Number of points measured on surfaces A, B, C and on the hole	4	9	16
S_π	Sampling method on A, B, C	Stratified random		Factorial
S_H	Sampling method on the hole	Stratified non-random sampling	Uniform on equispaced cross-sections	
<i>Blocking factors</i>				
h [mm]	Plate thickness	25	50	75
X_C [mm]	Horizontal boxed dimension	50	100	150
Y_C [mm]	Vertical boxed dimension	50	100	150
d [mm]	Hole diameter	25	50	75
σ [mm]	Error standard deviation	0.001	0.005	0.01

The examination of the computed 95% confidence regions of \vec{e}_p reveals that they are affected by a directional bias. This no surprise since a preferential direction was already noted for the DRF origin. A sample of confidence regions for different hole locations, i.e. different combinations of X_C and Y_C , are plotted in Figure 5.38. Interestingly the hole location does not exhibit any influence on the size of the uncertainty but does affect the orientation of its spatial distribution. This fact leads to the proposal of a more accurate acceptance rule for the tolerance which takes into account the (inexpensive) information on the measured angle of the position error. By centring the confidence region on the measured position error \vec{e}_{pm} , the following statistical acceptance rule can be formulated:

$$\max_{\gamma} |\vec{e}_{pm} + \vec{e}_{\gamma}| \leq \frac{t_0}{2} \quad (5.18)$$

where \vec{e}_{γ} is a vector departing from the centre of the confidence region towards a point on the boundary γ . The more biased the confidence region the more precision is gained in the control with respect to a rule independent of the error angle. Figure 5.39 illustrates the logic of the

statistical rule.

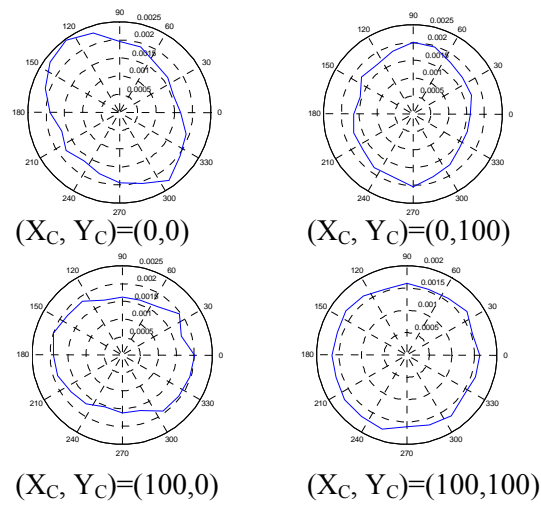


Fig. 5.38. 95% confidence regions for different hole locations in the DRF. Other factors are fixed (interpretation: surface; estimation method: OLS; material condition: MMC; $h=20\text{mm}$; $d=50\text{mm}$).

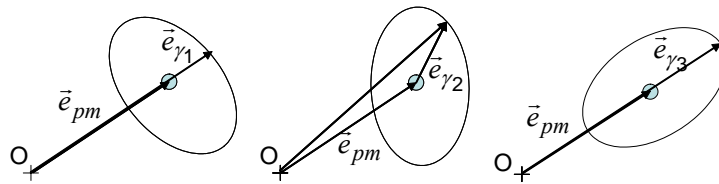


Fig. 5.39. Geometrical interpretation of the statistical acceptance rule of the position tolerance. Three cases are shown where the measured position error is unchanged and the confidence region has three different orientations: different

$$\max_{\gamma} |\vec{e}_{pm} + \vec{e}_{\gamma}| \leq \frac{t_0}{2} \text{ result.}$$

5.5.3. Final remarks

In the dissertation the use of the statistical analysis of uncertainty for the purpose of designing the measurement process is demonstrated for the position tolerance control on CMM. From the study a number of findings and considerations can be drawn.

1. In the case of position tolerance the problem of “methods divergence” appears very relevant. The statistical analysis reveals that the control procedure dictated by the standard leads to undesired characteristics of the geometric error (systematic bias, loss of the central symmetry).
2. The “surface” criterion for tolerance interpretation is highly preferable as it reduces uncertainty. The mix of hardware and software operations is typical of modern metrology and the soft choices, like the interpretation criterion here, may impact measurement quality more than the hardware ones.
3. The criterion of maximal coverage when probing the planar surfaces has proved effective in limiting the uncertainty. However, one should bear in mind that, in presence of form error on the part, the location of the most informative points may well change. Hence, the methodology should be applied on a virtual part incorporating the known form error.
4. A vectorial position error has been introduced. Basing on it a more consistent analysis of uncertainty is done and a statistical acceptance rule, which exploits the information on the error direction, is stated.
5. Contrarily to the common belief that it is convenient to probe more points on the primary planar datum, the analysis has shown that, in some instances, a good estimate of the secondary and tertiary datums is more beneficial for the reduction of the uncertainty of the position error.
6. OLS estimation which is generally considered more robust than other estimation methods, like the minimum zone algorithms, is not necessarily so when the envelope principle is eventually applied.
7. Thorough experimental studies are necessary to validate the findings and their generality. As an example, the hypothesis that the size of the measurement error is uniform on the part is certainly too restrictive. A realistic distribution of the measurement error on the part should be assessed through an intensive experimental characterisation, possibly exploiting the methods of uncertainty evaluation that are currently being proposed in the ISO/TS 15530 standards.

REFERENCES CHAPTER 5

- CAPELLO, E. AND SEMERARO, Q., 2001, "The harmonic fitting method for the assessment of the substitute geometry estimate error. Part II: statistical approach, machining process analysis and inspection plan optimisation ", *Int. Jou. of Machine Tools and Manufacture*, vol. 41, pp. 1103-1129.
- DOWLING, M.M., GRIFFIN, P.M., TSUI, K.-L. AND ZHOU, C., 1997, "Statistical Issues in Geometric Feature Inspection Using Coordinate Measuring Machines", *Technometrics* 39, no. 1, pp. 3-24.
- FENG, C. J., SAAL, A. L., SALSURY, J. G., NESS, A. R., LIN, G. C. S., 2006, "Design and analysis of experiments in CMM measurement uncertainty study", *Precision Engineering*, in press.
- LIN, Z.C., CHEN, C.C., 1997, "Study of the automatic planning of measurement points with basic element features", *Int. Jou. of Production Research*, vol. 35, no. 11, pp. 3157-3178.
- SUMMERHAYS, K. D., HENKE, R. P., BALDWIN, J. M., CASSOU, R. M., AND BROWN, C. W., 2002, "Optimizing discrete point sample patterns and measurement data analysis on internal cylindrical surfaces with systematic form deviations", *Precision Engineering*, no. 26, pp. 105-121
- SUN, A. Y. T., ANAND, S., TANG, J. S. Y., 2002, "Comprehensive design of experiments-based framework for optimal CMM inspection and uncertainty analysis of form tolerances", *Int. Jou. of Production Research*, vol. 40, no. 9, pp. 2097-2123
- ROMANO, D., AND VICARIO, G., 2003, "Assessing Part Conformance by Coordinate Measuring Machines", *Proc. of ESREL 2003 - European Safety and Reliability Conf.*, Maastricht (NL), June, T. Bedford and P.H. van Geldereds., Balkema Publishers, Lisse (NL), 1329-1336.
- VICARIO, G. AND ROMANO, D., 2002, "Inspecting Geometric Tolerances: Uncertainty In Position Tolerances Control On Coordinate Measuring Machines", *SMA (Statistical Methods & Applications)*, vol. 11 no. 1, Springer Verlag, Berlin Heidelberg (DE), 83-94.

6. APPLICATION TO FLATNESS TOLERANCES

According to ASME 14.5M (1995: 161-162), a form tolerance specifies a tolerance zone of minimum size defined by two parallel geometric features within which the actual feature must lie. However, the current standard does not provide guidelines for CMM inspection and verification of form tolerance. Decision made by CMM users about the sampling method, the number of probed points, and the form-fitting criterion are usually based on a purely economic criterion regardless of the possible implications on the accuracy of the result of the tolerance control. Typically very few points are probed according a very simple sampling strategy and the form error is calculated by the simplest form-fitting criterion. In such circumstances, the form error computed by the CMM software is prone to be affected by significant bias and uncertainty, particularly when the feature exhibits large and systematic form deviations. One possible countermeasure is to use model-based estimation of the geometric error, which requires that some form of a-priori knowledge of the surface error is available. In this chapter we apply the design methodology presented in chapter 4 to flatness tolerance. Differently from the application to position tolerance, here we also consider possible systematic form deviations of the feature. Its extension to straightness tolerance is straightforward. Finally, a new method is proposed for designing small-size inspection plans which also allow for an accurate estimation of flatness (or straightness) error. The method, based on the construction of a parametric model of the actual feature, directly accounts for possible systematic form deviations of the surface (or line).

6.1. Related work

Previous research analyzed the critical sampling strategy factors in a piece- or block-wise design (Dowling et al. 1995, Lee and Mou 1997, Choi et al. 1998). Conclusion drawn from these approaches were case-oriented and did not consider all the relevant factors simultaneously; therefore, they could not lead to generalized CMM inspection guidelines. The form-fitting criterion effect was usefully isolated from the model and the accuracy level was often predetermined whit certain assumptions leading to a non-integrated approach. Recent research on CMM inspection methods have been aimed at developing CMM inspection guidelines so as to combine factors such as form-fitting criterion; sampling method; simple size; type of form error due to various

manufacturing processes; and CMM measurement uncertainty. Sun and Anand (2002) establish a DOE-based framework to verify the estimation of flatness error using for the design, analysis and optimization of CMM inspection tasks. They use three levels for simple size, two form fitting criterion (normal least square and minimum zone) and three sampling methods (random, stratified and equispaced). As presented by Dowling et al. (1995) and Timoshenko (1959), they categorize and model the surface form error, which simulate different residual effects of the surface after machining.

More recently, attention is in experimenting new sampling methods and strategies for the identification of the characteristics of a surface resulting from a manufacturing process. Other sampling options for planar features are Hammersley sequence and Halton-Zaremba sequence (Woo, T.C. at al., 1995). As one strategy performs better than the others in a particular case, but the choice is largely a matter of convenience. Tabu search and hybrid search are employed in Badar at al.(2003), where an optimization search method is proposed. Result is that the number of points sampled is potentially less than that typically used to achieve the same accuracy. Raghunandan at al. (2006) use the LS (Least Squares) approach for flatness error estimation and by mean of a special search technique to arrive at the reduced sample size based on a surface error prediction model. Both previous works do not use an explicit model of the manufacturing process. At the end of this chapter we propose a new model-based approach competing with the last two. The approach is aimed at designing small-size inspection plans capable of producing accurate estimates of flatness and straightness errors.

6.2. Sample- based estimation of flatness error

As prescribed by ASME Y14.5 standards and already reported in chapter 1, the flatness tolerance specifies that all points of the surface must lie in some zone bounded by two parallel planes which are separated by not more than the specified tolerance t_0 . Ideally, the computational problem involved by the definition, is the search for the orientation of the pair of parallel planes enclosing the actual surface which assures the minimum distance, say t_R between the planes. Thus the tolerance specification is met if $t_R \leq t$. The following sub-sections are dedicated to the description of the most common sample-based methods for the estimation of flatness error. They are, in the order of presentation: Orthogonal Least Squares (OLS) method, Boundary Planes method, Convex-Hull method,

Reference Frame Changing method. Notice that the same methods can be also applied to estimate straightness error. As the latter is defined as the minimum distance between two parallel lines enclosing the feature, straightness tolerance is the two-dimensional equivalent of flatness tolerance. In this work two of the four estimation methods described are used. They are the OLS method and the Convex-Hull method, which are also the most frequently applied in industrial applications and in the scientific literature.

6.2.1. Orthogonal Least Square method

Given a set of points $P_i(x_i, y_i, z_i)$ resulting from a surface sampling, a plane can be fitted by multiple linear regression (single linear regression would apply to a two-dimensional set for straightness). The underlying method is ordinary Least Squares (LS). This would assume that two of the three coordinates are the independent variables (assumed to be without error) and the remaining coordinate is the dependent variables (assumed to have a random error), e.g. $z=f(x,y)$. However this conceptual distinction is by no mean evident for coordinates of a point sample. The main reason is that all the three point coordinates are affected by a measurement error. Therefore a modified version of ordinary LS method can be usefully adopted in this case: the Orthogonal Least Squares (OLS) method. Peculiarity of the OLS method is that the sum of the squared distances between sampled points and the OLS plane is minimized. This is a not the case of ordinary LS method where the sum of squared deviations in the direction of the dependent variable is minimized (e.g. $z_i - f(x_i, y_i)$). A major implication is that non linear regression is required for OLS. The mathematics of OLS is now summarized. The equation of a plane may be written in the form:

$$ax + by + cz + d = 0 \quad (6.1)$$

Assuming that the inspected surface is parallel to the XY plane, equation (6.1) can be arranged in the form:

$$z = \beta_0 + \beta_1 \cdot x + \beta_2 \cdot y \quad (6.2)$$

where

$$\beta_0 = -\frac{d}{c}, \quad \beta_1 = -\frac{a}{c}, \quad \beta_2 = -\frac{b}{c}.$$

Estimation of the OLS plane requires to identify the unknown parameters, β_0 , β_1 , and β_2 such that the sum of squares of the orthogonal deviations e_i between points P_i and the plane

$$\sum_i [e_i(\beta_0, \beta_1, \beta_2)]^2 \quad (6.3)$$

is minimized. Distances e_i in (6.3) are given by:

$$e_i = \frac{(z_i - \beta_0 - \beta_1 x_i - \beta_2 y_i)}{\sqrt{1 + \beta_1^2 + \beta_2^2}} \quad (6.4)$$

Parameters β_0 , β_1 , and β_2 , result from the solution of an unbounded optimization problem. Once the OLS plane is available, the two parallel planes required by the flatness definition are simply obtained by shifting the OLS plane both upward and downward until the points with the highest e_i and the lowest e_i respectively are enclosed by the two planes (see, Fig. 6.1). Therefore the resulting flatness error is the distance between the planes, namely:

$$t_R = \max_i e_i(\beta_0, \beta_1, \beta_2) - \min_i e_i(\beta_0, \beta_1, \beta_2) \quad (6.5)$$

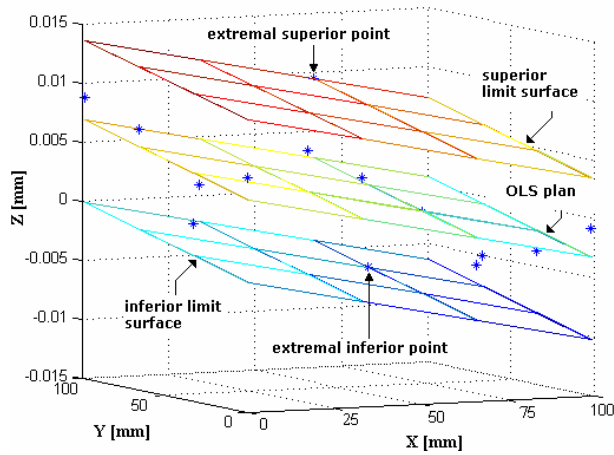


Fig. 6.1. Tolerance zone determined by the OLS method

The method, being simple and fast to compute, is the most widely used in the industrial practice. However it offers no guarantee that no other error computed by a different method is lower than the error computed by OLS. Yet it is very likely that equation (6.5) overestimates flatness error, see for example Figure 6.2. Anyway this is not necessarily bad given that sample-based evaluation of flatness generally underestimates the true flatness error of the inspected surface.

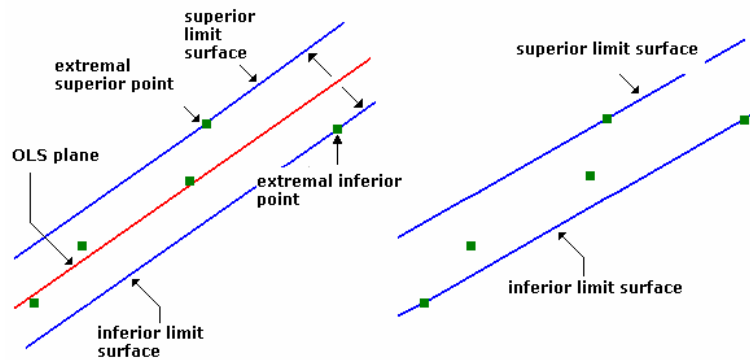


Fig. 6.2: OLS method overestimates flatness error of the point sample.

6.2.2. Boundary Planes method

The Boundary Planes method conforms more closely to the principle of “minimum zone” inherent to the definition of flatness (or straightness) than the OLS method does. The logic of the method is to identify the pair of parallel planes by letting them pass through extremal points of the sample (Takamasu et al., 1999). Let e a set of N probed points P_i be the result of a sampling of a surface nominally parallel to the XY plane. Therefore the z -coordinate deviations from the nominal plane are responsible for the form error. The assumption of the method is that the pair of parallel planes enclosing the minimum zone will be orthogonal to either XY plane or YZ plane. Then, given this constraint, each boundary plane is uniquely determined by imposing that two points of the sample belong to the plane. However, the orthogonality constraint, although it simplifies the computation, is indeed a limitation. Likewise OLS also the Boundary Planes method tends to overestimate the flatness error of the point sample. A step-by-step description of the method is provided below.

1. Identify the two sheaves of planes whose axis is parallel to x

direction and passing through the points having the maximum z ($P_N(x_{P_N}, y_{P_N}, z_{P_N})$) and the minimum z ($P_1(x_{P_1}, y_{P_1}, z_{P_1})$) respectively (see Fig. 6.3). The defining equations for the sheaves are respectively:

$$\lambda(z - z_{P_N}) + \mu(y - y_{P_N}) = 0 \text{ and } \lambda(z - z_{P_1}) + \mu(y - y_{P_1}) = 0 \quad (6.6)$$

2. (Analogous to step 1.) Identify the two sheaves of planes whose axis is parallel to y direction and passing through the points having the maximum z and the minimum z respectively. The defining equations for the sheaves are respectively:

$$\lambda(z - z_{P_N}) + \mu(x - x_{P_N}) = 0 \text{ and } \lambda(z - z_{P_1}) + \mu(x - x_{P_1}) = 0 \quad (6.7)$$

3. From the two sheaves defined at step 1. select two planes: one plane passing through the point with the second highest z ($P_{N-1}(x_{P_{N-1}}, y_{P_{N-1}}, z_{P_{N-1}})$) and another plane passing through the point with the second lowest z ($P_2(x_{P_2}, y_{P_2}, z_{P_2})$). The two planes, denoted by SUP_X and INF_X , are displayed in Fig. 6.4. They are obtained by rotating the planes $z - z_{P_N} = 0$ and $z - z_{P_1} = 0$ (belonging to the two sheaves) around the respective shief axis (parallel to x direction) by the angles γ_1 and γ_3 respectively.
4. (Analogous to step 3.) From the two sheaves defined at step 2. select two planes: one plane passing through the point with the second highest z ($P_{N-1}(x_{P_{N-1}}, y_{P_{N-1}}, z_{P_{N-1}})$) and another plane passing through the point with the second lowest z ($P_2(x_{P_2}, y_{P_2}, z_{P_2})$). The two planes, denoted by SUP_Y and INF_Y , are obtained by rotating the planes $z - z_{P_N} = 0$ and $z - z_{P_1} = 0$ (belonging to the two sheaves) around the respective shief axis (parallel to y direction) by the angles γ_2 and γ_4 respectively.

Defining equations for the four rotation angles are:

$$\gamma_1 = ar \cos \left[\frac{(y_{P_{N-1}} - y_{P_N})}{\sqrt{(z_{P_N} - z_{P_{N-1}})^2 + (y_{P_{N-1}} - y_{P_N})^2}} \right]$$

$$\begin{aligned} \gamma_2 &= ar \cos \left[\frac{(x_{P_{N-1}} - x_{P_N})}{\sqrt{(z_{P_N} - z_{P_{N-1}})^2 + (x_{P_{N-1}} - x_{P_N})^2}} \right] \\ \gamma_3 &= ar \cos \left[\frac{(y_{P_1} - y_{P_2})}{\sqrt{(z_{P_2} - z_{P_1})^2 + (y_{P_1} - y_{P_2})^2}} \right] \\ \gamma_4 &= ar \cos \left[\frac{(x_{P_1} - x_{P_2})}{\sqrt{(z_{P_2} - z_{P_1})^2 + (x_{P_1} - x_{P_2})^2}} \right] \end{aligned} \quad (6.8)$$

5. From each of the boundary planes obtained at steps 3., SUP_X and INF_X , obtain a pair of parallel planes enclosing the point sample. The first pair is made up of SUP_X and a plane parallel to it and passing through P_1 . The second pair is made up of INF_X and a plane parallel to it and passing through P_N . Denote by t_1 and t_3 the distances between the planes in each pair respectively. For instance equation for t_1 is:

$$t_1 = \frac{(z_{P_N} - z_{P_{N-1}})(y_{P_1} - y_{P_N}) + (y_{P_{N-1}} - y_{P_N})(z_{P_1} - z_{P_N})}{\sqrt{(z_{P_N} - z_{P_{N-1}})^2 + (y_{P_{N-1}} - y_{P_N})^2}} \quad (6.9)$$

6. (Analogous to step 5.) From each of the boundary planes obtained at steps 4., SUP_Y and INF_Y , obtain a pair of parallel planes enclosing the point sample. The first pair is made up of SUP_Y and a plane parallel to it and passing through P_1 . The second pair is made up of INF_Y and a plane parallel to it and passing through P_N . Denote by t_2 and t_4 the distances between the planes in each pair respectively.
7. The flatness error is determined as the minimum among distances t_1 , t_2 , t_3 , t_4 .

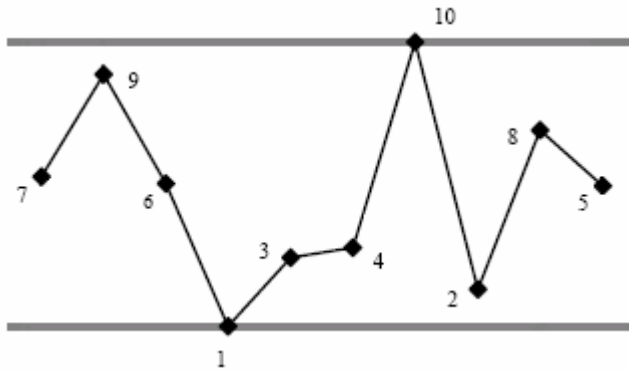


Fig. 6.3. Example of probed points projected on YZ plane (y is the horizontal direction, z is the vertical one). The two bold lines represent two sheaves of planes parallel to y direction and passing through P_N (point 10) and P_I (point 1) respectively.

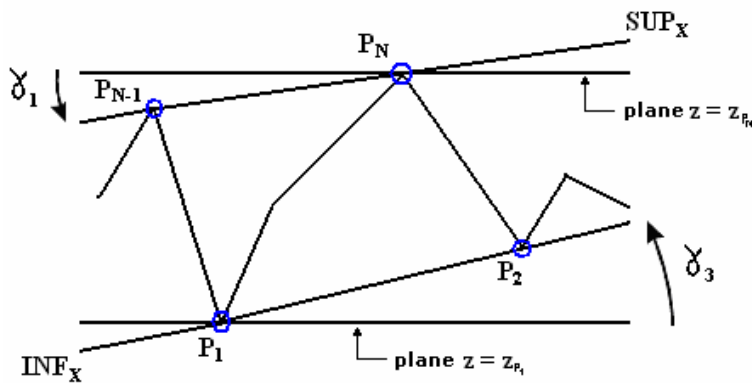


Fig. 6.4: Projection of tolerance zone on YZ plane and representation of the boundary planes SUP_X and INF_X . Also rotation angles γ_1 and γ_3 are indicated.

6.2.3. The Convex Hull method

In mathematics, the convex hull or convex envelope for a set of points X in a real vector space V is the minimal convex set containing X . (Note that X may be the union of any set of objects made of points).

To show this exists, it is necessary to see that every X is contained in at least one convex set (the whole space V , for example), and any intersection of convex sets containing X is also a convex set containing X . It is then clear that the convex hull is the intersection of all convex sets containing X , which is an alternative definition.

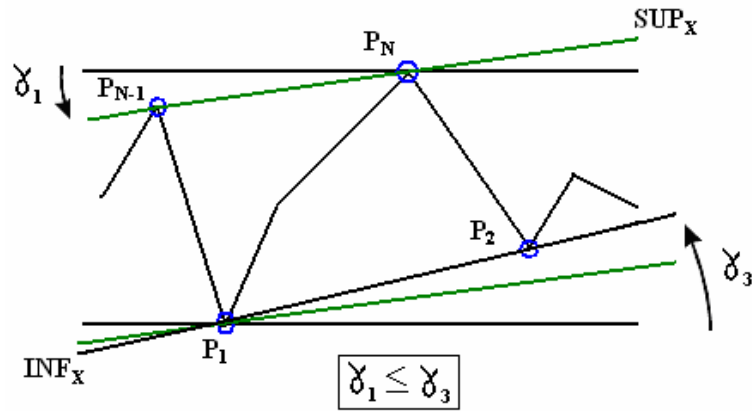


Fig. 6.5: Construction of the tolerance zone formed by the plane SUP_X and a plane parallel to it and passing through P_1 . The two planes are separated by the distance t_1 .

More directly, the convex hull of X can be described constructively as the set of convex combinations of points from X : that is, the set of points

of the form $\sum_{j=1}^n t_j x_j$, where n is an arbitrary natural number, the numbers

t_j are non-negative and sum to 1, and the points x_j are in X . It is simple to check that this set satisfies either of the two definitions above. In fact, if X is a subset of an N -dimensional vector space, sums of up to $N+1$ points are sufficient in the definition above. This is equivalent to saying that the convex hull is the union of all simplexes with vertices in X . This is known as Carathéodory's theorem. The convex hull is defined for any kind of objects made up of points in a vector space, which may have any number of dimensions. The convex hull of finite sets of points and other geometrical objects in a two-dimensional plane or three-dimensional space are special cases of practical importance. As explained later they are used for the estimation of straightness and flatness errors respectively.

Different algorithms exist to implement the convex hull problem. In two and three dimensions, specialized algorithms exist with complexity $O(n \ln n)$ (Skiena 1997, pp. 351-352). Yao (1981) has proved that any decision-tree algorithm for the two-dimensional case requires quadratic or higher-order tests, and that any algorithm using quadratic tests (which includes all currently known algorithms) cannot be done with lower complexity than $O(n \ln n)$. However, it remains an open problem whether better complexity can be obtained using higher-order polynomial tests (Yao 1981). Yao's analysis applies to the hardest cases, where the

number of vertices n is equal to the number of vertices in the hull h . In easier cases where $h < n$, the bound of $O(n \ln n)$ can be improved to $O(n \ln h)$ (Chan 1996). O'Rourke (1997) gives a robust two-dimensional implementation as well as an $O(n^2)$ three-dimensional implementation. The Qhull method works efficiently in 2 to 8 dimensions (Barber et al. 1997).

In this work we use the “*convhulln*” Matlab function, based on the Qhull algorithm and Delaunay triangle theory (see Fig. 6.6).

This is the procedure to compute flatness (or straightness) error. From the point sample the sub-sample containing the vertices of the polyhedron defining the convex hull of the sample is obtained, by means of the *convhulln* function. Then, for each triangular face of the polyhedron, the distances between that face and each vertex of the convex hull is computed and the largest is saved. Among the set of the largest distances the smallest distance is picked: it represents the estimated flatness (or straightness) error t_R . Its expression is:

$$t_R = \min_j \max_i d_{ij} \quad (6.10)$$

where index j designates the faces of the convex hull and i its vertices.

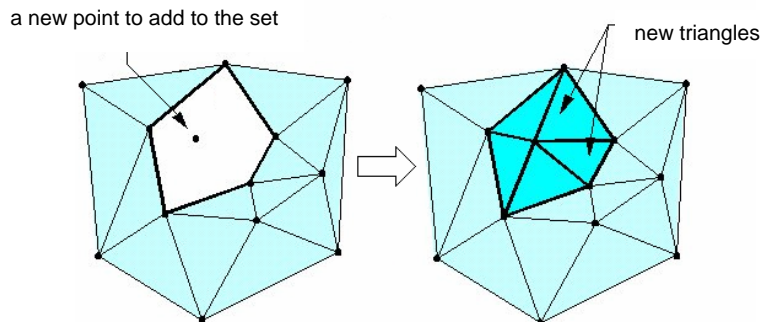


Fig. 6.6: Iterative construction of the convex hull 3D polyhedron.

6.2.4. Reference frame changing method

Finally we report a brief mention of another method which has been proposed in the literature (Kwon, O., Wu, J.-L., 1999). It is based on the minimum zone principle and requires the resolution of an optimization problem.

The idea is to move a generic pair of parallel planes in order to enclose the point sample within a minimum zone. Two reference frame are

defined: $R'(O_1, X', Y', Z')$ and $R(O, X, Y, Z)$. Coordinates of the N probed points P_i are expressed in the first frame and the two parallel planes are expressed in the second. Of the two planes one is coincident with the XY plane and the other is a parallel plane at distance t . This logic is represented in Figure 6.7. The objective of the optimization problem is to minimize t by applying an adequate roto-translation of system R with respect to system R' . This is equivalent to move the two planes around the point sample. Thus the parameters defining the roto-translation are the variables to be set by optimization.

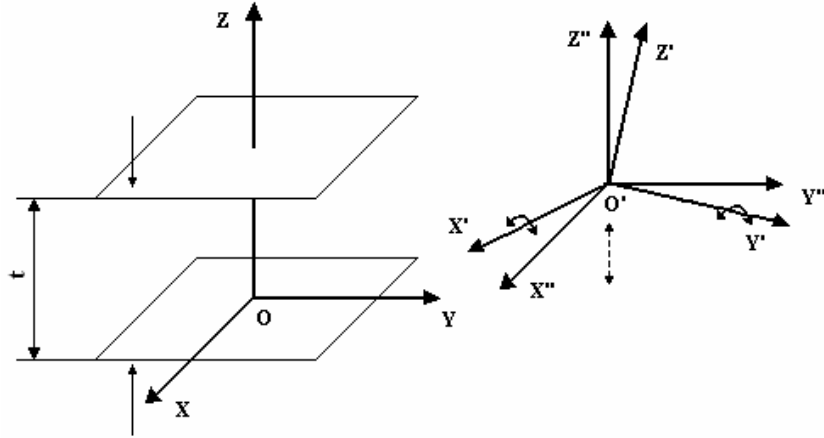


Fig. 6.7: Representation of the Reference Frame Changing method.

A system of equations represent the roto-translation:

$$\begin{cases} x = a_{11}x' + a_{12}y' + a_{13}z' + a \\ y = a_{21}x' + a_{22}y' + a_{23}z' + b \\ z = a_{31}x' + a_{32}y' + a_{33}z' + c \end{cases} \quad (6.11)$$

Where a_{ij} are the elements of the rotation matrix A (below) and a , b and c define the components of the translation vector for system R :

$$A = \begin{pmatrix} \cos\theta_2 \cos\theta_3 & -\cos\theta_2 \sin\theta_3 & \sin\theta_2 \\ \sin\theta_1 \sin\theta_2 \cos\theta_3 + \cos\theta_1 \sin\theta_3 & -\sin\theta_1 \sin\theta_2 \sin\theta_3 + \cos\theta_1 \cos\theta_3 & -\sin\theta_1 \cos\theta_2 \\ -\cos\theta_1 \sin\theta_2 \cos\theta_3 + \sin\theta_1 \sin\theta_3 & \cos\theta_1 \sin\theta_2 \sin\theta_3 + \sin\theta_1 \cos\theta_3 & \cos\theta_1 \cos\theta_2 \end{pmatrix}$$

where θ_1 , θ_2 and θ_3 , are the angles defining the rotation of system R around X' , Y' and Z' axes. Notice that, for the purpose of computing t_R

we are not interested in rotations around the Z-axis, hence matrix A simplifies to:

$$A = A_{X'} \cdot A_{Y'} = \begin{pmatrix} \cos \vartheta_2 & 0 & \sin \vartheta_2 \\ \sin \vartheta_1 \sin \vartheta_2 & \cos \vartheta_1 & -\sin \vartheta_1 \cos \vartheta_2 \\ -\cos \vartheta_1 \sin \vartheta_2 & \sin \vartheta_1 & \cos \vartheta_1 \cos \vartheta_2 \end{pmatrix}$$

By means of the previous relations, coordinate z of points P_i can be written as:

$$z''_i = -\cos \vartheta_1 \sin \vartheta_2 x'_i + \sin \vartheta_1 y'_i + \cos \vartheta_1 \cos \vartheta_2 z'_i + c \quad (6.12)$$

Finally the optimization problem can be formulated as:

$$\begin{aligned} & \text{minimize } t \\ & \text{subject to} \\ & z_i \leq t \\ & z_i \leq 0, \quad i=1, \dots, N \end{aligned} \quad (6.13)$$

6.3. Model-based estimation methods

In the previous section we have presented sample-based methods for estimating flatness error. However, an important warning should be taken in mind. The ASME definition of flatness would require the knowledge of the entire surface. Hence, as it was already pointed out for location tolerances, the crucial problem when using a CMM for flatness control is relying on a generally small sample for the estimation of the geometric error. The problem becomes particularly critical if the actual surface exhibits systematic form deviations. In such circumstance, flatness error, as computed by the available sample-based algorithms, may be dangerously underestimated. In the following sub-sections we present two estimation methods which utilize a parametric model of the surface. They can be extremely efficient when the surface is affected by a systematic form error. However model-based method need some form of a-priori knowledge on the surface to be inspected. An important question is where this kind of a-priori may come from. There are two major sources. The first is the knowledge of the manufacturing process

(machining operations and their parameters) which the part has undergone. Typically, machining operations leave peculiar signatures on the part surfaces that can be put in the form of a parametric model. The second source is a metrological one. Assume that a number of nominally identical parts are to be inspected, e.g. coming from mass or batch production. A preliminary large-sample inspection can be applied to one or a few parts from the lot. From this highly informative sample a reliable empirical model of the surface is estimated, for example by statistical regression. Then, an ad hoc designed small-sample can be used to inspect the rest of the lot. In fact, the small sample is only used to estimate parameters of the identified surface model. Needless to say, the method works well provided that parts inspected with the small sample have a form error similar to that of the parts inspected with the large sample. By the way, this condition is normally met when production machines are operated under reasonably controlled conditions. However, even if the population contains outliers, the model-based approach may offers some protection against the risk of wrong evaluations of the geometric error.

6.3.1. Regression Fit method

Its rationale is quite simple. Let us assume that we have a-priori knowledge on the possible systematic pattern of form error and that this a-priori knowledge can be put in the form of a parametric model. Then we can use the point sample to estimate the parameters of the model by statistical regression. In such a way sample information is transformed into inferential information about the population. Finally the geometric error is estimated by using the fitted model of the entire surface. Estimates can be easily obtained by applying one sample-based method to a discretized version of the fitted model. However, in principle, also analytical estimates are possible by working out on the model, usually at the cost of resorting to more involved mathematics. Possible outliers may be identified by the lack of statistical significance of the model fitted on the small sample. This method will be compared to two sample-based method in section 6.4.

6.3.2. Improved Regression Fit method

The previous method may have problems when the fitted model is not able to emulate accurately the surfaces of the typical part of the lot. However, statistical regression can reveal this circumstance by suitable

analyzing the regression residuals, namely the difference between experimental and fitted values. If the residuals exhibit a systematic pattern the model suffers from lack of fit. If this is the case, systematic bias may occur when estimating the geometric error.

To tackle this problem we can suppose that the form error depends on two pieces of information of different kind. One is the average pattern of the whole surface; this is a kind of global information, e.g. provided by a regression model. In the case of systematic form deviations this component may account for a large fraction of the form error. The second component is represented by those local patterns which, departing from the average, are responsible for the extra fraction of the error. Thus the problem is decomposed into two sub-problems. First, a statistical model of the surface is obtained from the large-sample datasets and a small point-sample that is able to estimate that model accurately is devised. Classical *Design of Experiments* theory is helpful for this purpose. Designed experiments are just good (sometimes optimal) samples for estimating an assumed model holding in a given input space. Then, extra points are added to the first sample to take into account the local departures (from the model) that have leverage on the form error. We propose to identify these extra points by contrasting the residuals originated by the fitted model with the convex-hull of the large sample. In fact, the convex hull contains sufficient information to rank the points in terms of their potential to affect the form error: points not in the convex-hull do not affect the error; points in the convex-hull affect it to a different degree which can be computed by an ad-hoc algorithm. Hence, the extra points are those fulfilling two conditions: they exhibit a large residual and belong to the convex hull with a high rank.

Originality of the approach lies in the two-scale analysis of measurement data and in the combination of statistical and numerical modelling. We believe this is key to design very small inspection plans. At the inspection stage, the method offers also two ways for protecting against the risk of a poor estimation of the form error. In fact, outliers in the lot may be identified either by the lack of statistical significance of the model (fitted to the small sample), or by the lack of leverage of the extra points on the estimated form error.

The application of the method and its merit are illustrated in section 6.6. by a case-study referring to straightness tolerances on face-milled surfaces.

6.4. Design of inspection plans for flatness (or straightness) control

This section is dedicated to the application of the methodology proposed in Chapter 4 for the selection of good inspection plans. In chapter 5 the methodology has been applied in the case of position tolerance. We will follow a similar structure for the presentation of the case-study. First we define the part to be inspected, then the experiment on the virtual CCM is described and the most significant results are discussed. The objective is to assess the effects of the sampling patterns (characterized by location and size of the sample) and of the flatness estimation methods on the bias and uncertainty of the estimated flatness error. Although also in this case the CMM measurement process is simulated, there are two important differences with respect to the position tolerance case-study. First systematic form deviations of the part surface, induced by the manufacturing process, are explicitly considered. Secondly the analyzed estimation methods comprise two sample-based methods (OLS and Convex-Hull methods) but also one model-based method. A major intent of the study is to demonstrate the superiority of the latter method, which is able to exploit a priori knowledge about the parts to be inspected.

6.4.1. The inspected part

The selected part is a cast-iron plate (dimensions $a \times b \times h$) as represented in Figure 6.8.

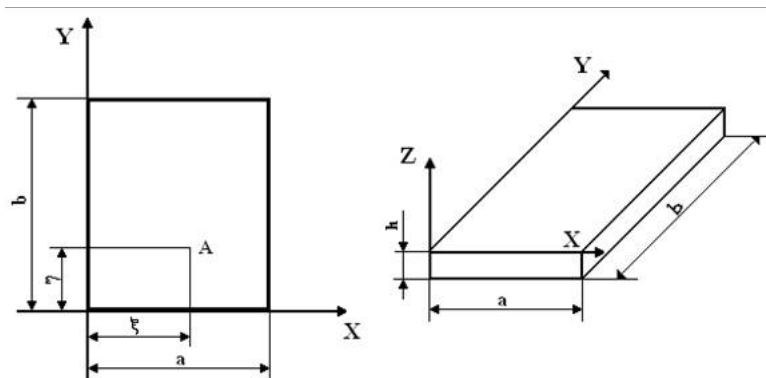


Fig. 6.8: The inspected part.

To analyse the effect of form error, we assume that the relevant manufacturing process is a commonly used one such as end milling, slab milling or grinding. We also assume that the plate is fixtured in such a

way that it is supported around all the four edges. In this conditions the vertical component of the cutting force applied by the tool generates vertical deflections on the part that peak at the centre of the plate.. Let ξ and η indicate the generic application point (A) of the vertical component of cutting force P. According to a model describing the effects of face milling on a flat surface in a vise, a good approximation of the process induced distortion of the machined surface when the fixturing force dominates is provided by (Timoshenko, S., 1959):

$$w = -\frac{4 \cdot P}{a \cdot b \cdot D \cdot \pi^4} \sum_{m=1}^{\infty} \sum_{n=1}^{\infty} \left[\frac{\sin\left(\frac{m\pi \cdot \xi}{a}\right) \cdot \sin\left(\frac{n\pi \cdot \eta}{b}\right)}{\left(\frac{m^2}{a^2} + \frac{n^2}{b^2}\right)} \cdot \sin\left(\frac{m\pi}{a} \cdot x\right) \cdot \sin\left(\frac{n\pi}{b} \cdot y\right) \right] \quad (6.14)$$

where w is the deflection in the z direction axis and D is the flexural rigidity of the plate. D is given by:

$$D = \frac{Eh^3}{12(1 - \nu^2)} \quad (6.15)$$

where E is the elasticity modulus of the material, and “ ν ” the Poisson’s ratio.

As the infinite series in model (6.14) converges rapidly, we can obtain the deflection at any point of the plate with sufficient accuracy by summing up only a few initial terms of the series (sixteen would suffice). For a square plate ($a=b=200$ mm) submitted to a vertical component of the cutting force, deflection on the plate (w) can be expressed in terms of the maximum deflection w_{\max} . occurring in the middle ($\xi = \eta = 1/2 a$). The series (6.14) Can be rewritten as:

$$w = -\frac{4 \cdot w_{\max}}{\alpha \cdot a^3 \cdot b \cdot \pi^4} \sum_{m=1,3,5,\dots}^{31} \sum_{n=1,3,5,\dots}^{31} \left[\frac{\sin\left(\frac{m\pi \cdot \xi}{a}\right) \cdot \sin\left(\frac{n\pi \cdot \eta}{b}\right)}{\left(\frac{m^2}{a^2} + \frac{n^2}{b^2}\right)} \cdot \sin\left(\frac{m\pi}{a} \cdot x\right) \cdot \sin\left(\frac{n\pi}{b} \cdot y\right) \right] \quad (6.16)$$

Taking the first sixteen terms of the series we find that parameter α is 0,0115944.

In addition to the deflection component, we also include two other sources of surface variation. One source, in face milling, is due to both the cutting tool vibrations and the commonly used up and down tool path

followed on a square part. This source generates a sinoidal wave pattern. There is empirical evidence of this effect in face milling. The other source is random noise in the process. Its effect on the surface is a deflection component modelled by a Normal random variable with zero mean and constant standard deviation σ_m . (Sun, Y. T., et al., 2002 and Dowling, M. et al., 1995).

Therefore, the complete form error model can be formulated as:

$$z = w + c_1 \sin(v_1 \cdot x + \varphi_1) + c_2 \sin(v_2 \cdot y + \varphi_2) + N(0, \sigma_m^2) \quad (6.17)$$

where c_1 and c_2 , v_1 and v_2 , and φ_1 and φ_2 are the amplitudes, the angular frequencies and the phase angles of the surface waviness, in the x and y directions respectively. As reported in the Table 6.1 w_{\max} value is 1 mm or 4 mm and c_1 and c_2 value is 0.01 mm or 0.04 mm. Both v_1 and v_2 are assigned the value of $\frac{2}{3} \pi \text{ rad}\cdot\text{mm}^{-1}$; the value for σ_m is fixed at 0,0003 mm. Figure 6.9 shows the form error deriving from model (6.17) when all the parameters take their maximum value.

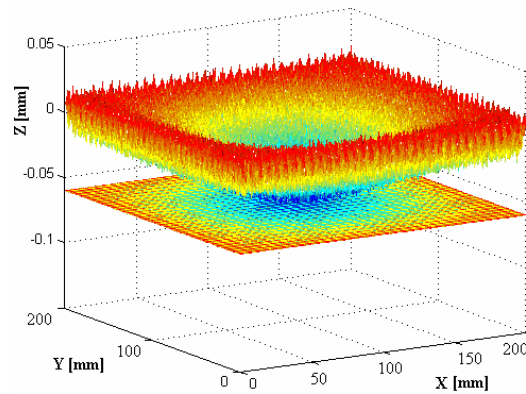


Fig. 6.9. The form error of the plate according to the complete model when all parameters are at their maximum value.

The first two components in model (6.17) are separately analyzed in the simulated experiment. Two cases are considered depending on which of the two first components (deflection and waviness) dominates on the other. Random process variation is present in both cases. The parameter values for each case are shown in Table 6.1 while the appearance of the form error is shown in Figure 6.10 and Figure 6.11.

Table 6.1: Values of parameter in model (17) when deflection or waviness are dominant.

Dominant error source	w_{\max} [mm]	c_1 [mm]	c_2 [mm]	v_1 [rad/mm]	v_2 [rad/mm]	ϕ_1 [rad]	ϕ_2 [rad]	σ_{rn} [μm]
Deflection	4	0,01	0,01	$\frac{2}{3}\pi$	$\frac{2}{3}\pi$	0	0	0,3
Waviness	1	0,04	0,04	$\frac{2}{3}\pi$	$\frac{2}{3}\pi$	0	0	0,3

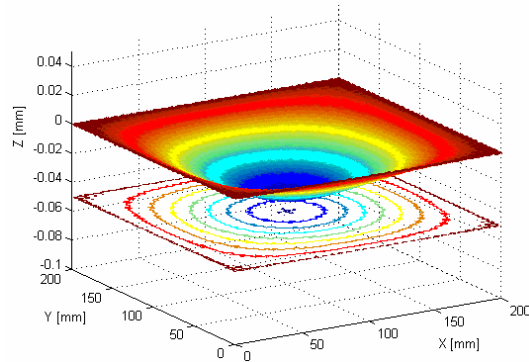


Fig. 6.10. Deflection is the dominant error component.

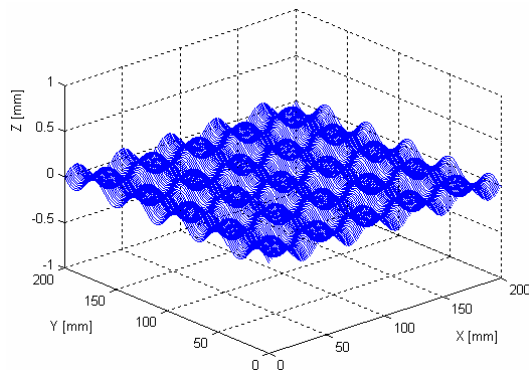


Fig. 6.11. Waviness is the dominant error component.

6.4.2. The planned experiment

The experiment run on the virtual CMM is a full factorial and studies the effects of four control factors on flatness error t . The experiment is run for two cases of surface error: in one case deflection is the dominant error, in the other case the waviness is. As both the mean and the

standard deviation of the estimated t are analyzed we will draw information on both systematic bias and uncertainty of the position error. More precisely, for any experimental setting we analyze the empirical mean and standard deviation of t obtained by Montecarlo simulation. The four control factors, all pertaining to the measurement process, are: sample size, sampling method, size of the random measurement error, and method for flatness error estimation. They are given six, four, three, and three levels respectively for a total run size of $6 \times 4 \times 3 \times 3 = 216$. Factor and levels are reported in Table 6.2. Each of the 216 experimental settings are repeated 10^4 times by using Montecarlo simulation. In different repetitions only the measurement error is randomly changed. Measurement errors of the CMM in x , y , z coordinates are simulated by i.i.d. normal random numbers with null mean and common standard deviation σ . The latter is the third experimental factor.

Six levels of sample size, n_p , are powers of two ($n_p = k^2$, $k=3$ to 8). Four sampling strategies are explored: pure random sampling (RS), stratified non-random sampling (SNRS), stratified non-random circular sampling (SNRCS), and Latin Hypercube sampling (LHS). The first two methods have been already introduced in the previous chapter. Stratified non-random circular sampling and Latin Hypercube sampling are illustrated hereafter, see also Fig. 6.12.



Fig. 6.12: Stratified non-random circular sampling (NRCS) and Latin Hypercube sampling (LHS).

Stratified non-random circular sampling is analogous to stratified non-random sampling (factorial). In this case points are located on a ring shaped pattern as shown in Figure 6.12. In practice, $\sqrt{n_p}$ equispaced points are located on $\sqrt{n_p}$ circumferences of increasing diameter. Point patterns on different circumferences are shifted in such a way that the n_p points are assigned n_p equispaced phase angles respectively. This strategy seems good because it reproduces the central symmetry which characterizes the deflection component of the surface error. The other strategy is the Latin Hypercube sampling, which works quite well since it

tends to spread the measurement over the feature surface while maintaining a fair amount of randomness. We use the Matlab function “*lhsdesign*”, which implements the sampling method as described in (McKay et al. 1979). An LH sample of n_p points is taken as follows. Peculiarities of LHS are that any sample size n_p can be realized, and that the n_p points, if projected onto any dimension of the factor space (2 dimensions, x and y , in our case), generate n_p different points realizing a nearly uniform space filling in each dimension. The procedure for generating a LH sample in our case is described below.

1. Partition the length of each side (in the x and y directions) of the plate into n_p equal sized intervals. The result is an n_p -by- n_p grid of rectangular cells of equal area. A cell in the grid is defined by its position (i,j) $i,j=1$ to n_p .
2. Draw without replacement numbers from 1 to n_p generating a random ordering of the numbers. Let k be the order of the draws and p_k the number drawn at step k .
3. Pick the set of cells $S=\{k, p_k\}$, $k=1$ to n_p .
4. for each cell in S , take a measurement at a random point within the cell.

Notice that two of the four analyzed sampling methods have a random mechanism (random sampling and LHS) while the remaining two are fully deterministic. This is an interesting issue for evaluating their performance. The third factor is the standard deviation of the random measurement error. It varies in the range 0,0005 to 0,0025 mm, spanning a broad spectrum of CMM quality. Last control factor is the method for estimating t . In particular we use two sample-based methods and one model-based method. Among the sample-based methods presented in section 5.2. OLS method and Convex-Hull (CH) method are selected. The model-based method is the Regression Fit (RF) method. When using this estimation method we assume that the structure (not the parameter values!) of the model expressing the surface error is known. At each simulation run the method entails the estimation of all parameters in the first two terms of model (6.17) via regression analysis. Notice that, since model (6.17) is non linear in the parameters v_1 v_2 φ_1 φ_2 , non linear regression has been used. Matlab routine for non linear regression is used.

Table 6.2: Factors and levels of the experiment, with their values.

Factors	Levels					
Number of points measured on plate surface	9	16	25	36	49	64
Sampling strategy	RS	SNRS	SNRCS	LHS		
Size of random measurement error (mm)	0,0005		0,0015		0,0025	
Method for flatness error estimation	OLS		CH		RF	

6.5. Results of the experiment

The analysis of the experiment is structured as follows. We apply the Analysis of Variance (ANOVA) to the two experimental responses, namely: empirical mean and standard deviation of the flatness error (calculated over 10^4 replications). The two responses are related to two primary metrological characteristics, i.e. bias and uncertainty of flatness estimates respectively. ANOVA allows for a quantitative evaluation of both single factor effects (main effects) and combined factor effects (interactions) on the responses. Then, main effects and interactions are visually assessed by displaying main effects plots and interaction plots.

6.5.1. Analysis of flatness bias

We define flatness bias as the deviation between the computed flatness error and the true flatness error:

$$b = t_{\text{est}} - t_{\text{true}} \quad (6.18)$$

A normalized measure of bias is obtained by taking the relative deviation:

$$B = \frac{t_{\text{est}} - t_{\text{true}}}{t_{\text{true}}} \quad (6.19)$$

Bias B defined in (6.19) is a random variable as t_{est} is a random variable. Thus it indicates a random deviation of the computed flatness from its true value. A negative bias denotes an underestimation of the true flatness error and a positive bias an overestimation.

If in equation (6.19) the estimated flatness error t_{est} is replaced by its mean $E(t_{\text{est}})$, a mean bias is obtained:

$$E(B) = \frac{E(t_{\text{est}}) - t_{\text{true}}}{t_{\text{true}}} \quad (6.20)$$

Mean bias is no longer a random variable; it is a parameter and denotes a systematic deviation of the computed flatness from its true value.

In the presentation of results we analyze a sample-based estimate of the mean bias, i.e.:

$$\hat{E}(B) = \frac{\hat{E}(t_{\text{est}}) - t_{\text{true}}}{t_{\text{true}}} \quad (6.21)$$

where

$$\hat{E}(t_{\text{est}}) = \frac{1}{10^4} \sum_{i=1}^{10^4} t_{\text{est}i} \quad (6.22)$$

is computer averaging over the 10^4 replications of each experimental run. In the following analyses, systematic bias in (6.21) is considered in percent.

6.5.1.1. Dominant form error: deflection

The true flatness error is quite large and amounts to 4,00734 mm. The ANOVA table includes single effects, two-factor interactions and one three-factor interaction, that involving sample size, sampling method and estimation method. It is reported in Table 6.3. Apart from random error size, the other single effects are significant in the order: estimation method, sample size, sampling method. All interactions involving these three factors are significant, even if to a lesser extent.

The variance decomposition captures more than 99% of the total variability (see the R^2 indices at the end of the table).

Table 6.3. Analysis of Variance for systematic flatness bias (%) when deflection is the dominant form error component.

Source	DF	SS	MS	F	P
Sample size	5	5245,29	1049,06	3128,28	0,000
Sampling method	3	629,72	209,91	625,94	0,000
Random error size	2	0,12	0,06	0,18	0,832
Estimation method	2	8035,67	4017,84	11981,15	0,000
Sample size*Sampl. meth.	15	4050,93	270,06	805,32	0,000
Sample size*Rand. err.size	10	2,29	0,23	0,68	0,739

Sample size*Estim. meth.	10	2694,48	269,45	803,49	0,000
Sampl. meth.*Rand. err.size	6	0,97	0,16	0,48	0,821
Sampl. meth.*Estim. meth.	6	542,23	90,37	269,49	0,000
Rand. err.size*Estim. meth.	4	1,66	0,41	1,24	0,299
Sample size*Sampl. meth.* Estim. meth.	30	2057,52	68,58	204,52	0,000
Error	122	40,91	0,34		
Total	215	23301,80			

S = 0,579091 R-Sq = 99,82% R-Sq(adj) = 99,69%

A clearer picture comes from looking at the plots of main effects and significant two-factor interactions. The most important result is that the model-based estimation method does not exhibit systematic bias regardless of which sample size and sampling method is used. A sizable negative bias appears when sample-based methods are used (OLS seems slightly better than CH only because, as it was noticed, it tends to overestimate the sample-based flatness). As expected, bias slowly tends to zero as sample size increases. However, while sampling methods incorporating randomness (pure random and LS) approach zero monotonically, deterministic sampling methods do not. This is explained by the fact that from one sample size to another it may happen that some point is in a position where form error is higher.

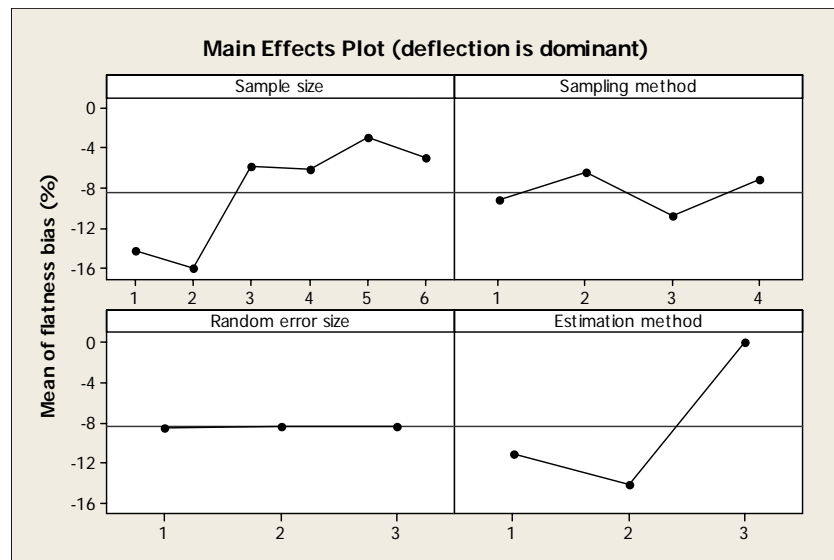


Fig. 6.13. Main effects for mean flatness bias (%) when deflection is the dominant form error component.

For example, for odd sample sizes (9,25, and 49) the factorial method (level 2) has a point in the middle of the plate where the deflection peaks. This is clearly seen in the interaction plot involving sample size and sampling method (red dots). Thus estimates of flatness may be very sensitive to sample size when deterministic sampling methods are used. From this viewpoint, samples with some randomness might be preferable. Finally notice that LH sampling is just a little better the pure random sampling for small sample sizes (up to 16) as it assures a good coverage of the surface.

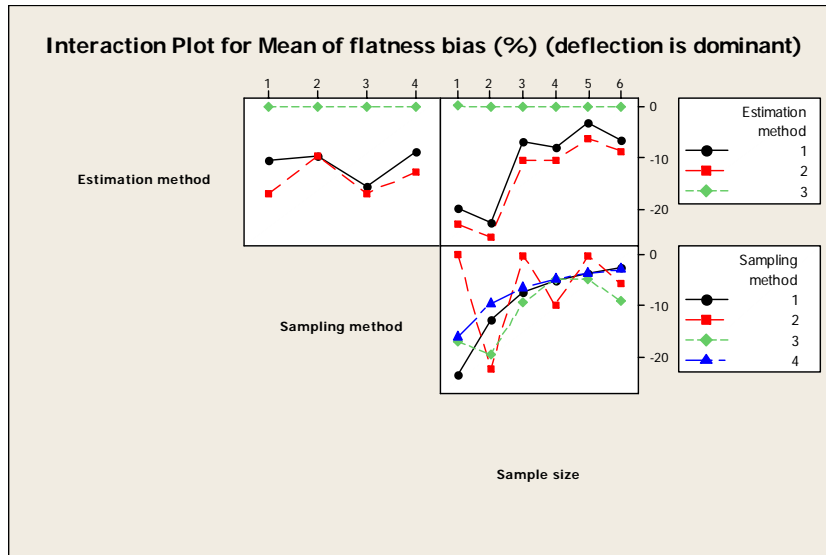


Fig. 6.14. Significant two-factor interactions for mean flatness bias (%) when deflection is the dominant form error component.

6.5.1.2. Dominant form error: waviness

The true flatness error is 1,00522 mm. The ANOVA table includes single effects, two-factor interactions and one three-factor interaction, that involving sample size, sampling method and estimation method. It is reported in Table 6.4. Results are very much similar to when deflection dominates. However a couple of considerations are in order. Both are related to the fact that waviness is periodic and exhibits faster variations than deflection. First, when using the Regression Fit estimation method it happens that, especially for small sample size and/or for deterministic sampling methods, parameters of the non linear sinoidal terms are

estimated with little less accuracy. This can be seen in the interaction plot where RF method is present. Moreover, for the same reason, the sensitivity of flatness to sample size when deterministic sampling methods are used is increased, see the third interaction plot in Fig. 6.16.

Table 6.4. Analysis of Variance for systematic flatness bias (%) when waviness is the dominant form error component.

Source	DF	SS	MS	F	P
Sample size	5	7546,81	1509,36	2144,57	0,000
Sampling method	3	1003,78	334,59	475,41	0,000
Random error size	2	0,01	0,00	0,00	0,996
Estimation method	2	8481,36	4240,68	6025,35	0,000
Sample size*Sampl. meth.	15	4425,94	295,06	419,24	0,000
Sample size*Rand. Err. size	10	5,64	0,56	0,80	0,627
Sample size*Estim. meth.	10	4264,76	426,48	605,96	0,000
Sampl. meth.*Rand. err. size	6	12,94	2,16	3,06	0,008
Sampl. meth.*Estim. meth.	6	655,83	109,30	155,30	0,000
Rand. err. size*Estim. meth.	4	4,73	1,18	1,68	0,159
SampleSize*Sampl.meth.* Estim. meth.	30	2341,40	78,05	110,89	0,000
Error	122	85,86	0,70		
Total	215	28829,06			

S = 0,838932 R-Sq = 99,70% R-Sq(adj) = 99,48%

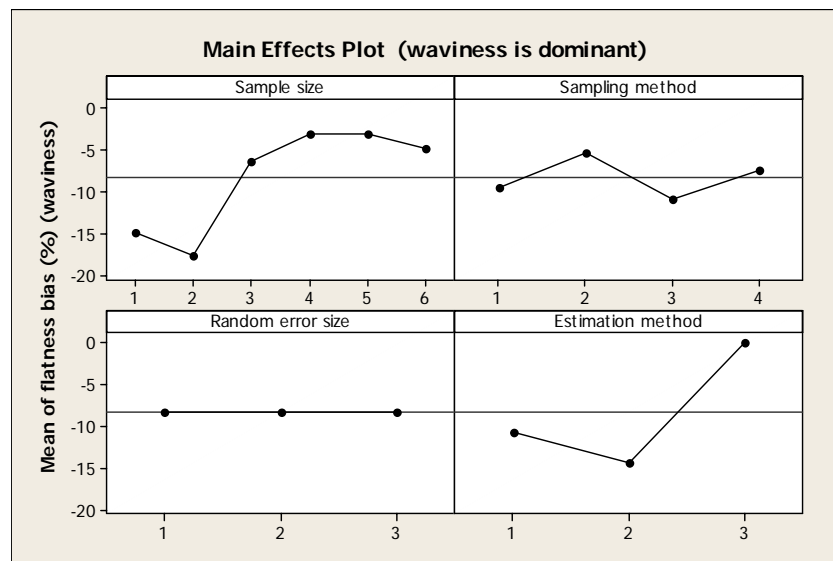


Fig. 6.15. Main effects for mean flatness bias (%) when waviness is the dominant form error component.

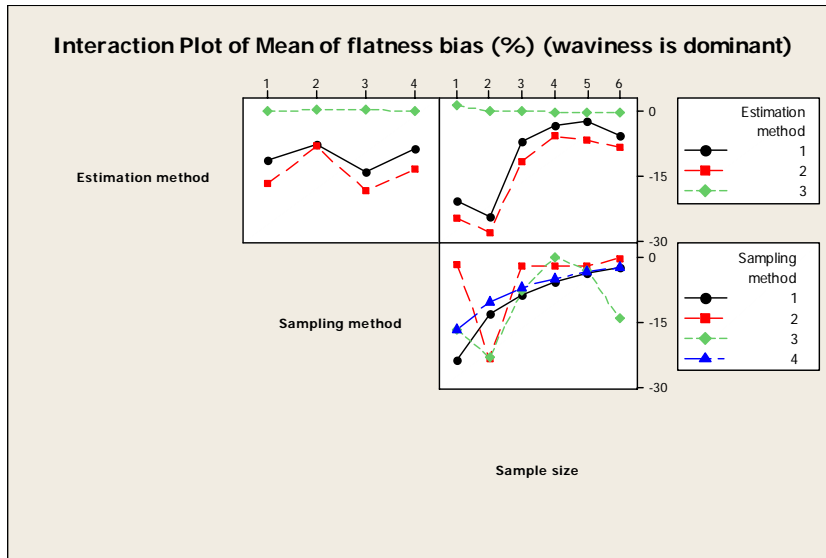


Fig. 6.16. Significant two-factor interactions for mean flatness bias (%) when waviness is the dominant form error component.

6.5.2. Analysis of flatness uncertainty

We define flatness uncertainty as the standard deviation of the computed flatness error:

$$u = \sigma_{t_{est}} \tag{6.23}$$

Analogously to bias, a normalized measure of uncertainty is obtained by dividing the standard deviation by the absolute value of the true flatness:

$$U = \frac{\sigma_{t_{est}}}{t_{true}} \tag{6.24}$$

In the presentation of results we analyze a sample-based estimate of flatness uncertainty, i.e.:

$$\hat{U} = \frac{\hat{\sigma}_{t_{est}}}{t_{true}} \tag{6.25}$$

where the sample standard deviation of the estimated flatness

$$\hat{\sigma}_{t_{\text{est}}} = \sqrt{\frac{1}{10^4 - 1} \sum_{i=1}^{10^4} (t_{\text{est}i} - \bar{t}_{\text{est}})^2} \quad (6.26)$$

is computer averaging over the 10^4 replications of each experimental run. In the following analyses, normalized uncertainty in (6.24) is considered in percent.

6.5.2.1. Dominant form error: deflection

The ANOVA table includes single effects, two-factor interactions and one three-factor interaction, that involving sample size, sampling method and estimation method. It is reported in Table 6.5. All single effects, including the size or the random measurement error, are significant in the order: sampling method, estimation method, sample size, random error size (the latter at 97% confidence level). All interactions involving the first three factors are also significant. The variance decomposition captures more than 99% of the total variability (see the R^2 indices at the end of the table).

Table 6.5. Analysis of Variance for normalized flatness uncertainty (%) when deflection is the dominant form error component.

Source	DF	SS	MS	F	P
Sample size	5	405,680	81,136	432,68	0,000
Sampling method	3	1543,674	514,558	2743,99	0,000
Random error size	2	1,350	0,675	3,60	0,030
Estimation method	2	704,908	352,454	1879,54	0,000
Sample size*Sampl. meth.	15	340,235	22,682	120,96	0,000
Sample size*Rand. err. size	10	2,041	0,204	1,09	0,376
Sample size*Estim. meth.	10	138,596	13,860	73,91	0,000
Sampl. meth.*Rand. err. size	6	0,560	0,093	0,50	0,809
Sampl. meth.*Estim. meth.	6	917,329	152,888	815,31	0,000
Rand. err. size*Estim. meth.	4	0,830	0,208	1,11	0,356
Sample size*Sampl. meth.* Estim. meth.	30	238,814	7,960	42,45	0,000
Error	122	22,878	0,188		
Total	215	4316,894			

S = 0,433038 R-Sq = 99,47% R-Sq(adj) = 99,07%

The most evident result is that a small uncertainty (considerably less than 1% of the true value) is obtained by using deterministic sampling methods and/or the moel-based estimation method. On the other hand, sampling methods incorporating randomness produce high uncertainty, especially for small sample size (from 6% to 12% of the true flatness for

sample sizes from 16 to 9). As expected, uncertainty decreases, but slowly, as sample size increases. Also for uncertainty, LH sampling is superior to pure random sampling.

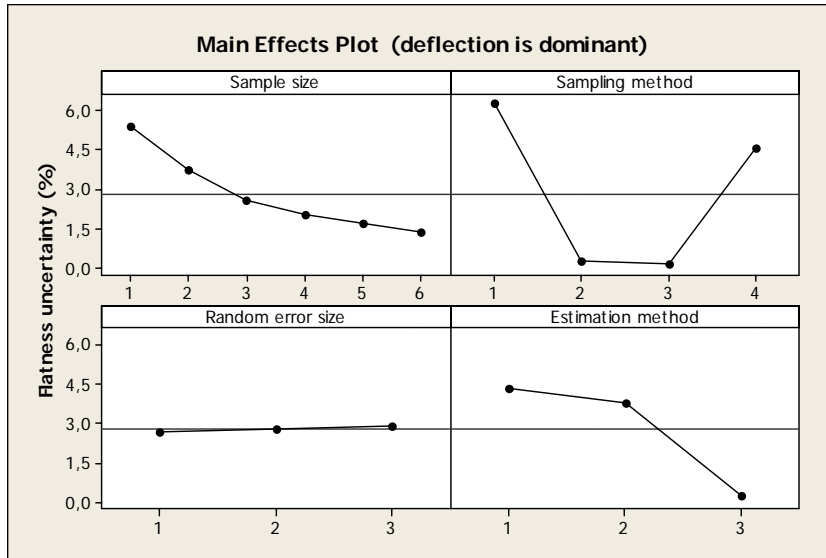


Fig. 6.17. Main effects for flatness uncertainty (%) when deflection is the dominant form error component.

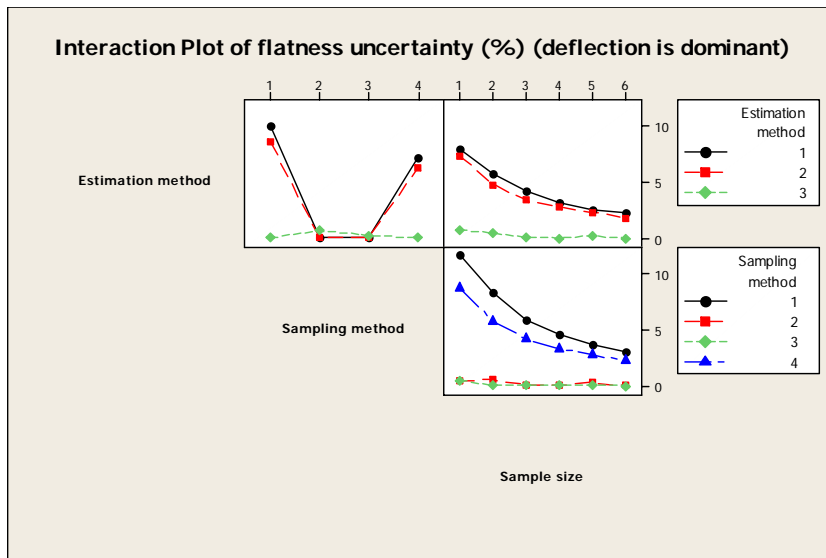


Fig. 6.18. Significant two-factor interactions for flatness uncertainty (%) when deflection is the dominant form error component.

6.5.2.2. Dominant form error: waviness

The ANOVA table includes single effects, two-factor interactions and one three-factor interaction, that involving sample size, sampling method and estimation method. It is reported in Table 6.6. Results are very much similar to those of the deflection case. Explained variability is just a little less than before (see the R^2 indices at the end of the table). Also plots of main effects and two-factor interactions are in close agreement with those for deflection. It can be noticed, however, that the model-based method, in association with deterministic sampling methods, produces a slightly higher uncertainty than it does in the case of deflection. This is again due to the fact that fixed point locations characterizing these sampling methods may happen to be unfavourable for a good estimate of the parameters of waviness, which is also the non linear part of the form error model (6.17).

Table 6.6. Analysis of Variance for normalized flatness uncertainty (%) when waviness is the dominant form error component.

Source	DF	SS	MS	F	P
Sample size	5	416,851	83,370	126,61	0,000
Sampling method	3	1555,221	518,407	787,26	0,000
Random error size	2	3,986	1,993	3,03	0,052
Estimation method	2	625,036	312,518	474,59	0,000
Sample size*Sampling method	15	193,340	12,889	19,57	0,000
Sample size*Rand. err. Size	10	5,846	0,585	0,89	0,547
Sample size*Estim. meth.	10	40,112	4,011	6,09	0,000
Sampl. meth.*Rand. err. size	6	7,950	1,325	2,01	0,069
Sampl. meth.*Estim. meth.	6	1184,021	197,337	299,68	0,000
Rand. err. size*Estim. meth.	4	7,971	1,993	3,03	0,020
Sample size*Sampl. meth.* Estim. meth.	30	302,830	10,094	15,33	0,000
Error	122	80,336	0,658		
Total	215	4423,500			

S = 0,811476 R-Sq = 98,18% R-Sq(adj) = 96,80%

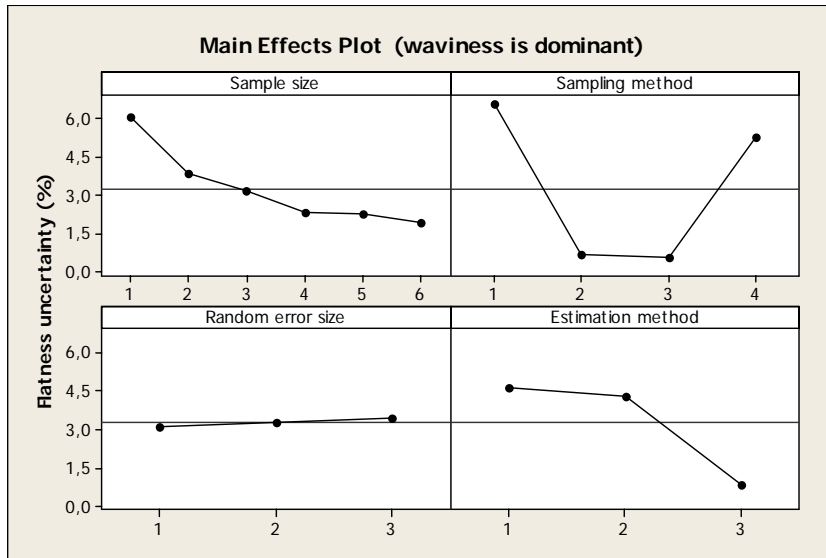


Fig. 6.19. Main effects for flatness uncertainty (%) when waviness is the dominant form error component.

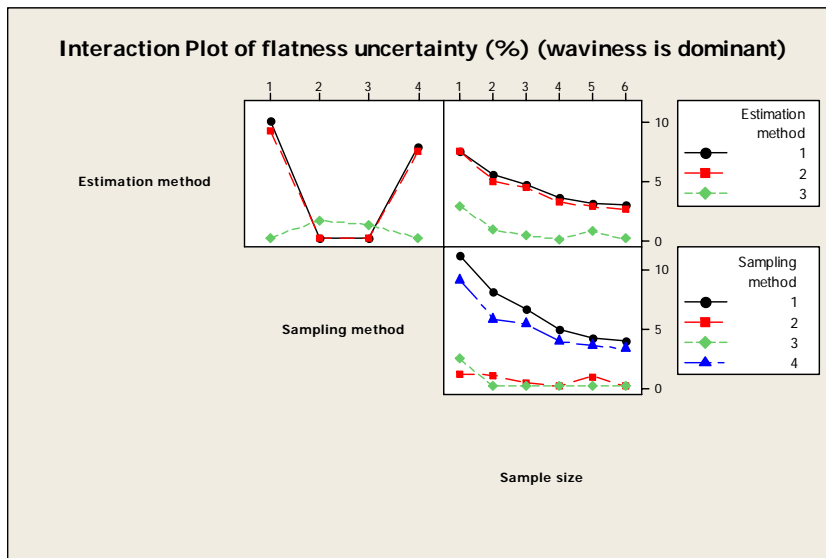


Fig. 6.20. Significant two-factor interactions for flatness uncertainty (%) when waviness is the dominant form error component.

6.6. Application of the Improved Regression Fit method

The Improved Regression Fit method described in section 6.3.2 is

applied to the control of straightness tolerance in a real case study. The objective is to illustrate its use and to validate it. The part is a square plate with a number of through holes of different sizes. It is displayed in Figure 6.21. On the upper surface of the plate a rectangular area of $165 \times 31 \text{ mm}^2$, defined by $4 \leq X \leq 35 \text{ mm}$ and $30.5 \leq Y \leq 195.5 \text{ mm}$ is selected, see

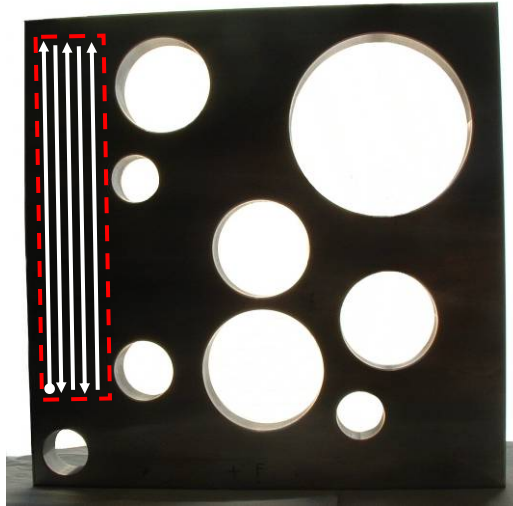


Fig. 6.21. Control of straightness tolerance in a real case study.

The area has been densely probed by a scanning probe of a CMM, travelling up and down paths along the Y direction. The probed are uniformly distributed in the area with a step of approximately 0.5 mm in both directions. Measurements (20816 points) have been carried out at the University of Salerno in November 2006.

The application concerns the control of straightness of successive lines along direction Y on the selected area. The validation of the IRF method envisages the following steps.

1. From the dense point dataset relative to one line selected from the set of scanned lines, a curve fit is obtained by linear regression.
2. Residuals of the curve fit are computed.
3. A minimum-size point sample (containing only Y coordinates) allowing for the estimation of the identified curve is designed.
4. The convex-hull of the line selected at step 1. is computed.
5. Extra points (containing only Y coordinates) are added to the small sample identified at step 3.. The extra points fulfil two conditions: (a)

they exhibit a large residual; (b) they are in the set of vertices of the convex hull that determine the straightness error according to the CH estimation method.

6. The sample comprising the minimum-size sample obtained at step 3. and the extra points obtained at step 5. is applied to a number of lines selected from the set of scanned lines. Z -coordinates corresponding to the Y -coordinates are obtained for each line.
7. From the minimum size sample of Y -coordinates, a curve, of the same form of that identified at step 1., is fitted. This operation is repeated for each line selected at step 7..
8. Straightness error of the ensemble of the curve fitted at step 7. and the extra points obtained at step 6. is computed. This operation is repeated for each line selected at step 7..
9. Straightness errors obtained at step 8. basing on the small-sample inspection plan are compared with the corresponding straightness errors computed from the large samples.

Steps from 1. to 5. concerns the design of the small-sample inspection plan. Steps from 6. to 8. apply the small-sample inspection plan on a sub-sample of the scanned lines and estimate the relevant straightness error. Step 9. validates the IRF method.

Figure 6.22 shows the elements for the design of the small-sample inspection plan.

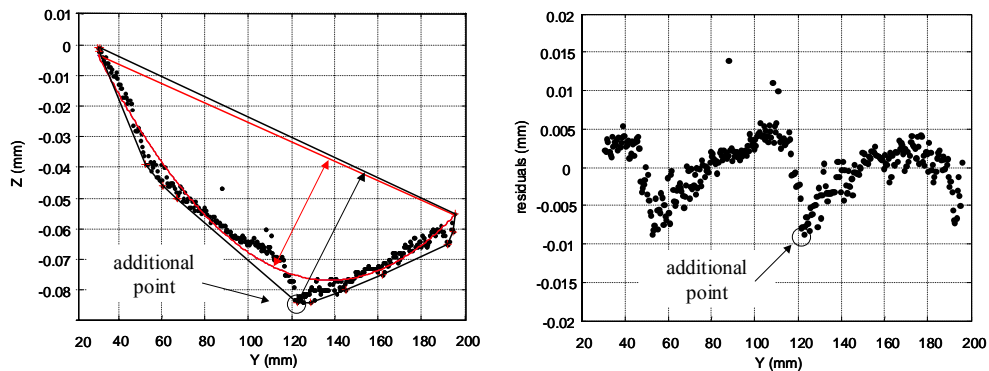


Fig. 6.22. Decomposition of a dense probed pattern on a flat surface (at fixed X) into a parabolic component (red curve, left) and its residuals (right). Parabola accounts for 84% of the straightness error. Solely one additional point, identified by crosschecking the residuals with the convex-hull of the sample (solid polygon, right) is responsible for the remaining error fraction.

Black dots are the large sample from the initially selected line. The red curve is the second-order polynomial fitted to the large sample (red curve). Residuals are plotted in the right diagram. Four points on the Y axis are selected to be included in the small inspection plan. They are the two extreme points ($Y_1=30.5$ mm, $Y_4=195.5$ mm). The other two are internally located at $Y_2=74.0$ mm and $Y_3=88.5$ mm. We have chosen these points because they are internal and have a very low residual. Although three points would suffice for fitting a second-order polynomial, we have decided to pick another point in order to have an additional degree of freedom for evaluating the goodness of fit at the inspection phase.

Only one extra point, $Y_5=122.0$ mm, is necessary to complete the small inspection plan. In fact, it is easily identified as the point (a) belonging to the convex-hull of the large sample (black polygon in the right diagram) and being critical for the straightness of the large sample, and (b) exhibiting a large residual.

The small inspection plan is then applied to four lines drawn at random from the population of 63 lines. The straightness error on these four lines is computed by applying the CH methods to the point dataset obtained by summing up the large sample from a dense discretization of the parabola (fitted to four points only) and the additional point $Y=122$ mm, $Z(Y=122.0$ mm). Fig. 6.23 to Fig. 6.26 show, for each of the four lines, all the geometrical elements relevant to the IRF method.

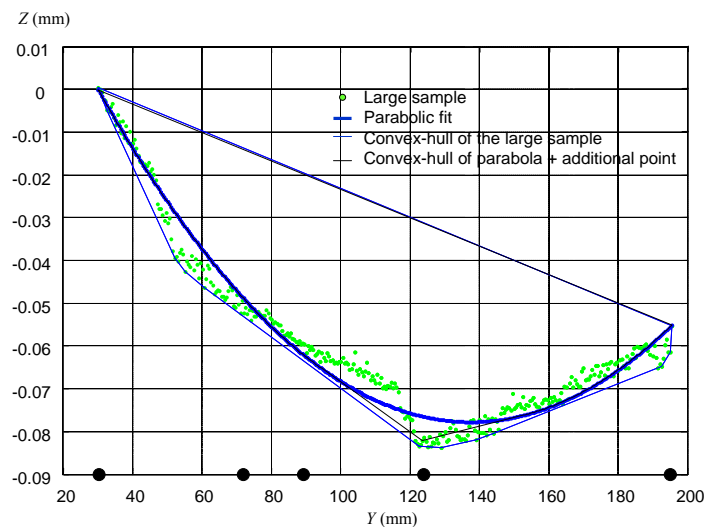


Fig. 6.23. Application of the IRF method to the line at $X=12$ mm. The black dots indicate the designed small sample of Y coordinates.

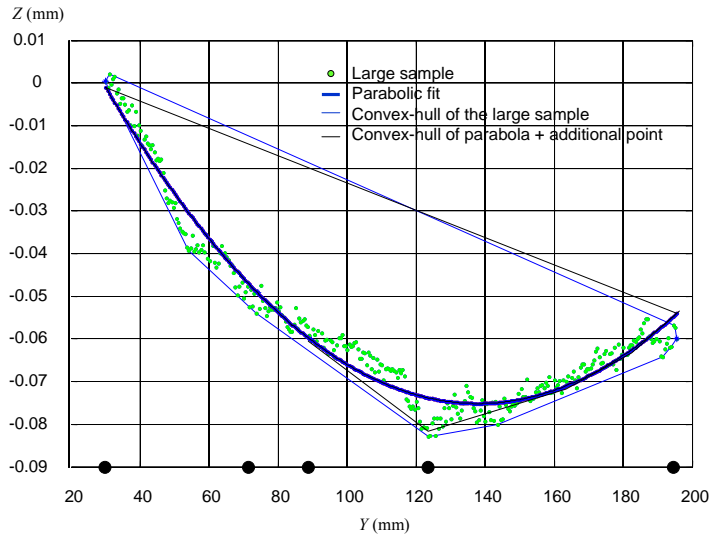


Fig. 6.24. Application of the IRF method to the line at $X=19$ mm.

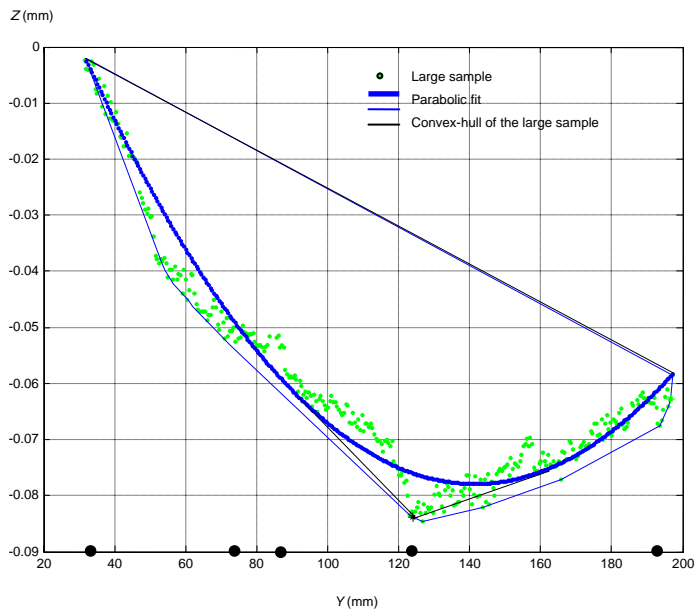


Fig. 6.25. Application of the IRF method to the line at $X=26$ mm

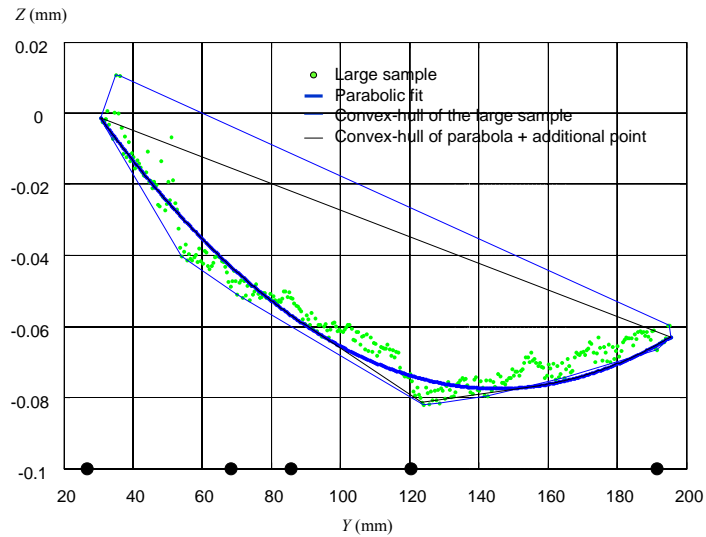


Fig. 6.26. Application of the IRF method to the line at $X=33$ mm.

Table 6.7 reports results of the validation, i.e. the comparison between the straightness errors estimated by the IRF method applied to the 5-point sample and those computed by the CH method applied to the large sample (some 330 points).

Table 6.7: Validation of the IRF method.

lines	Straightness error, (mm)		Relative deviation (%)
	5-point sample	large sample	
$X=12$ mm	0,0508	0,0528	-3.79
$X=19$ mm	0,0473	0,0494	-4.25
$X=26$ mm	0,0481	0,0504	-4.56
$X=33$ mm	0,0454	0,0536	-15.30

REFERENCES CHAPTER 6

- BADAR, M.A., RAMAN, S., PULAT, P.S., 2003, "Intelligent search-based selection of sample points for straightness and flatness estimation", *Journal of Manufacturing Science and Engineering* 125, 263–271.
- BARBER, C. B.; DOBKIN, D. P.; AND HUHDANPAA, H. T., 1996, "The Quickhull Algorithm for Convex Hulls" *ACM Trans. Mathematical Software* 22, 469-483.
- CHAN, T., 1996, "Optimal Output-sensitive Convex Hull Algorithms in Two and Three Dimensions", *Disc. Comput. Geom.* 16, 361-368.
- CHOI, W., KURFESS, T. R., CAGAN, J., 1998, "Sampling uncertainty in coordinate measurement data analysis", *Precision Engineering*, 22, 153-163.
- DOWLING M., GRIFFIN P.M., TSUI K.L., ZHOU C., 1995, "A comparison of the orthogonal least squares and minimum enclosing zone methods for form error estimation," *Manufacturing Review*, v8, n2, pp120-138.
- KWON O., WU J.-L., 1999, "Development of web-based program for evaluation of straightness and flatness tolerance", ME 220 Class Project, Berkeley Expert Systems Technology (University of California)
- LEE G., MOU J. SHEN Y., 1997, "Sampling strategy design for dimensional measurement of geometric features using coordinate measuring machine", *International Journal of Machine Tools & Manufacture*, v37, n7, pp 917-934.
- O'ROURKE, J., 1998, "Computational Geometry in C 2nd ed.", (Cambridge University Press).
- RAGHUNANDAN, R., VENKATESWARA RAO, P., 2006, "Selection of an optimum sample size for flatness error estimation while using coordinate measuring machine", *International Journal of Machine Tools & Manufacture*, in press.
- SUN Y. T., ANAND S., TANG J. S. Y., 2002, "Comprehensive design of experiments-base framework for optimal CMM inspection and uncertainty analysis of form tolerances", *International Journal of Production Research*, vol. 40, no. 9, 2097-2123.
- SKIENA, S. S., 1997, "Convex Hull", §8.6.2 in *The Algorithm Design Manual*, (Springer-Verlag), pp. 351-354, 1997.
- TAKAMASU K., FURUTANI R., OZONO S., 1999, "Statistical Evaluation of Minimum Zone Method in Coordinate Metrology", *IMEKO-XV World Congress*, pp. 101-106

- TIMOSHENKO S. P., WOINOWSKY S.-KRIEGER, 1954, "Theory of plates and shells", (Mcgraw-Hill Book Company).
- YAO, A. C.-C., 1981, "A Lower Bound to Finding Convex Hulls", J. ACM 28, 780-787.
- WOO, T. C., LIANG, R., HSIEB, C. C. AND LEE, N. K., 1995, "Efficient sampling for measurement of geometric features using coordinate measuring machines", International Journal of Machine Tools & Manufacture, 37(7), pp 917-934.

APPENDIX 1: Working Draft ISO/WD 15530-4:

Geometrical Product Specifications (GPS) - Techniques of Determining the Uncertainty of Measurement in Coordinate Metrology -Part 4: Estimating Task-Specific Measurement Uncertainty Using Simulation

At 6-8 September 2006 meeting in Turin, ISO/DTS 15530-4 was ready for submission to publication

Preliminary remark

For coordinate measuring machines (CMMs) used to inspect tolerances, the task-specific uncertainties of measurement according to ISO 14253-1 must be taken into account when tests for conformity/non-conformity are carried out. Thus knowledge of the uncertainty of measurement is of utmost importance. Up to the present, there have been only a few procedures that allow the task specific uncertainty of measurement to be stated. For simple measuring devices this uncertainty can be estimated by an uncertainty budget according to the recommendations of the Guide to the Expression of Uncertainty in Measurement (GUM). However, in the case of a CMM, the formulation of a classical uncertainty budget is impossible for the majority of the measurement tasks due to the complexity of the measuring process. Alternate methods that are consistent with the GUM can be used to determine the task-specific uncertainty of coordinate measurements. One of them, which estimates the uncertainty by numerical simulation of the measuring process allowing for uncertainty influences, is described in this standard.

A1.1. Scope

It is the objective of this standard to describe testing procedures for the evaluation of task specific uncertainty determination by simulation for specific measurement tasks carried out on CMMs, taking into account the measuring device, the environment, the measurement strategy and the object. The standard is to unify the general procedures without restricting the possibilities of the technical realization. A procedure for verification and evaluation of the simulation package is included. Measures are recommended that increase the procedure's transparency for the user, and methods are described that the user may apply to monitor it. The standard is not aimed at defining new parameters for the general evaluation of the accuracy of CMM measurements. The functional capability of the CMMs

is taken for granted, as agreement with specifications is checked on the basis of sheets 1 - 6 of VDI 2617 and of the ISO series of standards 10360.

A1.2. Terminology: (To be defined; descriptions are given when used first)

- Influence Quantity
- Input Quantity
- Uncertainty Evaluating Software (UES)
- Uncertainty Evaluating Software Evaluation (UESE)
- Uncertainty Evaluating Software Implementation Test (UESIT)
- Computer-aided Verification and Evaluation (CVE)

A1.3. Overview

The generation of task specific uncertainty statements for CMM measurements is a complex issue. To allow CMM users to easily create uncertainty statements, CMM suppliers and other third party companies have developed Uncertainty Evaluating Software (UES). UES is based on a computer-aided mathematical model of the measuring process. In this model, the measuring process is represented from the measurand to the measurement result, taking important influence quantities into account. In the simulation, these influences are varied within their possible or assumed range of values (described by probability distributions), and the measuring process is repeatedly simulated, using possible combinations of the influence quantities. The uncertainty is determined from the variation of the final result. This procedure is compatible with the fundamental principles of the internationally valid Guide to the Expression of Uncertainty in Measurement (GUM). The details of the UES are often hidden in compiled computer code making it difficult for the user to assess the reliability of the calculated uncertainty statements. This standard sets forth terminology and testing procedures for both the UES supplier and the CMM user to communicate and quantify the capability of UES.

This standard divides the problem into three major parts. The first part (section A1.4) is the declaration of influence quantities. The declarations identify which influence quantities, along with their ranges of values, the UES can account for in its uncertainty evaluation. For example, some

UES can include the effects of using multiple styli during a CMM measurement, while others cannot. Similarly, some UES can include the effects of temporal or spatial temperature gradients, while others cannot. The purpose of the declaration section is to clearly identify to the CMM user what influence quantities, and their ranges of values, the UES will consider in its uncertainty evaluation. This will allow the user to be able to make informed decisions. Purchasing a UES product with limited capabilities that do not include some influence quantities present during the CMM measurements requires the CMM user to independently evaluate these unaccounted-for influence quantities and combine them appropriately with those that are evaluated by the UES in order to produce a GUM compliant uncertainty statement.

The second part describes the testing procedure for the uncertainty evaluating software evaluation (UESE). The UESE is performed by a testing body and is only conducted once for each version of the UES. The UESE is a major evaluation that tests the UES for its ability to produce appropriate uncertainty statements under any combination of influence quantities permitted in the declaration section.

The third part describes the final test which is performed by the CMM user on a particular CMM. This Uncertainty Evaluating Software Implementation Test (UESIT) checks that the UES and its associated input values are correctly installed and working properly. The UESIT may also detect a large uncertainty source that is not taken into account by the UES but is present in the CMM system.

A1.4. Elements of the UES

The simulation can be integrated into a control and evaluation software of a CMM (on-line) or implemented as an independent system on an external computer (off-line). Both variants are covered by this standard.

A1.4.1 Uncertainty Contributors

The measuring process of a CMM is subject to a great number of uncertainty contributors (influence quantities) that affect the measurement result. When the uncertainty of a measuring process is evaluated using the UES, these influence quantities must be accounted for, recognizing that, in general, the UES accounts for only some of these influence quantities.

A1.4.2 UES Model

The model of the measuring process employed by the UES describes the mathematical relationship between the input quantities (measurand and influence quantities) and the output measurement result. The UES does not require that the model be described by a closed mathematical expression. Numerical algorithms, such as the calculation of derived features or filtering of measurement points can, therefore, be included in the model. This makes UES particularly suitable for complex measuring processes like coordinate measurements. The model used by UES of the measurement on a CMM can be described by a flow chart, in which the quantities influencing the measuring process are plotted. Figure 1 shows a typical flow chart.

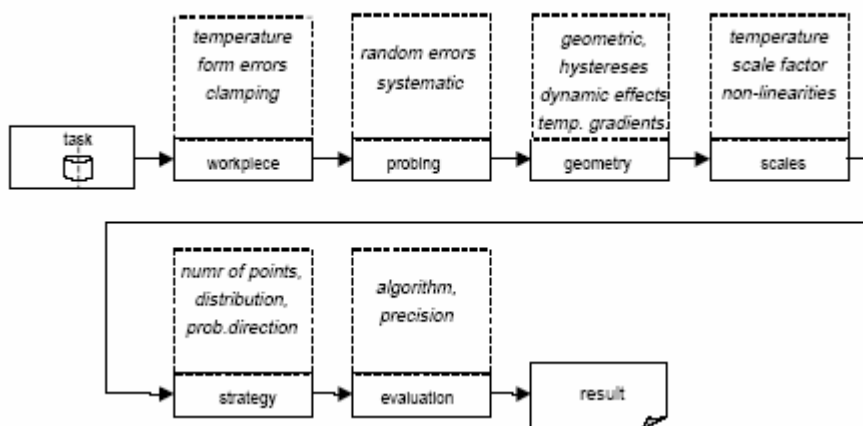


Fig. A1.1. Measurement on a coordinate measuring machine represented in the form of a flow chart

Usually, not all possible uncertainty influences are taken into account in the model. Influence quantities which have not been considered are to be estimated by other procedures and added to the total uncertainty as follows:

A1.4.3 Determination of the task-specific uncertainty of measurement

The parameters of the simulated measurement which are important from the metrological point of view should be as similar as possible to those of the real measurement. The standard uncertainty of a measurement result y is composed of - the uncertainty u_{sim} determined by the simulation, and the uncertainties u_i from the influence quantities which have not be taken

into account in the simulation and have been estimated by other appropriate means.

The combined standard uncertainty is then calculated with

$$u_{ges} = \sqrt{u_{sim}^2 + \sum u_i^2} \quad (\text{A1.1})$$

With the aid of coverage factors, this standard uncertainty can be brought to the desired confidence level. As a rule, the following is valid

$$U_{ges} = 2 \cdot u_{ges} \quad (\text{A1.2})$$

for a confidence level of 95%. If the uncertainty stated by the simulation already is an expanded uncertainty U_{sim} , the simulated uncertainty u_{sim} is to be calculated by division with the respective coverage factor.

A1.4.4 Requirements and information to be provided by the manufacturer

A1.4.4.1 Influence Quantities

The manufacturer of the UES shall explicitly declare which influence quantities (cf. A1.2.2.1) have been taken into account in the software, and what information is required from the user. In particular, the manufacturer should specify by means of this checklist, which uncertainty contributors the software claims to take into account:

Declaration of Influence Quantities

- CMM Types : moving bridge moving table horizontal arm gantry etc...
 Rotary Tables
- CMM Errors: static machine geometry errors dynamic machine geometry errors
 part loading effects Non 20 C temperature spatial gradients
 temporal gradients algorithm software accuracy
 hysteresis
- Probe Types: contact touch trigger contact analog non-contact optical
- Probe Errors: probe response (lobing) multiple styli multiple probe
 articulating head styli/probe changing scanning
- Nominal Parts: circles planes sphere cylinder splines etc.
- GD&T: datum ref frames form size location orientation
- Real Part Effects: surface roughness waviness form error
 non 20 C temp spatial gradients temporal gradients
 contamination fixturing
- Operator Effects: sampling strategies, i.e. the number and location of points in the
workpiece coordinate system
 workpiece position and orientation in machine coordinate system
 other operator effects...

The manufacturer shall state what measurements or other quantities are needed to characterize the CMM and its environment in order for the UES to produce uncertainty statements (A1.3.7).

The following contributors must at least be taken into account:

- The geometrical deviations of the CMM
- Deviations of the contacting system
- Influences of temporal and spatial temperature gradients on specimen and CMM

[Note: The details of which items should be on this list are yet to be determined]

A1.4.4.2 Operating conditions

Each factor “checked” in the declarations section (A1.3.1) implies that the simulation software will appropriately address this issue over a specified range of conditions. (For example, “non-standard temperature” might be defined as homogenous temperature in space and time, within the limits of 15 °C to 30 °C.). The software manufacturer shall specify these ranges defining the spectrum of measurement tasks and the environmental conditions for which the simulation is valid. Examples of these ranges to be specified includes but is not limited to:

- Permissible part spectrum (e.g. exclusion of flexible sheet-metal parts, a minimum arc length for circles, maximum cone apex angles, etc.)
- Permissible task spectrum (e.g. exclusion of scanning or form measurement)
- Permissible temperature range
- Permissible temporal temperature gradients dT/dt
- Permissible spatial temperature gradients dT/dx
- Other permissible environmental conditions

Within the scope of these restrictions, computer-aided verification and evaluation can be performed, as well as the user checks, both described in section A1.5.

A1.4.4.3 Input Quantities and How They Are Obtained

Along with the declarations described in section (A1.3.1), the simulation software manufacturer must specify in detail (or reference appropriate documents) what input quantities are required to characterize the measurement system and how these quantities are obtained. These are the values that are used by the simulation software to characterize the CMM, the environment, operator effects etc. (Operator effects might be assessed from gauge repeatability and reproducibility studies i.e., GR&R; analysis of variance, i.e. ANOVA; and from expert judgement, i.e. "type B estimation").

A1.4.4.4 Additional UES Requirements

- The manufacturer shall describe how the influence quantities are varied. As a rule, the probability distribution should be documented.
- The manufacturer must document how the uncertainties are derived from the simulated samples.
- The essential features of the model must be documented. Transparency of the model increases the user's confidence in the statement of the uncertainty. Documentation of model and procedure should be sufficient to enable the user to furnish proof of a statement of uncertainty in compliance with the standards. This is important in particular in connection with the requirements of ISO 9000 foll. requiring the documentation of the procedure used for the uncertainty determination.
- The result of the evaluation of the simulation should be a statement in the form $\pm U$ which describes the uncertainty range of the measurement result with a specified confidence level (cf. also GUM).
- It must be ensured that the statement of the uncertainty complies with the internationally valid principles of the expression of the uncertainty (GUM). This includes the statement of a confidence level or a coverage factor. The combined standard uncertainty may be indicated in addition to the expanded uncertainty.

A1.5 Uncertainty Evaluating Software Evaluation (UESE)

A1.5.1 General

The UES must account for all effects that are specified in the declaration of influence factors. The CMM user can gain confidence that the UES

performs as claimed if the UES has passed an UESE performed by a testing body. The UESE test attempts to verify that when all influence quantities that are identified in the declaration section are varied within their permitted ranges, the expanded uncertainty calculated by the UES contains a large fraction (typically 95%) of the measurement errors. Given the very large number of different measurands and combinations of influence factors that can occur in CMM measurements, each one of which leads to a particular measurement error that is to be compared to the expanded uncertainty as calculated by the UES, the task of the UESE is enormous. In particular, since the measurement error, which is the difference between the measured and true values of a quantity, is to be compared against the UES calculated uncertainty statement, this requires a “true value”, e.g. a calibrated artifact, to be available for every CMM measurement performed in the UESE. Fortunately, if an UES can demonstrate that it can properly calculate the measurement uncertainty under an extensive UESE test, this testing does not need to be repeated unless the UES is revised.

The UESE consists of some combination of physical measurements and software measurements. Ideally, for each measurand, all possible permitted influence quantities are varied over their full permitted extent. To illustrate the magnitude of this task, consider a measurand that is the diameter of a cylinder. Ideally, we would like to measure a calibrated cylinder on a very large number of CMMs, each having a different combination of geometrical, probing error, different thermal, etc. as permitted by the declaration section. On each of these CMMs we would like to measure the cylinder in many locations, orientations, with different probes, sampling strategies, etc. For each of these measurements the error (CMM result minus calibrated value) is compared to the UES calculated expanded uncertainty statement. Obviously this example of a single measurand, involves hundreds, perhaps thousands, of measurements on a large number of CMMs and becomes too expensive as a practical test.

A1.5.2 Evaluation

The UESE consists of two parts: TEST 1: a thorough, general software test covering a wide range of capabilities of the simulation software, and TEST 2: a test using a physical object on a specific implementation of the software on a particular CMM and covering the whole system composed of CMM, evaluation software, and simulation software. TEST 1 is

conducted only once on a specific software release, while TEST 2 is conducted on each software/CMM combination.

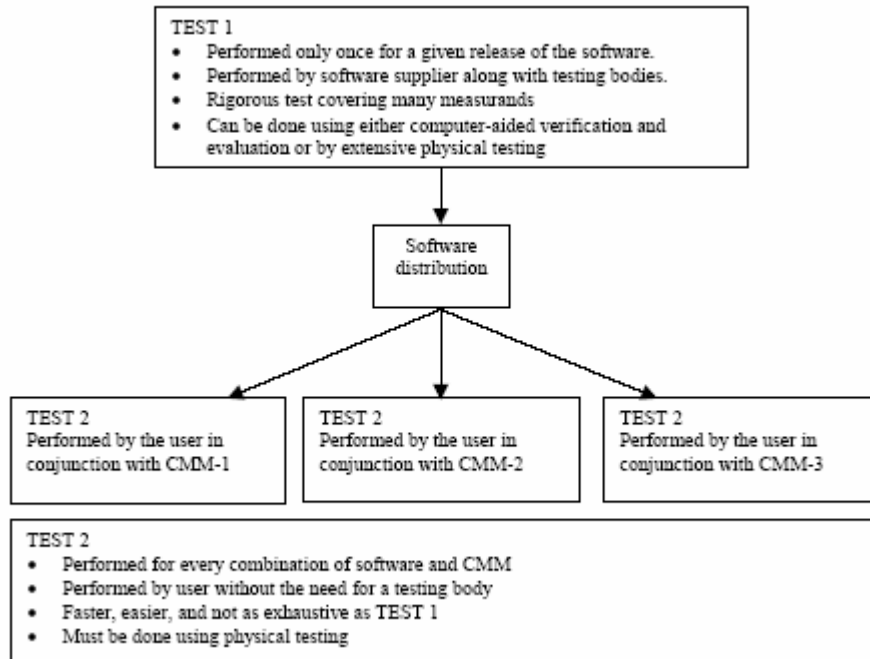


Fig. A1.2. Uncertainty Evaluating Software Evaluation (UESE) flow chart

A1.5.2.1 TEST 1

(DRAFT NOTE: Currently this standard briefly describes only the computer-aided verification and evaluation (CVE) for test 1. An alternate means for achieving TEST 1 by using extensive physical measurements is being investigated).

This procedure uses computer simulation to verify and evaluate the simulation software. The concept is to simulate a measuring instance, based on the claims in the declarations section (A1.3.1). Since the measuring instance is simulated and thus fully known in the CVE process, the error of the simulated measurement can be found. The software under test produces an uncertainty statement for this measurement and a simple comparison can determine if the error of the simulated measurement was contained in the uncertainty region reported by the software under test. This procedure can be repeated hundreds of times with varying conditions and statistics can be determined regarding

how often the errors of measurement were contained within their corresponding reported uncertainty ranges.

A1.5.2.1.1 Creation of a Simulated Measuring Instance used in CVE

When a CMM probes, there is generally a difference between the target contact point and the measured point, this difference being a vector. So a simulated measuring instance can be created by defining a vector field over the measuring volume of the CMM. That is, associated with each point in the CMM's measuring volume is a vector that represents the difference between the target contact point and the simulated measured point.

For the purposes of CVE, the declarations section (A1.3.1) determines what influences the definition of the vector field. For instance, if hysteresis is claimed in section (A1.3.1) then the vector associated with a particular point on one query would, in general, be different than on a subsequent query. If part form errors are included in the declarations section (A1.3.1) then the vector associated with a particular point would depend on the placement of the part in the measuring volume. This allows for testing the software's reported uncertainties without combining them with other uncertainties.

A1.5.2.1.2 Creation of Input Quantities

The declarations section includes the indication of the input quantities required by the software (A1.3.1, A1.3.7). These input quantities might arise from probes of special calibrated workpieces. Appropriate input quantities can be obtained as follows: A simulated measuring instance can be created in accordance with the specifications of the manner in which input quantities are obtained (A1.3.1, A1.3.7). Note, these conditions might be different than the ranges given in the checklist (e.g. the input quantities might be measured close to 20°C, while the software allows for measurements over a wider temperature range.) The target contact points used in the procedure to determine input quantities are provided to the testing body and the testing body returns the corresponding measured contact points from the simulated measuring instance. The software under test must be able to exchange this information.

A1.5.2.1.3 CVE Testing

The CVE testing should be performed over the entire spectrum of measurands for which the software is claimed to be valid. The CVE testing proceeds as shown in the following diagram:

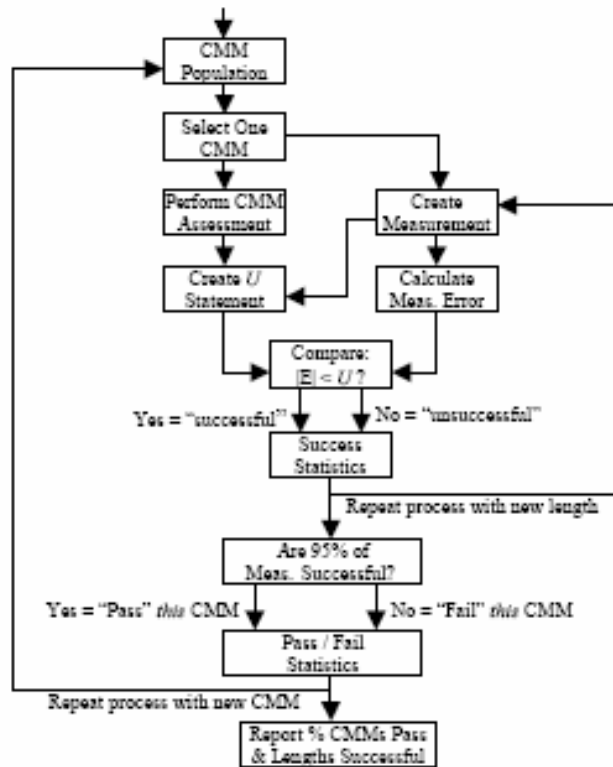


Fig. A1.3. CVE testing diagram

A1.5.2.1.4 Reporting CVE Results

CVE results consist of the following information:

- The percent of time true value lies in uncertainty interval; e.g. for "good" software the threshold might be 95%.
- The average amount of over-estimation of uncertainty, i.e. when the true value is contained within the uncertainty interval, on average how far is it from the nearest uncertainty interval limit.

- The average amount of under-estimation of uncertainty, i.e. when the true value is outside the uncertainty interval, on average how far is it from the nearest uncertainty interval limit.

A1.5.2.2 Verification Using a Calibrated Workpiece

In addition to the CVE, this procedure provides verification for a specific task for a specific software/CMM combination. Here, the statement of the uncertainty is checked by a test covering the whole system composed of CMM, evaluation software, and simulation software. The test is based on real measurements performed on calibrated objects. Any object permitted according to section A1.3.5 may be used. The object must have been calibrated by an independent procedure. In the Annex, an object and a procedure are given as an example, and show a number of measurement tasks to be simulated and which can also be calibrated with sufficient accuracy by independent procedures. For the measurement of such an object it is recommended to also vary the measurement strategy (position and orientation of the test object, distribution of measurement points) in order to check the influence on the measurement uncertainty stated. The following test objects may also be used: gauge blocks, step gauges, ball plates, ball bars and other standards. However any specific object is only suited to a limited extent to test the statements of task-specific uncertainty.

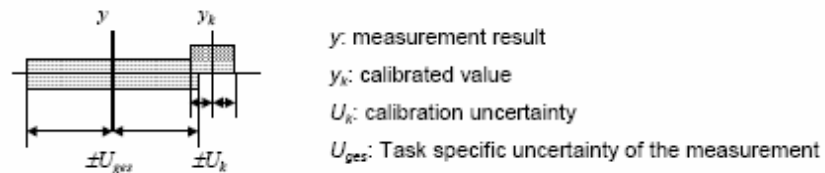
A1.5.2.2.1 Procedure

The measurements on the calibrated test objects are carried out on the real CMM for which the uncertainty of measurement is to be determined. The real measurement results y are calculated and the related task-specific uncertainties of measurement U_{ges} are determined by simulation.

A1.5.2.2.2 Calculation of the test result

Performing a number of measurements on calibrated objects, the coverage of the uncertainty ranges is checked. A statement of uncertainty will be plausible if:

$$\frac{|y_k - y|}{\sqrt{U_k^2 + U_{ges}^2}} \leq I \quad (\text{A1.3})$$



A reasonable relationship between the uncertainty of the calibration and the uncertainty of the individual measurement is to be aimed at. As a rule, the following should be valid: $U_K \ll U_{ges}$. The higher the calibration uncertainty U_K of the test object, the smaller the meaningfulness of the test.

A1.5.2.2.3 Re-verification

The Re-verification is to be carried out at regular intervals. Its type and scope comply with the procedure described in §A1.5. In addition, a Re-verification is to be carried out

- when the coordinate measuring machine has been modified,
- when one or several input parameters of the simulation model have been changed,
- when, in addition, the environmental conditions have changed beyond the specified range,
- when there are doubts about the uncertainties determined for other reasons.

After the first installation on the CMM concerned, short intervals (≤ 3 months) should be selected for the Re-verification. The positions of the test object in the measurement volume should, if possible, be varied for each intermediate test to guarantee as high a number of independent samples as possible. The intervals may be prolonged when sufficient experience has been gained regarding the stability of the measurements.

A1.5.2.2.4 Interim check of the input quantities

In the course of the intermediate test it is to be determined to what extent the present state of the CMM complies with the assumptions. The procedure has to state whether or not the estimation of the influence

quantities is still valid. The following influence quantities should in particular be monitored:

- Scale factors
- Rectangularities
- Probing errors
- Temperature and temperature gradients

The input quantities should preferably be monitored by the procedures usually applied in coordinate measurement technology.

APPENDIX 2: Architecture of the Software

The aim of this appendix is to present the software developed to evaluate the geometric error in the two case-studies discussed in this dissertation (a plane with a hole and a surface affected by position error and flatness error respectively). The software is an implementation of the general design methodology for the design of the inspection plan presented in the work. The adopted rationale is to run planned experiments in a suitable space of the design variables of interest. The experiments are run on a digital representation of the CMM (virtual CMM).

First we outline the general architecture and the interfaces of the software platform, and then we provide the code of the most relevant routines. Each code is introduced by a brief description of the implemented functionalities.

All routines are implemented in the Matlab environment. The control of the different software elaborations is assigned to the scripts “main.m”. They call a graphic interface where each different functionality can be mastered at a higher level. These functionalities are implemented by the individual sub-programs. When required the main program calls one or more sub-programs which solve a given problem.

The software has been tested with both Matlab 5.3 (R12) and 6.5 (R13) releases. It utilizes the general Matlab functions as well as the specific functions of the Matlab statistical toolbox.

The platform is designed in such a way that further modules relative to other geometric tolerances can be easily integrated. In this sense it represents a prototype of a possible software package for industrial use.

A schematic diagram of the software architecture is displayed in the next page (see Fig. A1). Notice that this diagram illustrates the software relative to position tolerances, while Figure A2 shows the software relative to flatness and straightness tolerances.

A2.1. Software configuration in the position tolerance evaluation case.

A Graphical User Interface provides the user with a set of possible configurations of the main program (see the red-dashed frame in Fig. A2.1). By means of the algorithms for planar surface sampling, measurement points on the plate are simulated.

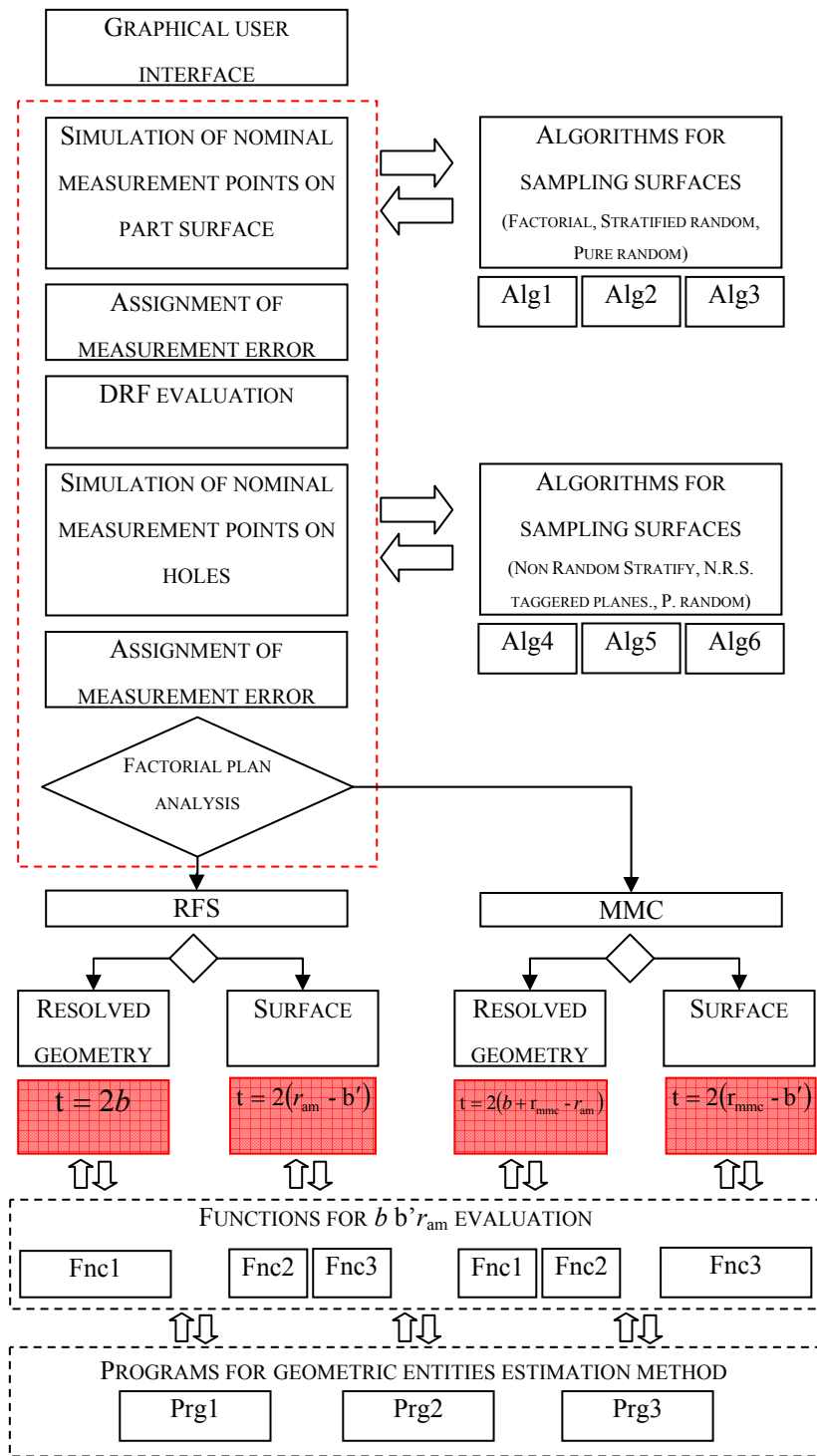


Fig.A2.1.General architecture of the developed software platform

For this purpose three different algorithms (Alg1, Alg2 and Alg3), may be used. Points generated are modified by the addition of the measurement error before the experiment is run. Then points on the holes are probed. Also in this case three different algorithms (Alg4, Alg5 and Alg6), can be used. At this point, according to the factorial plan (or to user choices), the software computes the geometric error (in this case the position error). For doing this it is necessary to find the values of all components forming position error t . Ad hoc functions are implemented for this purpose (Fnc1, Fnc2, Fnc3). All the three functions use as many programs (Prg1, Prg2, Prg3) to estimate the involved geometric entities

A2.2. Simulation of nominal measurement points on part surface

This routine calls algorithms which implements different measurement strategies on plate flat surface: Alg1: puntiDRF_fattoriale; Alg2: puntiDRF_LHS; Alg3: puntiDRF_random.

Input: sample size (na, nb, nc), geometric parameters (lu, la, percbordi).

Output: coordinates of probe points.

```
switch strpunpiano      %%scelta della strategia adottata
                        per tastare i punti sulle superfici di riferimento
case 1      %%FATTORIALE
    puntiDRF=puntiDRF_fattoriale(na,nb,nc,lc,lu,la,percbordi)
    %%funzione che individua i punti tastati sugli elementi
    di rif.
    puntiDRF_A=puntiDRF(:,1:na)';      %%matrice che contiene
    le coordinate degli na punti tastati sull'elemento di
    riferimento A
    puntiDRF_B=puntiDRF(:,na+1:na+nb)';      %%matrice che
    contiene le coordinate degli nb punti tastati
    sull'elemento di riferimento B
    puntiDRF_C=puntiDRF(:,na+nb+1:na+nb+nc)';      %%matrice che
    contiene le coordinate degli nc punti tastati
    sull'elemento di riferimento C
case 2      %%RANDOM STRATIFIED
    puntiDRF=puntiDRF_RS(na,nb,nc,lc,lu,la,percbordi);
    %%funzione che individua i punti tastati sugli elementi di
    rif.
    puntiDRF_A=puntiDRF(:,1:na)';      %%matrice che contiene le
    coordinate degli na punti tastati sull'elemento di
    riferimento A
    puntiDRF_B=puntiDRF(:,na+1:na+nb)';      %%matrice che
    contiene le coordinate degli nb punti tastati
    sull'elemento di riferimento B
    puntiDRF_C=puntiDRF(:,na+nb+1:na+nb+nc)';      %%matrice che
    contiene le coordinate degli nc punti tastati
    sull'elemento di riferimento C
```

```

case 3          %%RANDOM
puntiDRF=puntiDRF_random(na,nb,nc,hc,lu,la,percbordi);
  %funzione che individua i punti tastati sugli elementi di
  rif.
puntiDRF_A=puntiDRF(:,1:na)';          %matrice che contiene le
  coordinate degli na punti tastati sull'elemento di
  riferimento A
puntiDRF_B=puntiDRF(:,na+1:na+nb)';    %matrice che
  contiene le coordinate degli nb punti tastati
  sull'elemento di riferimento B
puntiDRF_C=puntiDRF(:,na+nb+1:na+nb+nc)'; %matrice che
  contiene le coordinate degli nc punti tastati
  sull'elemento di riferimento C
end

```

A2.2.1. Alg1: puntiDRF_fattoriale

See theory in § 5.3.4.

```

function[puntiDRF]=puntiDRF_fattoriale(na,nb,nc,hc,lu,la,pe
rcbordi);

lu_drf=lu-lu*percbordi;          %la lunghezza della piastra
  viene decurtata della percbordi imposta (1%) per tener
  conto degli smussi
la_drf=la-la*percbordi;          %la larghezza della piastra
  viene decurtata della percbordi imposta (1%) per tener
  conto degli smussi
hc_drf=hc-hc*percbordi*20;      %l'altezza della piastra viene
  decurtata del 20% per tener conto degli smussi

puntiDRF_A= zeros(na,3);
for k=1:sqrt(na)
  for h=1:sqrt(na)
    puntiDRF_A((k-1)*sqrt(na)+h,:)= [lu*percbordi/2+lu_drf/...
      (sqrt(na)-1)*(k-1), la*percbordi/2+la_drf/(sqrt(na)-
      1)*(h-1), 0];
  end
end

puntiDRF_B= zeros(nb,3);
for k=1:sqrt(nb)
  for h=1:sqrt(nb)
    puntiDRF_B((k-1)*sqrt(nb)+h,:)= [lu*percbordi/2+lu_drf/...
      (sqrt(nb)-1)*(k-1), 0, hc*percbordi*20/...
      2+hc_drf/(sqrt(nb)-1)*(h-1)];
  end
end
end

```

```

puntiDRF_C= zeros(nc,3);

for k=1:sqrt(nc)
    for h=1:sqrt(nc)
        puntiDRF_C((k-
            1)*sqrt(nc)+h,:)= [0,la*percbordi/2+la_drf/... (sqrt(nc)-
            1)*(k-1),hc*percbordi*20/2+hc_drf/(sqrt(nc)-1)*(h-1)];
        end
    end

puntiDRF=[puntiDRF_A',puntiDRF_B',puntiDRF_C'];    %matrice
    contenente l'insieme dei punti tastati per determinare il
    DRF

```

A2.2.2. Alg2: puntiDRF_RS

See theory in § 5.3.4.

```

function[puntiDRF]=puntiDRF_RS(na,nb,nc,hc,lu,la,percbordi)

lu_drf=lu-lu*percbordi;    %la lunghezza della piastra
    viene decurtata della percbordi imposta (1%) per tener
    conto degli smussi
la_drf=la-la*percbordi;    %la larghezza della piastra
    viene decurtata della percbordi imposta (1%) per tener
    conto degli smussi
hc_drf=hc-hc*percbordi*20; %l'altezza della piastra viene
    decurtata del 20% per tener conto degli smussi

puntiDRF_A= zeros(na,3);    %inizializzo la matrice che
    conterrà le coordinate degli na punti tastati
    sull'elemento di riferimento A
for k=1:sqrt(na)
    for h=1:sqrt(na)
        puntiDRF_A((k-1)*sqrt(na)+h,:)= [lu*percbordi/2+lu_drf/...
            sqrt(na)*(k-1+rand),la*percbordi/2+la_drf/sqrt(na)*(h-
            1+rand),0];
        end
    end
puntiDRF_B= zeros(nb,3);
for k=1:sqrt(nb)
    for h=1:sqrt(nb)
        puntiDRF_B((k-
            1)*sqrt(nb)+h,:)= [lu*percbordi/2+lu_drf/sqrt(nb)*(k-
            1+rand),0,hc*percbordi*20/2+hc_drf/... sqrt(nb)*(h-
            1+rand)];
        end
    end

puntiDRF_C= zeros(nc,3);    %inizializzo la matrice che

```

```

    conterrà le coordinate degli nc punti tastati
    sull'elemento di riferimento C
for k=1:sqrt(nc)
    for h=1:sqrt(nc)
        puntiDRF_C((k-1)*sqrt(nc)+h,:)= [0,la*percbordi/2+la_drf/...
            sqrt(nc)*(k-
            1+rand),hc*percbordi*20/2+hc_drf/sqrt(nc)*(h-1+rand)];
    end
end
puntiDRF=[puntiDRF_A',puntiDRF_B',puntiDRF_C']; %matrice
    contenente l'insieme dei punti tastati per determinare il
    DRF

```

A2.2.3. Alg3: puntiDRF_random

See theory in § 5.3.4.

```

function[puntiDRF]=puntiDRF_random(na,nb,nc,hc,lu,la,percbordi);

lu_drf=lu-lu*percbordi; %la lunghezza della piastra
    viene decurtata della percbordi imposta (1%) per tener
    conto degli smussi
la_drf=la-la*percbordi; %la larghezza della piastra
    viene decurtata della percbordi imposta (1%) per tener
    conto degli smussi
hc_drf=hc-hc*percbordi*20; %l'altezza della piastra viene
    decurtata del 20% per tener conto degli smussi

puntiDRF_A= zeros(na,3); %inizializzo la matrice che
    conterrà le coordinate degli na punti tastati
    sull'elemento di riferimento A
for k=1:na
    puntiDRF_A(k,:)= [lu*percbordi/2+lu_drf*rand,la*percbordi/
        2+la_drf*rand,0];
end

puntiDRF_B= zeros(nb,3);
for k=1:nb
    puntiDRF_B(k,:)= [lu*percbordi/2+lu_drf*rand,0,hc*percbord
        i*20/2+hc_drf*rand];
end

puntiDRF_C= zeros(nc,3); %inizializzo la matrice che
    conterrà le coordinate degli nc punti tastati
    sull'elemento di riferimento C
for k=1:nc
    puntiDRF_C(k,:)= [0,la*percbordi/2+la_drf*rand,hc*percbord

```

```

    i*20/2+hc_drf*rand];
end

puntiDRF=[puntiDRF_A',puntiDRF_B',puntiDRF_C'];    %matrice
           contenente l'insieme dei punti tastati per determinare il
           DRF

```

A2.3. Assignment of measurement error

See theory in § 5.3.3.

```

pDRF_Amis=normrnd(puntiDRF_A,sigma);    %simulazione dei
           punti tastati sull'elemento di riferimento A
pDRF_Bmis=normrnd(puntiDRF_B,sigma);    %simulazione dei
           punti tastati sull'elemento di riferimento B
pDRF_Cmis=normrnd(puntiDRF_C,sigma);    %simulazione dei
           punti tastati sull'elemento di riferimento C

```

A2.4. DRF evaluation

See theory in § 5.3.4.

```

orthopA = zeros(3,1);
orthopB = zeros(3,1);
orthopC = zeros(3,1);

servA=pDRF_Amis-kron(mean(pDRF_Amis),ones(na,1));
AA=servA'*servA;
[eigenvectA,lamdaA]=eigs(AA);
orthopA(:,1)=eigenvectA(:,3);
servB= pDRF_Bmis-kron(mean(pDRF_Bmis),ones(nb,1));
AB=eigenvectA(:,1:2) '*servB'*servB*eigenvectA(:,1:2);
[eigenvectB,lamdaB] = eigs(AB);
orthop23 = eigenvectA(:,1:2)*eigenvectB;

if lamdaB(1,1)< lamdaB(2,2)
    orthopB(:,1) = orthop23(:,1);
    orthopC(:,1) = orthop23(:,2);
else
    orthopB(:,1) = orthop23(:,2);
    orthopC(:,1) = orthop23(:,1);
end

if orthopB(2,1)<0
    orthopB(:,1)=-orthopB(:,1);
end
if orthopC(1,1)<0
    orthopC(:,1)=-orthopC(:,1);
end

```

```

end

alfa0_pA=-mean(pDRF_Amis)*orthopA(:,1);
alfa0_pB=-mean(pDRF_Bmis)*orthopB(:,1);
alfa0_pC=-mean(pDRF_Cmis)*orthopC(:,1);

A = [orthopA(:,1) orthopB(:,1) orthopC(:,1)]';
b = [-alfa0_pA;-alfa0_pB;-alfa0_pC];

DRF_orig(:,1) = A\b;
M=[orthopC(:,1),orthopB(:,1),orthopA(:,1)];

Prtrasl=(M'*(puntif-ones(npf,1)*DRF_orig'))';

```

A2.5. Definition of measurement error

```
P=normrnd(Prtrasl, sigma);
```

A2.6. Simulation of nominal measurement points on part surface (holes).

This routine calls algorithms which implement different measurement strategies on holes: Alg4: `puntif_fattoriale`; Alg5: `puntif_psfalsati`; Alg6: `puntif_random` (see §5.3.5).

Input: sample size (n_{pf}), geometric parameters (x_c , y_c , $raggio$, hc , $percbordi$).

Output: coordinates of probed points.

```

switch strpunforo          %scelta della strategia adottata
per tastare i punti sulle superfici del foro

case 1 %%FATTORIALE
puntif=puntif_fattoriale(npf,x_c,y_c,raggio,hc,percbordi);
case 2 %%PIANI SFALSATI
puntif=puntif_psfalsati(npf,x_c,y_c,raggio,hc,percbordi);
case 3 %%RANDOM
puntif=puntif_random(npf,x_c,y_c,raggio,hc,percbordi);
end

```

A2.6.1. Alg4: `puntif_fattoriale`

See theory §5.3.5

```

function[puntif]=puntif_fattoriale(npf,x_c,y_c,raggio,hc,pe
rcbordi);
hc_f=hc-hc*percbordi*20;    %l'altezza della piastra (del

```



```

foro) viene decurtata del 20% per tener conto degli
smussi

puntif=zeros(npf,3); %inizializzo la matrice che conterrà
le coordinate degli npf punti tastati sulla superficie
interna del foro
if npf==4 %distinzione necessaria per evitare che i
quattro punti proiettati su XY del DRF si sovrappongono
(vengono alternati)
for k=1:2
z=hc*percbordi*20/2+(k-1)*hc_f; %calcolo la z dei fori
for h=1:2
puntif((k-1)*2+h,:)= [x_c+raggio*cos((k-1)*pi/2+(h-
1)*pi),y_c+raggio*sin((k-1)*pi/2+(h-1)*pi),z];
end
end
else
for k=1:sqrt(npf)
z=hc*percbordi*20/2+(k-1)*hc_f/(sqrt(npf)-1); %calcolo
la z dei fori
for h=1:sqrt(npf)
puntif((k-1)*sqrt(npf)+h,:)= [x_c+raggio*cos((h-
1)*2*pi/sqrt(npf)),y_c+raggio*sin((h-
1)*2*pi/sqrt(npf)),z];
end
end
end
end

```

A2.6.2. Alg5: puntif_psfalsati

See theory §5.3.5

```

function[puntif]=puntif_psfalsati(npf,x_c,y_c,raggio,hc,per
cbordi);

hc_f=hc-hc*percbordi*20; %l'altezza della piastra (del
foro) viene decurtata del 20% per tener conto degli
smussi

puntif=zeros(npf,3); %inizializzo la matrice che conterrà
le coordinate degli npf punti tastati sulla superficie
interna del foro
salta=2*pi/npf; %calcolo l'angolo di cui saranno
sfalsati i piani
for k=1:sqrt(npf)
z=hc*percbordi*20/2+(k-1)*hc_f/(sqrt(npf)-1); %calcolo
la z dei fori
for h=1:sqrt(npf)
puntif((k-1)*sqrt(npf)+h,:)= [x_c+raggio*cos(salta*(k-
1)+(h-1)*2*pi/sqrt(npf)),y_c+raggio*sin(salta*(k-1)+(h-

```

```

    1)*2*pi/sqrt(npf)),z];
end
end

```

A2.6.3. Alg5: puntif_random

See theory §5.3.5

```

function[puntif]=puntif_random(npf,x_c,y_c,raggio,hc,percbo
rdi);

hc_f=hc-hc*perc bordi*20;    %l'altezza della piastra (del
foro) viene decurtata del 20% per tener conto degli
smussi

puntif=zeros(npf,3);    %inizializzo la matrice che conterrà
le coordinate degli npf punti tastati sulla superficie
interna del foro
for k=1:sqrt(npf)
    z=hc*perc bordi*20/2+(k-1)*hc_f/(sqrt(npf)-1);    %calcolo
    la z dei fori
    for h=1:sqrt(npf)
        puntif((k-1)*sqrt(npf)+h,:)= [x_c+raggio*cos(2*pi*rand),
        y_c+raggio*sin(2*pi*rand),z];
    end
end
end

```

A2.7. Factorial plan analysis

This section performs the computation of position error t . The main program calls functions that compute b , b' , r_{am} .

1. RFS-resolved geometry interpretation: Fnc1 (trovab) (see §5.3.6.1).
2. RFS-surface interpretation: Fnc2 (trovacilindroam) and Fnc3 (trovabprimo) (see §5.3.6.2).
3. MMC-resolved geometry interpretation: Fnc1 (trovab) and Fnc2 (trovacilindroam) (see §5.3.6.3).
4. MMC-surface interpretation: Fnc3 (trovabprimo) (see §5.3.6.4).

For details on inputs and outputs see the section where each function is described.

```

switch materiale

```

```

case 1    %%condizione del materiale applicata: RFS

if inter==1    %%interpretazione della geometria
    risolta

    bdir_trovab(p, hc, mcerchio, x_c, y_c, raggio); %%funzione
        che trova b, ram e la direzione di t
    b=bdir_trovab(1,1);    %%valore di b
    t=2*b;    %%valore misurato della tolleranza reale t
    x_dir_trovab(bdir_trovab(1,3));    %%direzione in x associata al
        valore di t calcolato riferita alle coordinate del
        centro nominale
    y_dir_trovab(bdir_trovab(1,4));    %%direzione in y associata al
        valore di t calcolato riferita alle coordinate del
        centro nominale
    dati_incertezza(i,:)=[materiale inter t b x_dir_trovab
        y_dir_trovab bdir_trovab(1,2) 0 0 0 x_c y_c raggio rmmc
        bdir_trovab(1,5) bdir_trovab(1,6) 0 0];

else    %%interpretazione della superficie

    riscer_trovacilindroam(p, mcerchio, raggio);    %%funzione
        che trova i parametri del cilindroam
    ram=riscer_trovacilindroam(1,5);    %%valore di ram
    bprimodirt_trovabprimo(p, mcerchio, x_c, y_c, raggio);
        %%funzione che trova bprimo e la direzione associata
        al valore di t misurato
    bprimo=bprimodirt_trovabprimo(1,1);    %%valore di bprimo
    t=2*(ram-bprimo);    %%valore misurato della tolleranza
        reale t
    x_dir_trovabprimo(bprimodirt_trovabprimo(1,2));    %%direzione in x associata
        al valore di t calcolato riferita alle coordinate del
        centro nominale
    y_dir_trovabprimo(bprimodirt_trovabprimo(1,3));    %%direzione in y associata
        al valore di t calcolato riferita alle coordinate del
        centro nominale
    dati_incertezza(i,:)=[materiale inter t bprimo x_dir_trovabprimo
        y_dir_trovabprimo bprimodirt_trovabprimo(1,4:6) ram x_c y_c raggio rmmc -
        riscer_trovacilindroam(1,1) -riscer_trovacilindroam(1,2) 0 0];

end

case 2    %%condizione del materiale applicata: mmc

if inter==1    %%interpretazione della geometria risolta

    bdir_trovab(p, hc, mcerchio, x_c, y_c, raggio); %%funzione
        che trova b, ram e la direzione di t
    b=bdir_trovab(1,1);    %%valore di b
    ram=bdir_trovab(1,2);    %%valore di ram

```

```

t=2*(b+rmmc-ram);           %%valore misurato della
toleranza reale t
x_dirt=bdirt(1,3);         %%direzione in x associata al
valore di t calcolato riferita alle coordinate del
centro nominale
y_dirt=bdirt(1,4);         %%direzione in y associata al
valore di t calcolato riferita alle coordinate del
centro nominale
dati_incertezza(i,:)=[materiale inter t b x_dirt
y_dirt 0 0 0 ram x_c y_c raggio rmmc bdirt(1,5)
bdirt(1,6) 0 0];

else    %%interpretazione della superficie

bprimodirt=trovabprimo(p,mcerchio,x_c,y_c,raggio);
%%funzione che trova bprimo e la direzione associata
al valore di t misurato
bprimo=bprimodirt(1,1);    %%valore di bprimo
t=2*(rmmc-bprimo);        %%valore misurato della
toleranza reale t
x_dirt=bprimodirt(1,2);    %%direzione in x associata
al valore di t calcolato riferita alle coordinate del
centro nominale
y_dirt=bprimodirt(1,3);    %%direzione in y associata
al valore di t calcolato riferita alle coordinate del
centro nominale
distcc1=sqrt(x_dirt^2+y_dirt^2);
dati_incertezza(i,:)=[materiale inter t bprimo x_dirt
y_dirt distcc1 bprimodirt(1,4:6) x_c y_c raggio rmmc
0 0 0 0];
end
end

```

A2.7.1. Fnc1: trovab

Input: coordinate of probed points (P), geometric parameters (hc, x_c, y_c, raggio), geometry evaluation function (mcerchio).

Output: *b* value

```

function [bdirt]=trovab(P,hc,mcerchio,x_c,y_c,raggio);

riscer=trovacilindroam(P,mcerchio,raggio); %%funzione che
trova i dati del più grande cilindro contenuto nel foro
ram=riscer(1,5);    %%valore di ram
w=-riscer(1,1);    %%valore di w rispetto al DRF
f=-riscer(1,2);    %%valore di f rispetto al DRF
Rw=[1,0,0;0,cos(w),sin(w);0,-sin(w),cos(w)]; %%matrice di
rotazione di w

```

```

Rf=[cos(f),0,-sin(f);0,1,0;sin(f),0,cos(f)]; %matrice di
    rotazione di f
passeam1=[riscer(1,3) riscer(1,4) 0]; %punto appartenente
    all'asse del più grande cilindro contenuto nel foro nel
    DRF ruotato di w, f
passeam2=[riscer(1,3) riscer(1,4) 10]; %punto appartenente
    all'asse del più grande cilindro contenuto nel foro nel
    DRF ruotato di w, f
passe(1,:)=(Rw*Rf*passeam1)'; %punto appartenente
    all'asse del più grande cilindro riferito al DRF misurato
passe(2,:)=(Rw*Rf*passeam2)'; %punto appartenente
    all'asse del più grande cilindro riferito al DRF misurato
t1r=(0-passe(1,3))/(passe(2,3)-passe(1,3)); %valutiamo il
    parametro t dell'equazione parametrica di una retta nello
    spazio con z0=0
plr=[passe(1,1)+(passe(2,1)-passe(1,1))*t1r
    passe(1,2)+(passe(2,2)-passe(1,2))*t1r]; %valore della
    proiezione del primo estremo dell'asse
t2r=(hc-passe(1,3))/(passe(2,3)-passe(1,3)); %valutiamo il
    parametro t dell'equazione parametrica di una retta nello
    spazio con z0=hc
p2r=[passe(1,1)+(passe(2,1)-passe(1,1))*t2r
    passe(1,2)+(passe(2,2)-passe(1,2))*t2r]; %valore della
    proiezione del secondo estremo dell'asse
c_nom=[x_c y_c]; %%coordinate del centro nominale del foro
distanza(1,:)=dist(plr,c_nom'); %distanza proiezione
    primo estremo, centro nominale
distanza(2,:)=dist(p2r,c_nom'); %distanza proiezione
    secondo estremo, centro nominale
[b sss]=max(distanza); %valore di b
if sss==1
    x_dirt=plr(1)-x_c; %direzione in x associata al valore
        di t calcolato riferita alle coordinate del centro
        nominale
    y_dirt=plr(2)-y_c; %direzione in y associata al valore
        di t calcolato riferita alle coordinate del centro
        nominale
else
    x_dirt=p2r(1)-x_c; %direzione in x associata al valore
        di t calcolato riferita alle coordinate del centro
        nominale
    y_dirt=p2r(2)-y_c; %direzione in y associata al valore
        di t calcolato riferita alle coordinate del centro
        nominale
end
bdirt=[b,ram,x_dirt,y_dirt, riscer(1,1), riscer(1,2)];
    %matrice che conserva i valori di b, ram e la direzione
    associata al valore di t misurato

```

A2.7.2. Fnc2: trovacilindroam

Input: coordinate of probed points (P), geometric parameters (raggio), geometry evaluation function (mcerchio).

Output: r_{am}

```

riscer=trovacilindroam(P,mcerchio,raggio);    funzione che
trova i dati del più grande cilindro contenuto nel foro

switch cerchio

case 1      %%proprietà geometriche
    angmax=0.0014;
    fino=5;
case 2      %%ottimizzazione non lineare
    angmax=0.0014;
    fino=5;
otherwise   %%minimi quadrati ortogonali
    angmax=0.0028;
    fino=6;
end

for conta=1:1:fino;%%imposto il grado di risoluzione voluto
for w=wmin:avanza:wmax;    %%variazione di w
for f=fmin:avanza:fmax;    %%variazione di f
    Prot=zeros(1,3); %%inizializzo la matrice che conterrà
    i valori dei punti proiettati sul nuovo piano XY
    for i=1:dim(1)    %%esprimo le coordinate dei punti
    tastati rispetto ai nuovi assi ottenuti dalla
    rotazione
        Rw=[1,0,0;0,cos(w),sin(w);0,-sin(w),cos(w)];
        %%matrice di rotazione di w
        Rf=[cos(f),0,-sin(f);0,1,0;sin(f),0,cos(f)];
        %%matrice di rotazione di f
        Prot(i,:)=(Rf*Rw*P(i,:))'; %%rotazione di P attorno
        a w e a f
    end
    Pproiez=Prot(:,1:2);    %% proiezione dei punti sul
    nuovo piano XY

%%Stima della più grande circonferenza inscritta tra i
punti proiettati sul nuovo piano XY

switch mcerchio
case 1      %%proprietà geometriche
    [x_c1 y_c1 r_c1]=cerchiomax...
    ...allcerchi(Pproiez,raggio);
case 2      %%ottimizzazione non lineare

```

```

[x_c1 y_c1 r_c1]=cerchiomaxopt(Pproiez);
case 3      %%minimi quadrati ortogonali
[x_c1 y_c1 r_c1]=min_quadrati(Pproiez);
end

cilindroam(ii,:)= [w f x_c1 y_c1 r_c1]; %%parametri
dei cilindri individuati al variare di w e f
ii=ii+1;
end
end

[a,b]=max(cilindroam(:,5)); %%valori di w e f e
rispetto cerchio massimo ottenuto
riscer=cilindroam(b,:); %%valori finali di w f x_c1
y_c1 r_c1 riferiti ad ram massimo
avanza=avanza/2;
wmax=riscer(1,1)+avanza;
wmin=riscer(1,1)-avanza;
fmax=riscer(1,2)+avanza;
fmin=riscer(1,2)-avanza;

w=-riscer(1,1); %%valore di w rispetto al DRF
f=-riscer(1,2); %%valore di f rispetto al DRF
Rw=[1,0,0;0,cos(w),sin(w);0,-sin(w),cos(w)]; %%matrice
di rotazione di w
Rf=[cos(f),0,-sin(f);0,1,0;sin(f),0,cos(f)]; %%matrice
di rotazione di f

passeam1=[riscer(1,3) riscer(1,4) 0]; %%punto
appartenente all'asse del più grande cilindro contenuto
nel foro nel DRF ruotato di w, f
passeam2=[riscer(1,3) riscer(1,4) 10]; %%punto
appartenente all'asse del più grande cilindro contenuto
nel foro nel DRF ruotato di w, f

passe(1,:)=(Rw*Rf*passeam1)'; %%punto appartenente
all'asse del più grande cilindro riferito al DRF misurato
passe(2,:)=(Rw*Rf*passeam2)'; %%punto appartenente
all'asse del più grande cilindro riferito al DRF misurato

t1r=(0-passe(1,3))/(passe(2,3)-passe(1,3)); %%valutiamo
il parametro t dell'equazione parametrica di una retta
nello spazio con z0=0
p1r=[passe(1,1)+(passe(2,1)-passe(1,1))*t1r;passe(1,2)
+(passe(2,2)-passe(1,2))*t1r]; %%valore della
proiezione del primo estremo dell'asse
t2r=(hc-passe(1,3))/(passe(2,3)-passe(1,3)); %%valutiamo
il parametro t dell'equazione parametrica di una retta
nello spazio con z0=hc
p2r=[passe(1,1)+(passe(2,1)-passe(1,1))*t2r;passe(1,2)+
(passe(2,2)-passe(1,2))*t2r]; %%valore della

```

```

    proiezione del secondo estremo dell'asse
c_nom=[x_c y_c]; %%coordinate del centro nominale del foro

distanza(1,:)=dist(p1r,c_nom'); %%distanza proiezione
    primo estremo, centro nominale
distanza(2,:)=dist(p2r,c_nom'); %%distanza proiezione
    secondo estremo, centro nominale
[b sss]=max(distanza); %%valore di b

if sss==1
    x_dirt=p1r(1)-x_c; %%direzione in x associata al valore
        di t calcolato riferita alle coordinate del centro
        nominale
    y_dirt=p1r(2)-y_c; %%direzione in y associata al valore
        di t calcolato riferita alle coordinate del centro
        nominale
else
    x_dirt=p2r(1)-x_c; %%direzione in x associata al valore
        di t calcolato riferita alle coordinate del centro
        nominale
    y_dirt=p2r(2)-y_c; %%direzione in y associata al valore
        di t calcolato riferita alle coordinate del centro
        nomina
end

```

A2.7.3. Fnc3: trovabprimo

Input: coordinates of probed points (P), geometric parameters (x_c, y_c, raggio), geometry evaluation function (mcerchio).

Output: b' value

```

function[bprimodirt]=trovabprimo(P,mcerchio,x_c,y_c,raggio)
Pproiez=P(:,1:2); %%proiezione dei punti tastati sul
    foro sul piano XY del DRF misurato

switch mcerchio
    case 1 %%proprietà geometriche
        [x_c1 y_c1 r_c1]=cerchiomaxallcerchi(Pproiez,raggio);
    case 2 %%ottimizzazione non lineare
        [x_c1 y_c1 r_c1]=cerchiomaxopt(Pproiez);
    otherwise %%minimi quadrati
        [x_c1 y_c1 r_c1]=min_quadrati(Pproiez);
end
bprimo=r_c1-dist([x_c1 y_c1],[x_c y_c]); %%calcolo di
    bprimo
x_dirt=x_c1-x_c; %%direzione in x associata al valore di
    t calcolato riferita alle coordinate del centro nominale
y_dirt=y_c1-y_c; %%direzione in y associata al valore di

```



```

t  calcolato  riferita  alle  coordinate  del  centro
nominale
bprimodirt=[bprimo,x_dirt,y_dirt,x_c1,  y_c1,  r_c1]  ;
%matrice che conserva i valori di bprimo e la direzione
associata al valore di t misurato

```

A2.7.4. Prg1: min_quadrati

See theory §5.4

```

function [x_c1,y_c1,r_c1]=min_quadrati(P)

Xp=P(:,1);
Yp=P(:,2);
nh1=size(P);
nh1=nh1(1);
sigmastop=0.0001;

servc=cat(2,Xp,Yp);
c0 = [mean(servc(:,1)) mean(servc(:,2))];

for h=1:nh1
distances1(h,1) = norm(servc(h,:) - c0); % valore misurato
del raggio
end

r0 = mean (distances1);

conta=0;
epsilon=1;

while epsilon > 0.01*sigmastop
  conta=conta+1;

  W = ones (nh1,3);
  W(:,2) = (servc(:,1)-c0(1,1))./distances1;
  W(:,3) = (servc(:,2)-c0(1,2))./distances1;
  Z = distances1-r0;
  delta = (W'*W)\(W'*Z);
  c = c0 + [delta(2:3,1)'];
  r = r0 + delta(1,1);
  epsilon = max (abs(delta));
  c0=c;
  r0=r;
  for h=1:nh1
    distances1(h,1) = norm(servc(h,:) - c0);
  end
end
C = c;
R=r;

```

```

distanze=dist(P,C');
mindist=min(distanze);
if mindist<R
    R=mindist;
else
end

x_c1=C(1,1);
y_c1=C(1,2);
r_c1=R;

```

A2.7.5. Prg2: cerchiomaxopt

See theory §5.4

```

function [x_c1,y_c1,r_c1]=cerchiomaxopt(P)

Xp=P(:,1);
Yp=P(:,2);
nh1=size(P); %
servc=cat(2,Xp,Yp);
c0 = [mean(servc(:,1)) mean(servc(:,2))];
for h=1:nh1
    distances1(h,1) = norm(servc(h,:) - c0); % primo valore
    misurato del raggio
end
r0 = mean (distances1);
x0 = [r0 c0(1) c0(2)]; lb = []; % Limite inferiore X >= 0
ub = []; % Nessun limite superiore
[x,fval,exitflag,output] =
    fmincon('objfun',x0,[],[],[],[],lb,ub,'confun',options,Xp
    ,Yp);

x_c1=x(2);
y_c1=x(3);
r_c1=x(1);

function f = objfun(x,Xp,Yp)

% Funzione obiettivo: f=diametro
f=-2*x(1);

function [c, ceq] = confun(x,Xp,Yp)

aa=size(Xp);
for j=1:aa
    a(j)=-sqrt((Xp(j)-x(2))^2+(Yp(j)-x(3))^2)+x(1);
end

```

```
c=a;
ceq = [];
```

A2.7.6. Prg3: cerchiomaxopt

See theory §5.4

```
function [x_c1,y_c1, r_c1]=cerchiomaxallcerchi(P,raggio)

bb=size(P);   c_m=mean(P);
dist_bar = dist(P(:,1:2),c_m(:,1:2)'); % primo valore
      misurato del raggio
r_med = mean (dist_bar);

XP=nchoosek(P(:,1),3); %%creazione di tutte le possibili
      terne di coordinate x
YP=nchoosek(P(:,2),3); %%creazione di tutte le possibili
      terne di coordinate y
aa=size(XP);
for cc=1:aa(1)
  %Soluzione di un sistema lineare
  x(1)*xp+x(2)*yp+x(3)=xp^2-yp^2
  %Sia A la matrice dei coefficienti delle incognite ovvero
  la matrice dei punti
  %B il vettore termine noti xp^2-yp^2
  A=ones(3,3);
  A(:,1:2)=cat(2,XP(cc,:)',YP(cc,:)'); %tre coppie di
      punti delle length(XP) combinazioni dei punti misurati
  B=(power(A(:,1),2)+power(A(:,2),2));
  D=B'*(inv(A)');
  xc=D(1)/2;
  yc=D(2)/2;
  % rc=sqrt(D(3)+xc^2+yc^2);
  p_c=[XP(cc,1),YP(cc,1)];
  c_c=[xc,yc];
  rc=dist(p_c,c_c');
  ris(cc,:)=[xc yc rc];
end
ord=sortrows(ris,3); %ordina le circonferenze dalla più
      piccola alla più grande
for ccc=1:aa(1)
  [anglec distc]=cart2pol(P(:,1)-repmat(ord(aa(1)+1-ccc,1),
      bb(1),1) , P(:,2)-repmat(ord(aa(1)+1-ccc,2),bb(1),1));
  mindistc=min(distc);
  raggioc=ord(aa(1)+1-ccc,3);
  if (mindistc-raggioc)>= -10^-12 & ... %%%la differenza
      darebbe un valore diverso da zero piccolo ma più
      grande della definizione 10^-16
    dist(c_m(1,1:2),ord(aa(1)+1-ccc,1:2)')< r_med/10
      %%%controlla che il centro del foro sia interno ai
```

```
    punti, 5 fattore di sicurezza
    break
end
end
x_c1=ord(aa(1)+1-ccc,1);
y_c1=ord(aa(1)+1-ccc,2);
r_c1=ord(aa(1)+1-ccc,3);
```

A2.8 Software configuration for the case of flatness (and straightness) tolerance.

A Graphical User Interface provides the user with a set of possible configurations of the main program ((see the red-dashed frame in Fig. A2.1). By means of factorial sampling method, large sampling is simulated. Then a fitting routine estimates the parameters of the form error model (flatness and straightness). Notice that in the routine three functions of the Matlab optimization toolbox are used (nonlinfit, fminunc, fmincon). According to the experiment design, a small point sample is simulated. For this purpose four different algorithms (Alg7, Alg8, Alg9 and Alg10), may be used. Points generated are then modified by adding both the measurement error and the form error.

Finally flatness error is computed either by using two possible algorithms (Prg4, Prg5) or by using the previous fitting routine.

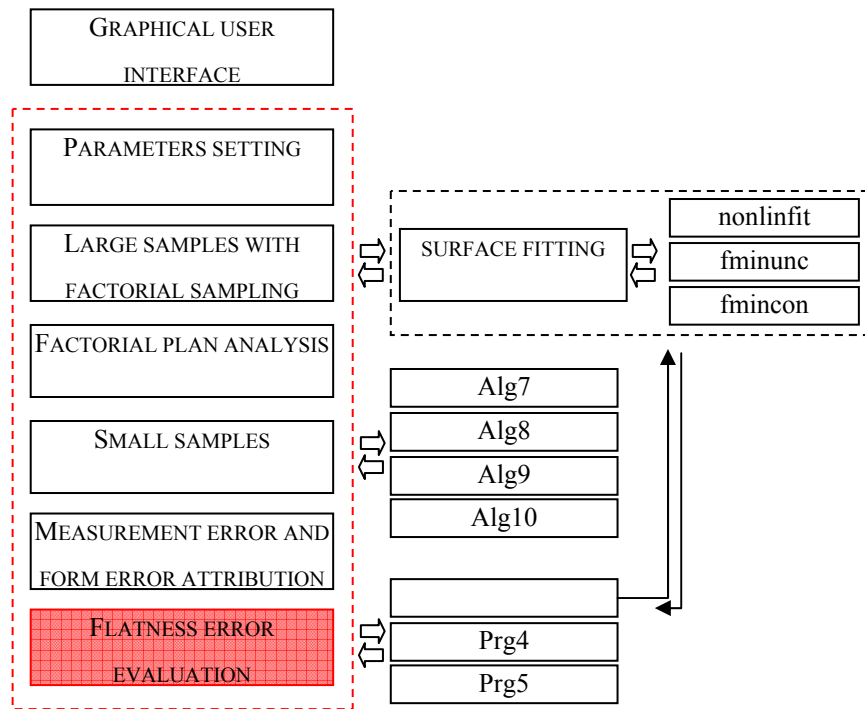


Fig.A2.1.General architecture of the developed software platform

A2.9. Parameters setting

This section of the main program assigns a value to the parameters used for flatness error computation.

```

npi=22500; %22500 numero di punti con i quali calcolare i
           coefficienti realistici della funzione che approssima la
           superficie della piastra
n_it=100;  % numero di ripetizioni dei calcoli per ogni
           stato di prova del DOE
lu=200;   % dimensione relativa all'asse X
la=200;   % dimensione relativa all'asse Y
percbordi=0.01;
% Dati generali del modello superficiale della piastra :
a=la;     % larghezza dell'intera piastra in mm
b=lu;     % lunghezza dell'intera piastra in mm
alfa=0.01159440356513; %valore della formula calcolato con
           16 iterazioni, forza applicata x=100 y=100 e a=b
% parametri delle funzioni che descrivono il profilo
           superficiale
csi=(a/2);
% eta e csi : ordinata del punto di applicazione del carico

```

```

    che assume quel valore per simulare la
    %      deformazione che lascia l'utensile
eta=(b/2);
ss=size(DOE);
nconf=ss(1);
risul=zeros(nconf,9); % matrice con 6 colonne contenenti
    l'output di ogni stato di prova: PAB   VC   MED   ST
    DEV T REAL      T TEST      P%   RANGE
ttt=zeros(n_it,nconf);
for iu=1:nconf
    prova=iu      %%PROVE DEL PIANO FATTORIALE
    switch DOE(iu,1)
        case 1
            na=36; % na: numeri di punti campionati sull'intera
                superficie
        case 2
            na=49; % na: numeri di punti campionati sull'intera
                superficie
        case 3
            na=64; % na: numeri di punti campionati sull'intera
                superficie
    end
    switch DOE(iu,2)
        case 1
            tast=1; %1=random
        case 2
            tast=2; %2=fattoriale
        case 3
            tast=3; %3=fattoriale radiale
        case 4
            tast=4; %4=ipercubi latini
    end
    switch DOE(iu,3)
        case 1
            sigma1=0.0005;
        case 2
            sigma1=0.0015;
        case 3
            sigma1=0.0025;
    end
    if iu==1
        R_iniz=4;          % massima flessione in mm al centro
            della piastra dovuta al solo carico concentrato
        a1_iniz=0.01;     % ampiezza dell'onda sinusoidale che
            si propaga in direzione X
        a2_iniz=0.01;     % ampiezza dell'onda sinusoidale che
            si propaga in direzione Y
        %R_iniz=1;        % massima flessione in mm al centro
            della piastra dovuta al solo carico concentrato (1-4)
    end
end

```

```

%a1_iniz=0.04;           % ampiezza dell'onda sinusoidale
                        che si propaga in direzione X   (0,04 -0,01)
%a2_iniz=0.04;           % ampiezza dell'onda sinusoidale che
                        si propaga in direzione Y   (0,04 -0,01)
wmax=R_iniz
T=3;
nil_iniz=((2*pi)/T);
ni2_iniz=((2*pi)/T);
fil_iniz=0;
fi2_iniz=0;
sigma2=0.0003; % deviazione standard della distribuzione
               normale dei fenomeni esterni
% sigma2=0;
R=R_iniz;           % massima flessione in mm al centro
                  della piastra dovuta al solo carico concentrato
al=a1_iniz;         % ampiezza dell'onda sinusoidale che si
                  propaga in direzione X
a2=a2_iniz;         % ampiezza dell'onda sinusoidale che si
                  propaga in direzione Y
nil=nil_iniz;
ni2=ni2_iniz;
fil=fil_iniz;
fi2=fi2_iniz;

```

A2.10. Large samples with factorial sampling

A large amount of points is simulated by means of a factorial strategy. Then the fitting function is called.

```

riferim=[R_iniz;a1_iniz;a2_iniz;nil_iniz;ni2_iniz;fil_iniz;
         fi2_iniz];

[coef_real,t_rif]=fitting(lu,la,sigma1,sigma2,riferim,npi,a
                          lfa,eta,csi);
R_real=coef_real(1,1);
al_real=coef_real(2,1);
a2_real=coef_real(3,1);
nil_real=coef_real(4,1);
ni2_real=coef_real(5,1);
fil_real=coef_real(6,1);
fi2_real=coef_real(7,1);
t_real=t_rif;

```

A2.10.1. Surface fitting

Function “fitting” estimates the parameters of the form error model and compute a realistic value of the form error t .

```

function[real_coeff,t_riferim] =
    fitting(lu,la,sigma1,sigma2,rif,npi,alfa,eta,csi)
na=npi;
a=la;           % larghezza dell'intera piastra in mm
b=lu;           % lunghezza dell'intera piastra in mm
percbordi=0.01;
R=rif(1,1);
wmax=R;
a1=rif(2,1);
a2=rif(3,1);
ni1=rif(4,1);
ni2=rif(5,1);
fi1=rif(6,1);
fi2=rif(7,1);
p_piastra=zeros(na,2);
p_piastra=piastra_fattoriale(na,lu,la,percbordi);
p_piastra_r=normrnd(p_piastra, sigma1); % sovrapposizione
    dell'errore di misura con dev st sigma1 ai punti tastati
    x y
for jj=1:na
    x=p_piastra_r(jj,1);
    y=p_piastra_r(jj,2);
    somma=0;
    for m = 1:2:32           % viene eseguita la sommatoria di8
        termini
        for n =1:2:32
            somma=somma+(sin(m*pi*csi/a)*...
                sin(n*pi*eta/b))/(m^2/a^2+n^2/b^2)^2*sin(m*pi*x/a)
                *sin(n*pi*y/b);
        end
    end
    w=-4*wmax/(alfa*a^3*b*pi^4)*somma;
    onde=(a1*sin(x*ni1+fi1)+a2*sin(y*ni2+fi2)); % solchi
        lasciati dall'utensile
    z(jj,1)=(w+onde);
    z=normrnd(z,sigma1); % sovrapposizione dell'errore
        di misura con dev st sigma1 a z
    z=normrnd(z,sigma2); % sovrapposizione dei fenomeni
        casuali esterni con dev st sigma2 a z

beta0=zeros(7,1);
beta0(1,1)=wmax; % R: max flessione al centro della
    piastra
beta0(2,1)=a1; % a1: ampiezza della sinusoide che si
    propaga in direzione X
beta0(3,1)=a2; % a2: ampiezza della sinusoide che si
    propaga in direzione Y
beta0(4,1)=ni1; % ni1: pulsazione della sinusoide che
    si propaga in direzione X

```



```

beta0(5,1)=ni2;          % ni2: pulsazione della sinusoida
    che si propaga in direzione Y
beta0(6,1)=fi1;         % fi1: sfasamento della sinusoida che
    si propaga in direzione X
beta0(7,1)=fi2;         % fi2: sfasamento della sinusoida che
    si propaga in direzione Y
real_coeff=zeros(7,1);
real_coeff=nlinfit(p_piastra,z,@superf_sup,beta0);

v1 = [100 100]; %punto iniziale per minimo
v2=[0,0;200,0;0,200;200,200]; %punto iniziale per max
options = optimset('GradObj','off');
options = optimset(options,'Display','off');
[coord_min,f_min] =
    fminunc(@eric_trif,v1,options,real_coeff);
coord=zeros(4,3);
for k=1:4
    options = optimset('LargeScale','off');
    options = optimset(options,'Display','off');
    [coord_max,f_max] =
        fmincon(@eric_trif_bound,v2(k,:),[],[],[],[],[0 200],[0
        200],[],options,real_coeff);
    coord(k,1:2)=coord_max;
    coord(k,3)=f_max;
end

f_mas=min(coord);
t_riferim=-f_min-f_mas(3)

```

A2.11. Small samples

According to the experiment design, a small point sample is generated, using one of four sampling methods: Alg7: tast_random; Alg8: piastra_fattoriale; Alg9: fatt_rad and Alg10: punti_latino.

```

mat_t=zeros(n_it,1); % vettore riga che contiene i calcoli
    di t_reale ripetuti in ogni stato di prova
for kk=1:n_it
    z=zeros(na,1);
    rip=kk;
    p_piastra=zeros(na,2);
    switch(tast)
        case 1
            p_piastra=tast_random(na,lu,la,percbordi);
        case 2
            p_piastra=piastra_fattoriale(na,lu,la,percbordi);
        case 3
            p_piastra=fatt_rad(na,lu,percbordi);
        case 4

```

```
p_piastra=punti_latino(na,lu,la,percbordi);
end
```

A2.12. Measurement error and form error attribution

Coordinates of simulated measurement points are modified by adding measurement error and form error.

```
for jj=1:na
    x=p_piastra(jj,1);
    y=p_piastra(jj,2);
    somma=0;
    for m = 1:2:32          % viene eseguita la sommatoria di 8
        termini
        for n =1:2:32
            somma=somma+(sin(m*pi*csi/a)*sin(n*pi*eta/b))/(m^2/a^2+n
                ^2/b^2)^2*sin(m*pi*x/a)*sin(n*pi*y/b);
        end
    end
    w=-4*wmax/(alfa*a^3*b*pi^4)*somma;
    onde=(a1*sin(x*ni1+fi1)+a2*sin(y*ni2+fi2)); % solchi
        lasciati dall'utensile
    z(jj,1)=(w+onde); %%%quota z ideale
end
z=normrnd(z,sigma1); % sovrapposizione dell'errore di
    misura con dev st sigma1 a z
z=normrnd(z,sigma2); % sovrapposizione dei fenomeni
    casuali esterni con dev st sigma2 a z
```

A2.13. Flatness error evaluation

In this section flatness error is computed. Two different methods may be used: Prg4: `olsmsemp` and Prg5: `conv3Dsemp`.

```
switch DOE(iu,4)
case 1
    p_sper=[p_piastra,z];
    mat_t(kk,1)=[olsmsemp(p_sper,na)];
case 2
    p_sper=[p_piastra,z];
    mat_t(kk,1)=[conv3Dsemp(p_sper,na)];
case 3
    beta0=zeros(7,1);
    beta0(1,1)=R_iniz; % R: max flessione al centro
        della piastra
    beta0(2,1)=a1_iniz; % a1: ampiezza della sinusoida
        che si propaga in direzione X
    beta0(3,1)=a2_iniz; % a2: ampiezza della sinusoida
        che si propaga in direzione Y
```

```

beta0(4,1)=ni1_iniz;          % ni1: pulsazione della
    senoide che si propaga in direzione X
beta0(5,1)=ni2_iniz;          % ni2: pulsazione della
    senoide che si propaga in direzione Y
beta0(6,1)=fi1_iniz;          % fi1: sfasamento della
    senoide che si propaga in direzione X
beta0(7,1)=fi2_iniz;          % fi2: sfasamento della
    senoide che si propaga in direzione Y
fit_coeff=zeros(7,1);
fit_coeff=nlinfit(p_piastra,z,@superf_sup,beta0);
v1 = [100 100]; %punto iniziale per minimo
v2=[0,0;200,0;0,200;200,200]; %punto iniziale per max
options = optimset('GradObj','off');
options = optimset(options,'Display','off');
[coord_min,f_min] = fminunc(@eric_trif,v1,[],fit_coeff);
minimo=[coord_min,-f_min];
coord=zeros(4,3);
for k=1:4
options = optimset('LargeScale','off');
options = optimset(options,'Display','off');
[coord_max,f_max] =
    fmincon(@eric_trif_bound,v2(k,:),[],[],[],[],[0 ;200],[0;
    200],[],options,fit_coeff);
coord(k,1:2)=coord_max;
coord(k,3)=f_max;
end
coord=sortrows(coord,3);
f_mas=coord(1,:);
massimo=f_mas;
mat_t(kk,1)=-f_min-f_mas(3) ;

vett=mat_t';

```

A2.13.1. Alg7: tast_random

```

function [punti]=tast_random(na,lu,la,percbordi);

lu_drf=lu-lu*percbordi; %la lunghezza della piastra viene
    decurtata della percbordi imposta (1%) per tener conto
    degli smussi
la_drf=la-la*percbordi; %la larghezza della piastra viene
    decurtata della percbordi imposta (1%) per tener conto
    degli smussi
punti= zeros(na,2); %inizializzo la matrice che conterrà
    le coordinate degli na punti tastati sull'elemento di
    riferimento A
for k=1:na
punti(k,:)=[lu*percbordi/2+lu_drf*rand,la*percbordi/2+la_
    drf*rand];

```

end

A2.13.2. Alg8: piastra_fattoriale

```
function [p_superf]=piastra_fattoriale(na,lu,la,percbordi);
lu_drf=lu-lu*percbordi;
la_drf=la-la*percbordi;
p_superf= zeros(na,2);
for k=1:sqrt(na)
    for h=1:sqrt(na)
        p_superf((k-
            1)*sqrt(na)+h, :)= [lu*percbordi/2+lu_drf/(sqrt(na)-1)*(k-
            1), la*percbordi/2+la_drf/(sqrt(na)-1)*(h-1)];
    end
end
```

A2.13.3. Alg9: fatt_rad

```
function [punti]=fatt_rad(n,lu,percbordi);

lu_drf=lu-lu*percbordi;
indriga=0;
fi=0;
for h=0:(sqrt(n)-1)
    r=(lu_drf/2)*(1-(h/(sqrt(n))));
    fi=fi+(pi/sqrt(n));
    for k=1:sqrt(n)
        indriga=indriga+1;
        teta=(fi+k*((2*pi)/sqrt(n)));
        punti(indriga, :)= [ ((lu/2)+r*cos(teta)), ((lu/2)+r*sin(tet
            a))];
    end
end
```

A2.13.4. Alg10: punti_latino

```
function [punti]=punti_latino(na,lu,la,percbordi);

lu_drf=lu-lu*percbordi;
la_drf=la-la*percbordi;
punti= zeros(na,2);
camp = lhsdesign(na,2);
punti(:,1)=(0.5*lu*percbordi+camp(:,1)*lu_drf);
punti(:,2)=(0.5*la*percbordi+camp(:,2)*la_drf);
```

A2.13.5. Prg4: olsmsemp

See theory §6.2.1

```
function [treale]=olsmsemp(punti,na);

Xp=[punti(:,1)];
Yp=[punti(:,2)];
Zp=[punti(:,3)];
n=na; % numero di punti tastato sulla superficie in esame
x(2)=beta1=0, x(3)=beta2=0
x0 = [0 0 0];
options = optimset('Maxfunevals',3000,'Display','off');
x = lsqnonlin('obpianoOLSM',x0,[],[],options,Xp,Yp,Zp,n);
e=zeros(n,1);
for k= 1:n
    e(k,1)=( (Zp(k)-x(1)-x(2)*Xp(k)-
             x(3)*Yp(k)) / (sqrt(1+x(2)^2+x(3)^2)) );
end
treale=max(e)-min(e);
```

A2.13.6. Prg5: conv3Dsemp

See theory §6.2.3

```
function [treale]=conv3Dsemp(pA,na);

K=convhulln(pA);
numrighe=length(K);
dist=zeros(na,numrighe);
for p = 1:numrighe % scansione delle faccie del poliedro
    a=( (pA(K(p,2),2)-pA(K(p,1),2)) * (pA(K(p,3),3) -
        pA(K(p,1),3)) - (pA(K(p,3),2)-pA(K(p,1),2)) * (pA(K(p,2),3) -
        pA(K(p,1),3))) );
    b=( (pA(K(p,3),1)-pA(K(p,1),1)) * (pA(K(p,2),3) -
        pA(K(p,1),3)) - (pA(K(p,2),1)-pA(K(p,1),1)) * (pA(K(p,3),3) -
        pA(K(p,1),3))) );
    c=( (pA(K(p,2),1)-pA(K(p,1),1)) * (pA(K(p,3),2) -
        pA(K(p,1),2)) - (pA(K(p,3),1)-pA(K(p,1),1)) * (pA(K(p,2),2) -
        pA(K(p,1),2))) );
    for q = 1:na % calcolo ripetuto per tutti i punti
        dist(q,p)=abs( (a*(pA(K(p,1),1)-pA(q,1))+b*(pA(K(p,1),2)-
            pA(q,2))+c*(pA(K(p,1),3)-
            pA(q,3))) / (sqrt((a)^2+(b)^2+(c)^2)) );
    end
end
distanze=max(dist);
treale=min(distanze);
```